Design and Synthesis of Small Molecule Ligands Targeting Protease-Activated Receptor 2 as Potential Diagnostic and Therapeutic Agents

A Thesis Presented to

The Faculty of Graduate Studies Of

Lakehead University

By

YANG MAO

In partial fulfillment of requirements for the degree of
Master of Science
26 August 2021

©Yang Mao, 2021

ABSTRACT

Positron emission tomography (PET) imaging requires radionuclides (positron-emitters) labeled molecules (tracers) to image biochemical and physiological processes *in vivo* and helps diagnose diseases noninvasively. The success of PET imaging depends on validated radiopharmaceuticals targeting biologically relevant receptors. Protease-activated receptors (PARs) are cell membrane receptors that belong to a class of the G protein-coupled receptors (GPCRs) family. Protease-activated receptor 2 (PAR2) is the second member of the PARs family. Aberrant activation of PAR2 is associated with various cancers, through downstream signaling that contributes to cancer progression and tumor metastasis. It has been found that PAR2 exhibited up to 16-fold over-expression in lung cancer. The upregulation of PAR2 in cancers indicates that it may serve as potential drug target for cancer screening and treatment. Blocking PAR2 activity with small molecules is proposed to provide a therapeutic benefit. In addition, the development of ^{18}F-radiolabeled small molecules targeting PAR2 receptor has the potential to non-invasively diagnose some types of cancers such as lung and breast cancers. A library of AZ3451 analogues (14 compounds) was designed with the assistance of molecular modelling, and was synthesized, and characterized by Mass Spectrometry, and ^{1}H-NMR. All compounds have greater than 95% purity as confirmed by HPLC. Collaborator Dr. Rithwik Ramachandran at Western University (UWO) will perform functional assays including calcium-signalling, β-arrestin recruitment, MARK signaling assays etc. to evaluate all compounds for the therapeutic potential; the candidate molecule will be selected for radiolabelling and PET imaging studies using animal models of cancer at the TBRHRI. The novel compounds synthesized in the thesis are potentially useful for the treatment of PAR2-driven cancers while the radioligand has potential for non-invasive cancer diagnosis with PET.

Keywords

Positron emission tomography (PET), PET imaging agent, radiopharmaceuticals, G protein-coupled receptor (GPCR), protease-activated receptor 2 (PAR2), antagonist, AZ3451 analogues, Fluorine-18 (^{18}F), inflammatory diseases, lung, and breast cancer, non-invasively.

Acknowledgments

In a thesis paper of more than 100 pages, I thought this page would be the easiest, so I left it to the last minute. But when I recall the memory of these two years, I even do not know where and how to start, because I have had a lot of help along the way, there are so many people I would like to thank.

It is a great pleasure to join Lakehead University and become a member of the Department of Chemistry. Here, I met nice and excellent faculty, professors, and committees. Firstly, I would like to thank my supervisor, Dr. Jinqiang Hou. He is a nice and responsible supervisor. I appreciated that he introduced me to the field of radiopharmaceutical and gave me a lot of help with my studies. He always takes his time to listen to my questions and help me to solve them. Dr. Hou was very willing to share his studying and research experience with us when we met some problems in the experiment. In addition, Dr. Hou has always gathered us together and made us an inclusive and cohesive team. And I also would like to thank Dr. Taylor Hari, who is the research advisor in our group. He is willing to help, whenever I had problems with my slides and paper, I can always get advice from him.

Next, I would like to thank Dr. Mike Campbell for being on my committee. I enjoyed Dr. Campbell's class on medicinal chemistry, I learned a lot of knowledge about drugs, which helped in my research very much. I am grateful to be able for running the MS samples in his lab. I would like to thank Dr. Christine Gottardo for being on my committee I enjoyed Dr. Gottardo's chromatography module, it helped me gain knowledge of GS and HPLC. I am grateful for her letting me borrow the chemicals from her lab, that were helpful for making my new compounds.

I would like to thank Dr. Justin Jiang. I used to take a class about carbohydrates when I was an undergraduate, so I was interested in his carbohydrates chemistry and learned more about this. And more, I would like to extend my thanks to Dr. Robert Mawhinney. He always patiently explained lots of questions about the graduate program and the courses to me. And I also learned the knowledge of computational chemistry and how to run the program Gaussian from his molecular modeling module.

Further, I would like to thank Debbie Puumula and Brad Miller for all the chromatography module assistance, obtaining chemicals, and refilling solvent. I would also like to thank Mike Sorokopud for his kind help with running NMR samples.

In addition, I would like to thank my lab mates, Wenjie Liu, Austin Hopkins, and Dong Zhao. Wenjie and I were the first two graduate students in Dr. Hou's group, so we discussed lots of research and laboratory issues together. Austin and I worked on similar research; we usually talk to each other about the research. I want to give him a special thanks for helping me edit this thesis.

Lastly, I would like to thank my family for supporting me all the time, despite they are being so far away. And I also like to thank my wife, Rui Zhu, and my son, Ryan Mao. They two really give me a lot of motivation during the time of my graduate studies.

All figures were created with BioRender.com, Chemdraw, MestRenova, and Discovery Studio 2021 software.

TABLE OF CONTENTS

PAGE

ABSTRACT

ACKNOWLEDGMENTS....i

LIST OF TABLES....v

LIST OF FIGURES....vi

LIST OF SCHEMES....viii

LIST OF APPENDICES....ix

LIST OF ABBREVIATIONS AND SYMBOLS....x

CHAPTER ONE

Introduction....11

1.1 Cancer and Molecular Imaging....11

1.2 Positron Emission Tomography Study....12

1.3 Positron Emission Tomography Imaging with Fluorine-18....14

1.4 Protease-Activated Receptors....18

1.5 Protease-Activated Receptor 2....21

1.6 Known Ligand Targeting PAR2....24

1.7 Labeling Strategy....28

1.8 Purpose of Thesis....29

CHAPTER TWO: DESIGN AND SYNTHESIS OF SMALL MOLECULE LIGANDS TARGETING PAR2 AS POTENTIAL DIAGNOSTIC AND THERAPEUTIC AGENTS.

2.1 Introduction..30

2.2 Ligand Design...33

2.3 Results and Discussion..36

2.31 Organic Synthesis of AZ3451...36

2.32 Conformational isomer of AZ3451...42

2.33 Organic synthesis of AZ3451 Analogues..46

2.4 Molecular Docking...49

2.5 Discussion of compound 8c..55

2.6 Other series of AZ3451 analogues...56

2.61 The design and synthesis of the second series of AZ3451 analogue........................56

2.62 The design and synthesis of the third series of AZ3451 analogue.......................... 57

CHPATER THREE

3.1 Conclusion...59

3.2 Future Work...60

3.21 Organic Synthesis...60

3.22 Biology Assay..60

3.23 Radiolabel Approach.. 61

CHAPTER FOUR

Experimental procedures...63

REFERENCES...79

APPENDICES..92

List of Tables

Table 1. Summary of PAR2 related disease models and effect of PAR2 knockout (KO) 23

Table 2. Purities of 14 analogues…………………………….……………………………37

Table 3. Binding affinity of the reference compound (AZ3451), and the analogues…………...51

Table 4. In vitro pharmacology of AZ3451 and AZ2623…………..…………………….........55

List of Figures

Figure 1. Cancer diagnosis and therapy by molecular imaging..........12

Figure 2. The key steps for development of PET imaging agent process..........14

Figure 3. Production of Fluorine-18..........15

Figure 4A. Positron Emission **4B.** Diagram of the operation of PET scanner. 16

Figure 5. Structure of [^{18}F]-FDG..........17

Figure 6. GPCRs and PARs activation comparison..........20

Figure 7. Activation of PAR2..........22

Figure 8. PAR2 antagonists reported in literature..........25

Figure 9. Structure of PAR2 agonists..........27

Figure 10. Direct radio-fluorination of aromatic ring..........28

Figure 11. Interplay of antagonist AZ3451 (orange) with PAR2, and pharmacology and binding affinity of AZ3451..........31

Figure 12. AZ3451 - PAR2 interactions in three-D and two-D diagram..........32

Figure 13. Ligand design of AZ3451 analogues with R group..........34

Figure 14. A) Scheme of the third step. B) Results of TLC of third step from 1 hour to 5 hours…39

Figure 15. The spectrum of ^{1}H-NMR for the reaction at the first hour (ester) and the fifth hour (carboxylic acid) 40

Figure 16. The spectrum of ^{1}H-NMR for AZ3451..........41

Figure 17. Structure of AZ3451 and 4 types of potential conformational isomer..........43

Figure 18. The spectrum of ^{1}H-NMR of carboxylic acid compound 4..........44

Figure 19. The spectrum of ^{1}H-NMR for carboxylic acid compound 4 on 25°C, 50°C, 75°C and 100°C..45

Figure 20. AZ3451 analogues with R-group...47

Figure 21. The spectrum of ^{1}H-NMR of compound 6b...48

Figure 22. The diagram of binding interaction between a ligand and its target protein………...50

Figure 23. Ligand-receptor interaction for analogues 6a-8a. AZ3451 is shown in yellow stick, analogues 6a-8a are shown as green sticks……..……………………………………………….52

Figure 24. Ligand-receptor interactions for analogues 9a-10a. AZ3451 is shown in yellow stick. Analogues 9a-10a are shown as green sticks.……………………………………………….53

Figure 25. Ligand-receptor interactions for analogues 11a-13a. AZ3451 is shown in yellow stick. Analogues11a-13a are shown as green sticks.…………………。………………………54

Figure 26. Structure of AZ3451 and AZ2623…………………………………………………...55

Figure 27. Structure of AZ3451 and compound 11. …………………………………...……...58

List of Schemes

Scheme 1. The reported synthetic scheme for AZ3451..36

Scheme 2. Proposed mechanism of Iodine-mediated Cyclization...37

Scheme 3. The proposed synthetic scheme for the second series of analogues............................56

Scheme 4. The proposed synthetic scheme for the third series of analogues................................57

Scheme 5. Proposed radiolabelling scheme for AZ3451-derived ligand......................................62

List of Appendices

Appendix 1: Structures of AZ3451 Analogues..78

Appendix 2: Spectrum of Mass Spectroscopy, HPLC, and ^{1}H-NMR for compound 4 (Carboxylic group) and Compound 5 (AZ3451) 79

Appendix 3: Spectrum of Mass Spectroscopy, HPLC and ^{1}H-NMR for AZ3451 analogues......83

Appendix 4: Spectrum of MS and ^{1}H-NMR for Compound 15..117

List of Abbreviations and Symbols

cAMP	cyclic adenosine monophosphate
DCM	methylene chloride
DIPEA	N, N-Diisopropylethylamine
DMSO	dimethyl sulfoxide
ECL2	extracellular loop 2
ERK	extracellular signal-regulated kinase
EtOAc	Ethyl acetate
^{18}F	fluorine-18
FDG	[^{18}F]-fluorodeoxyglucose
FLIPR	fluorescent imaging plate reader
GDP	guanosine diphosphate
GPCR	G-protein-coupled receptor
GTP	guanosine triphosphate
HATU	1-Bis(dimethylamino)methylene-1H-1,2,3-triazolo 4,5-b pyridinium 3-oxid hexafluorophosphate
IC_{50}	half-maximal inhibitory concentration
IP3	inositol 1,4,5-triphosphate
K_{222}	Krypto fix $_{222}$
K_D	dissociation constant
MAPK	mitogen-activated protein kinase
MRI	magnetic resonance imaging
PAR	protease-activated receptor
PET	positron-emission tomography
RCY	radiochemical yield
SCIDY	spirocyclic iodonium ylide
SPECT	single-photon emission computed tomography
TGF-β1	transforming growth factor beta 1
TMD	transmembrane receptor domain

Chapter One

Introduction

1.1 Cancer and Molecular Imaging

Cancer is caused by the uncontrolled growth and reproduction of cells resulting from a series of mutations in normal cells[1,2]. Cancer cells lack adhesion molecules that stick the cells in place, therefore, they can metastasize and spread throughout the body[3]. In fact, the spread of cancer cells is a major reason for cancer deaths.[4] In the past two years, nearly 50,000 Canadians have been diagnosed with different stages of lung cancer with rates slightly higher in men than women[5,6] About 20,000 people die of lung cancer each year[6]. Furthermore, more than 30,000 women have been diagnosed with various stages of breast cancer in 2020 alone[5,7]. This accounts for about 25 percent of new cancer cases[7]. About 5,000 women die of breast cancer each year, accounting for 13 percent of all cancer deaths in Canada[7]. Fortunately, cancer survival rates are improving due to three main advances in: 1) improved prevention efforts, 2) screening for several cancers, and 3) clinical cancer treatment[8]. The purpose of screening and diagnosing cancer is to detect cancer before symptoms appear[9] often providing the best chance for a cure. This monitoring includes blood tests, DNA tests, and medical imaging[8,10]. Over the past thirty years, imaging technology has become an indispensable tool in cancer research, clinical trials, and medical practices[1,8]. One type of medical imaging involves injecting a radiotracer (radioactive isotope) into a healthy individuals and using imaging techniques to track its movement through the body (Figure 1)[11].

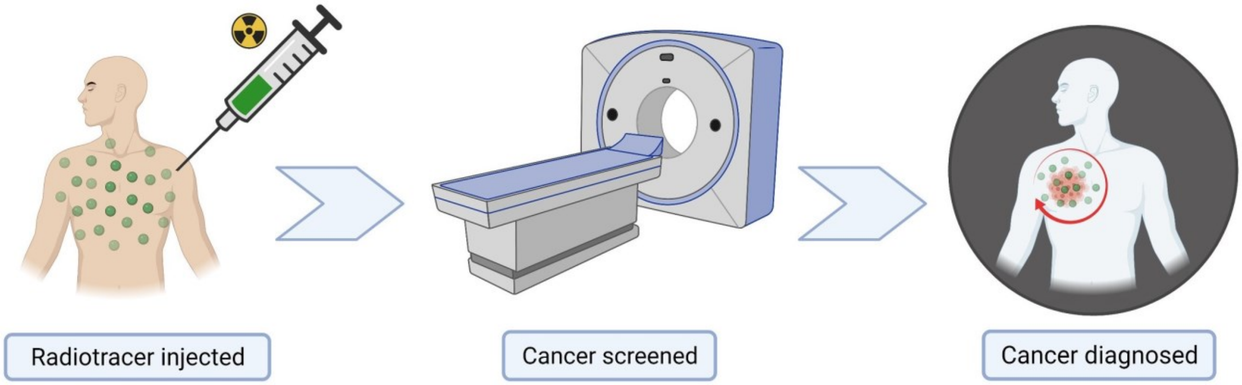

Figure 1. Cancer diagnosis by medical imaging.

This technique allows researchers and clinicians to better observe the real-time location, expression, and activity of cancer cells in the body[8]. This can effectively diagnose cancer and determine the cancer targets, which is also beneficial to the research and development of targeted therapeutic drugs[11,12].

1.2 Positron Emission Tomography Studies

In recent decades, the way that researchers and physicians approach the inner workings of living systems and the diagnosis and assessment of diseases has been gradually altered by medical imaging[11]. There are several different types of medical imaging techniques that are based on the amount of energy used to capture visual information, the difference of spatial resolution, and the mode of information acquired. These imaging technologies include X-rays, computed tomography (CT), magnetic resonance imaging (MRI), and the nuclear medicine techniques of single photon emission computed tomography and Positron Emission Tomography (PET)[11,13]. Nuclear medical imaging uses small amounts of radioactive substances. The radioactivity can be detected by a radiation detector, which transfers electrical signals to a computer to construct three dimensional images highlighting the bio-distribution of a radiotracer in the body[14]. In the early 20th century, researchers were only able to use Geiger counters to crudely measure the bio-distribution of radioactive substances in the body due to a lack of imaging subassembly[15]. It wasn't until 1956 that, an initial photographic part was created in the rectilinear scanner (an imaging device, designed by B. Cassen in 1950)[15]. This improvement greatly increased the resolution and sensitivity of the imaging instrument to radioactivity.

The key steps of PET imaging agent development are outlined in Figure 2[13]. In Step 1, the purpose of target identification is to find a biomarker of the disease of interest[13]. The biomarker can be used as an indicator of the physiological state of the disease and can be a protein or nucleic acid[16]. Once a promising target has been identified, the aim of hit identification is to identify a compound that can perfectly interact with and modify the target[17]. This can be done by using a process called high-throughput screening (HTS) (Step 2)[18]. The lead optimization of the compounds is accomplished by using advanced organic synthetic methods[13,18]. The purpose of this process is to improve the potency, solubility and reduce the side effects of the compounds, making them more 'drug-like'[13,17]. This step provides a lead compound for further *in vitro* testing (Step 3). Radiochemistry is the combination of radionuclides with bioactive compounds to form radiopharmaceuticals[13,19]. The candidates with the highest binding affinity in Step 3 will be radiolabeled to make radiotracers, which will be injected into small-animal models inflicted with human diseases in PET imaging studies (Step 4 and Step 5)[13]. These compounds need to be tested in vivo to evaluate the target-specificity of the imaging[20]. The use of small animal models is an important component of testing new drugs before they are translated into clinical practice[13,14]. Eventually, these drugs will be studied in clinical trials and need to be approved for the market (Step 5-8)[13].

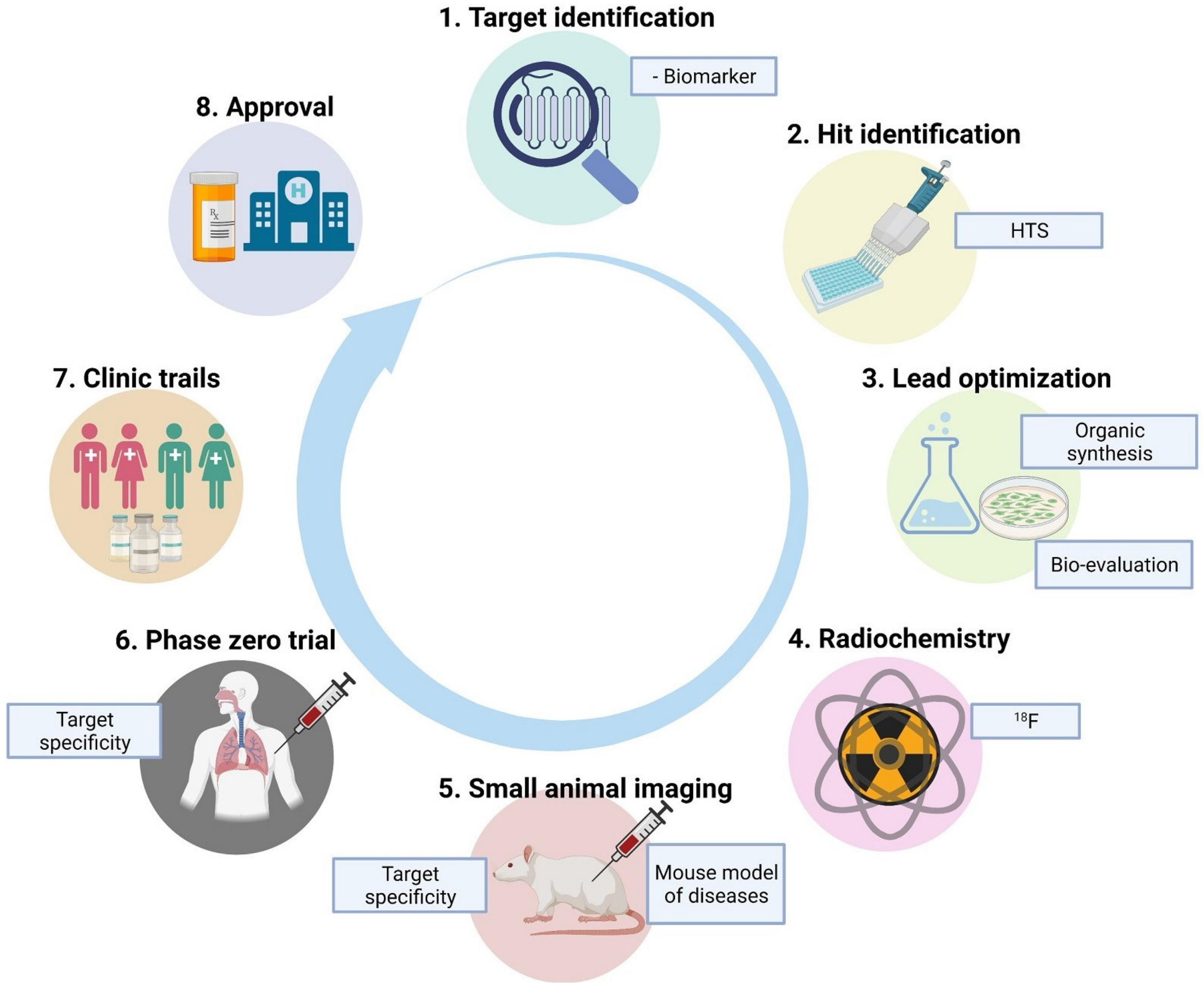
1. Target identification
- Biomarker
2. Hit identification
HTS
3. Lead optimization
Organic synthesis
Bio-evaluation
4. Radiochemistry
^{18}F
5. Small animal imaging
Target specificity
Mouse model of diseases
6. Phase zero trial
Target specificity
7. Clinic trails
8. Approval

Figure 2. The key steps for development of PET imaging agent process.

1.3 Positron Emission Tomography Imaging with Fluorine-18

Positron emission tomography (PET), is one nuclear imaging techniques[14]. PET imaging is a sensitive and non-invasive imaging approach that allows physicians to look at internal organs function without having to perform exploratory surgery[21]. PET imaging is a three-Dimensional imaging technique in which, information regarding the bio-distribution of an injected radiolabelled compound (radiotracer) in the body can be obtained by detecting the radiation[22]. PET imaging is based on positron-emitting radionuclides-labeled compounds. The most common radioisotopes for the PET imaging modality include ^{11}C (half-life = 20.3 minutes), ^{18}F (half-life = 109.8 minutes), ^{13}N (half-life = 9.97 minutes), ^{64}Cu (half-life = 12.7 hours) and ^{68}Ga (half-life = 67.8 minutes)[23]. Of greatest significance for radiotracer design and research is the half-life of radionuclides[24]. Radiotracers with longer-lived radionuclides enable metabolic processes to be studied over a few hours[23]. Fluorine-18 (^{18}F) was one of the earliest radionuclides used in research and is considered an ideal radionuclide for routine PET imaging based on its excellent chemical and positron-emitting properties[24]. In radiopharmaceutical production, PET radioisotopes are produced in cyclotrons, a type of particle accelerator that can produce charged particles in the ion chamber[25]. Fluorine-18 is produced by using a cyclotron to bombard water (enriched with oxygen-18), with high energy protons; this is the most used reaction for the productions of ^{18}F (Figure 3)[24]. Protons are accelerated in the cyclotron to obtain sufficient energy to bombard the oxygen-18 enriched water[22].

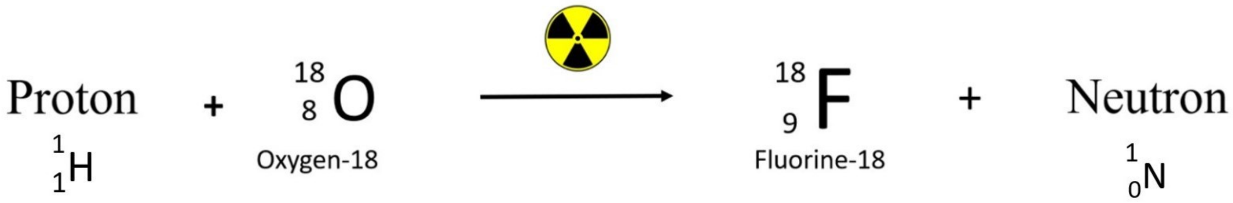

Figure 3. Production of Fluorine-18.

The mechanism of PET imaging begins when radionuclides (^{18}F) undergo beta decay to produce positrons (Figure 4A)[26]. The newly formed positrons collide with the negative electrons in the organism and annihilate, resulting in a pair of photons with equal energy in opposite directions[26]. By making use of the ring detector of the PET scanner (radiation detector), the time and location of the annihilation events can be inferred from the simultaneous detection of the produced photons[27]. The detectors in the PET scanner measure these photons and use this information to create a three-dimensional image of the distribution of radiotracer in the body (Figure 4B)[26].

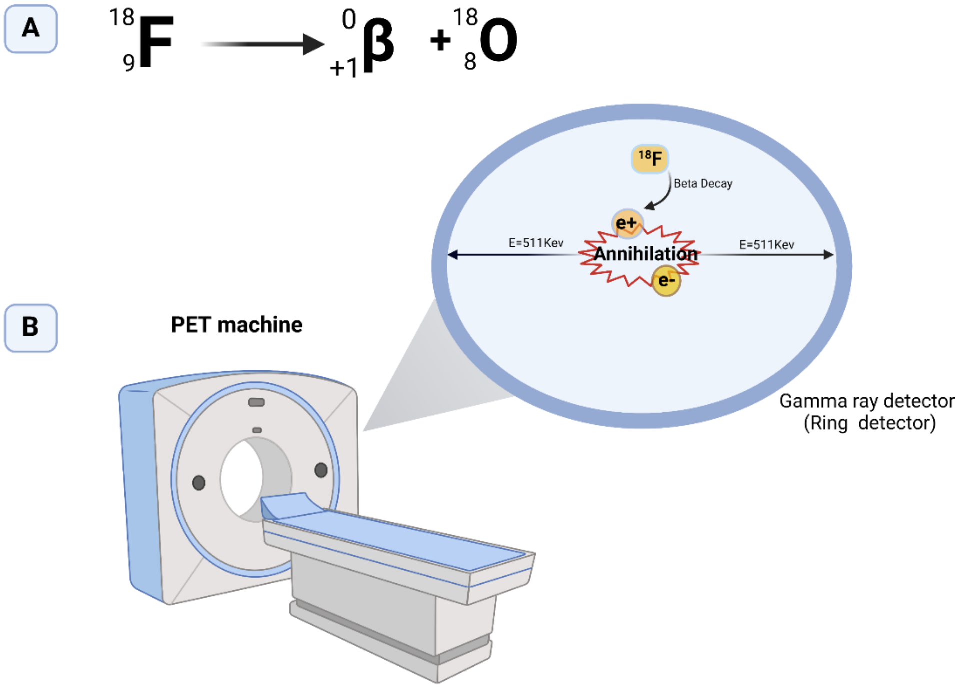
A
$^{18}_{9}F \longrightarrow ^{0}_{+1}\beta + ^{18}_{8}O$
B
PET machine
18F
Beta Decay
e+
E=511Kev
Annihilation
E=511Kev
e-
Gamma ray detector
(Ring detector)

Figure 4A. ^{18}F decay via positron Emission to ^{18}O **4B.**The annihilation event following positron decay generates two 511keV photons which travel antiparallel. These photons are detected by the PET scanner in coincidence, leading to multiple line of response forming a 3D image to localized radiotracers in vivo.

As a result, PET imaging allows for the diagnosis, staging, treatment planning, and response assessment of human diseases at different stages[28]. Currently, the most common radiotracer used in PET is ^{18}F-Fluorodeoxyglucose (FDG) (Figure 5). [^{18}F]FDG, a glucose analogue with ^{18}F substituted at carbon-2 position in glucose.[29]

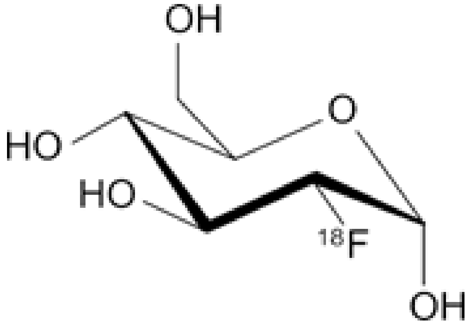

Figure 5. Structure of [^{18}F]FDG.

Since the development of [^{18}F]FDG in 1976, FDG-PET has gradually become the main clinical tool for detecting malignant cancer cells[21]. A key utility of FDG-PET is that it can be used to guide targeted biopsies at the high intensity sites of metabolic activity[21]. It assists in cancer diagnosis staging and subsequent cancer therapy[30]. The biological basis for [^{18}F]FDG in cancer is called the Warburg effect[31]. This effect is a form of cellular metabolism found in cancer cells that favours aerobic glycolysis rather than the aerobic respiration route favored by most cells in the body[29]. Malignant cancer cells take advantage of this effect to increase the rate of cell division and promote cell proliferation[32]. As aerobic glycolysis produces energy less efficiently than aerobic respiration, cancer cells typically need to metabolize more glucose to produce the same level of energy[33]. Given [^{18}F]FDG is a glucose analogue, the high consumption of glucose leads to the accumulation of [^{18}F]FDG in cancer cells[23,29]. This allows for the use of PET scans, which produce a clear three-dimensional picture of radioactive material in the body that can be used to diagnose and evaluate cancer[23].

Although widely useful, [^{18}F]FDG has limitations[31]. For example, in breast cancer, one of the problems is specificity[31]. High uptake of FDG may be related to tumors or it may be the result of inflammatory conditions[31]. FDG can also be accumulated by fatty tissue instead of mammary cancers, causing a high false positive rate[20,34]. These false positives reduce the specificity for the staging of breast cancer[34]. FDG is also not a reliable tool for detecting patients with infectious lung disease, because the high FDG uptake could be due to tuberculosis or sarcoidosis and not cancers[20,34]. Therefore, to improve the clinical use of radiotracers, there is an urgent need for diagnostic and therapeutic tools that possess greater accuracy.

1.4 Protease-Activated Receptors

A successful PET imaging agents is a validated radiopharmaceuticals that targets a relevant receptor. Cells respond to the environment through a complex series of interdependent signal transduction pathways[35]. The largest family of cell surface proteins involved in signal transduction is the G protein-coupled receptor (GPCRs) family[35]. GPCRs mediate a variety of biological processes, and their functioning is related to a variety of pathological conditions, making them an important target for modern drugs[36]. As of 2017, according to the list of approved drugs the by U.S. Food and Drug Administration (FDA), 108 out of 475 (35 per cent) drugs are targeting GPCRs[37].

GPCRs pass through the membrane seven times with alpha-helical segments between intracellular and extracellular loop regions (Figure 6A)[38]. As the name implies, GPCRs interact with G-proteins, by binding to guanosine triphosphate (GTP) and guanosine diphosphate (GDP)[38,39]. There are two families of G-proteins described, the family of G-proteins associated with GPCRs is heterotrimeric, meaning they have three different subunits: α-, the β- and γ-subunit[35]. While the α- and γ-subunit are attached to the cell membrane by lipid anchors, the β- subunit stays connected with the γ-subunit to form a complex called a heterodimer[40]. The α-subunit of the G protein is bound in its resting-state to GDP; the receptor is sitting and waiting in this condition. On the extracellular side of the cell membrane, a ligand, binds, and activates a GPCR causing a conformational change within the cell[39]. This change allows the α-subunit to bind with GTP and release GDP. This replacement allows the α-subunit to separate from the complex of β- and γ- subunits,[39,40] resulting in an activated α-subunit and an activated β- and γ- subunits dimer[40]. The activated α-subunit then regulates a membrane-bound protein which can catalyze a reaction that produces a second messenger, acting as an amplifier to the first signal from the ligand[41]. Furthermore, the ligand-induced conformational change can cause intracellular phosphorylation of GPCR. And this phosphorylated receptor binds with high affinity to β-arrestin-1 and 2, inducing the internalization and desensitization of the GPCR[39,41,42].

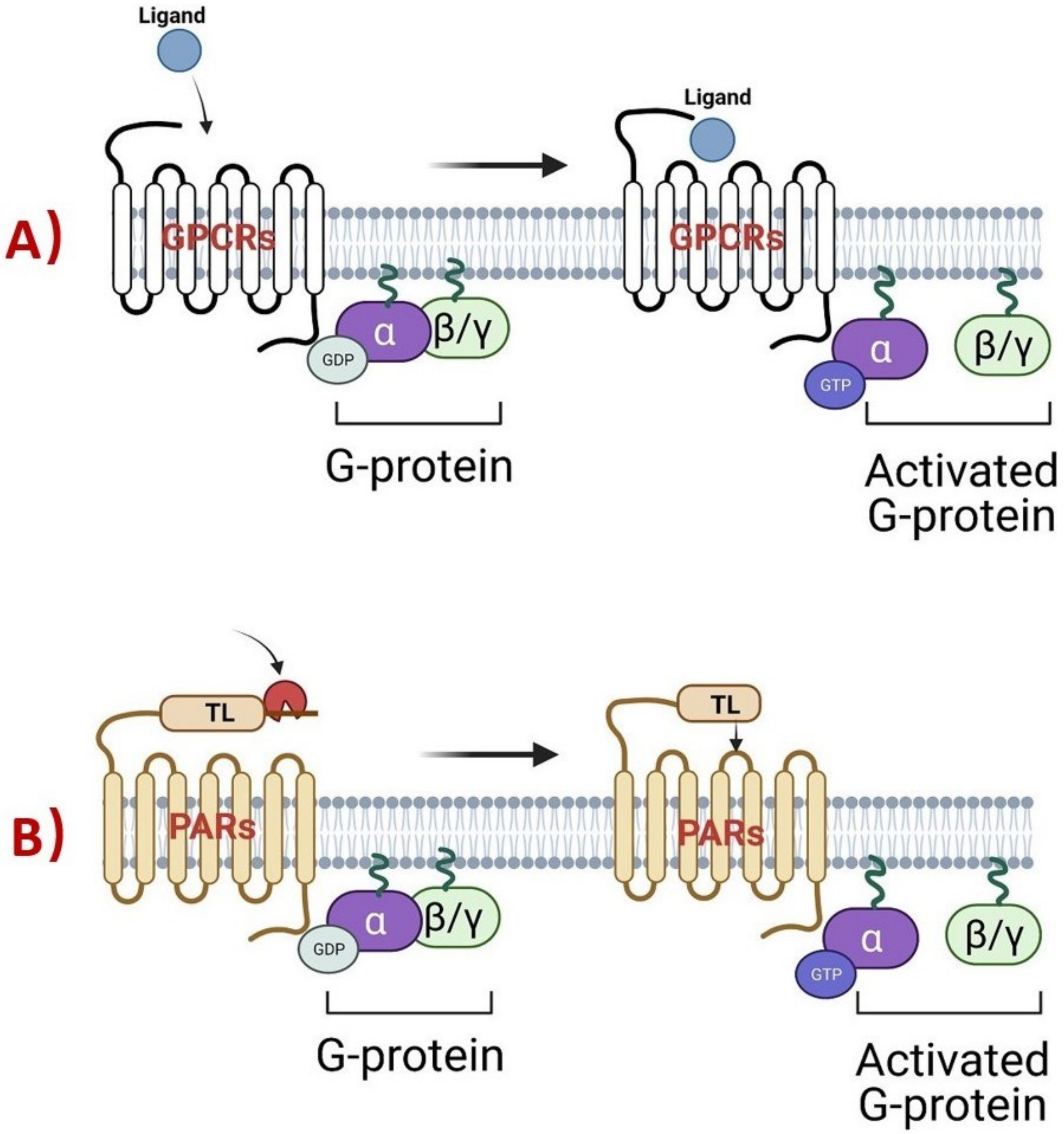
Ligand
A)
GPCRs
α
β/γ
GDP
G-protein
Ligand
GPCRs
α
β/γ
GTP
Activated G-protein
B)
TL
PARs
α
β/γ
GDP
G-protein
TL
PARs
α
β/γ
GTP
Activated G-protein

Figure 6. GPCRs and PARs activation comparison. TL = tethered ligand.

Since protease-activated receptors (PARs) belong to the cell membrane GPCRs superfamily, the pathways of activation are like to those of other GPCRs. A unique feature of these receptors is the method of ligand binding (Figure 6B)[39,43]. PARs are activated by proteases, and among these, mainly serine protease. In the inactive state, PARs have an amino terminus (N-terminal) that ‘wraps’ the ligand. In the active state, this ligand can be revealed after a specific protease cleaves the N-terminal portion, generating a newly formed N-terminal known as a tethered ligand. The ligand can then interact with the activation domain on the receptor to initiate receptor activation[43,44]. PARs have important functional roles in angiogenesis, inflammation, and cancer, making these important drug targets. Although GPCRs have proven to be the most successful class of drug targets, the unique method of receptor activation presents a distinctive challenge to the development of receptor-specific antagonists targeting PARs[45]. Currently, the only clinical agent targeting PARs is called Vorapaxar[44]. It is a selective small-molecule PAR1 antagonist. Functionally, vorapaxar inhibits the aggregation of human platelets induced by thrombin. Vorapaxar lowers the risk of heart attacks by reducing occlusive thrombus formation[45,46]. As an antagonist, vorapaxar binds to PAR1 preventing receptor activation. Once bound, platelets are no longer activated and inhibit the amplification process that leads to an occlusive thrombus, thereby lowering the risk of occlusive thrombus or heart attack[45,47].

1.5 Protease-Activated Receptor 2

There are four PARs encoded in the mammalian genome specified by IUPHAR[48]. (International Union of Basic and Clinical Pharmacology) as PAR1, PAR2 PAR3, PAR 4[45]. Since human PAR1 was discovered in 1991, significant advances have been made in the study of the *in vivo* function of the PAR family, including receptor signaling characteristics in different cellular environments and regulation of receptor signaling and function[43,45]. PARs are activated by a serine protease, the pathways of activation of PAR members are similar, except the thrombin-like proteases act on PAR1, PAR3, and PAR4, and trypsin-like proteases act on PAR2 (Figure 7)[43]. For PAR2, activating proteases, such as trypsin or tryptase, can recognize a substrate sequence (SLIGKV-human, SLIGRL-rat) on the N-terminus located in the extracellular domain[43,48]. Upon proteolytic cleavage, a new N-terminus sequence (SLIGKV-humanL) is revealed as a tethered ligand that binds to the extracellular loop 2 (ECL2) and initiates the activated state of the PAR2[49]. The unique activation of PAR2 makes it a favorable drug target.

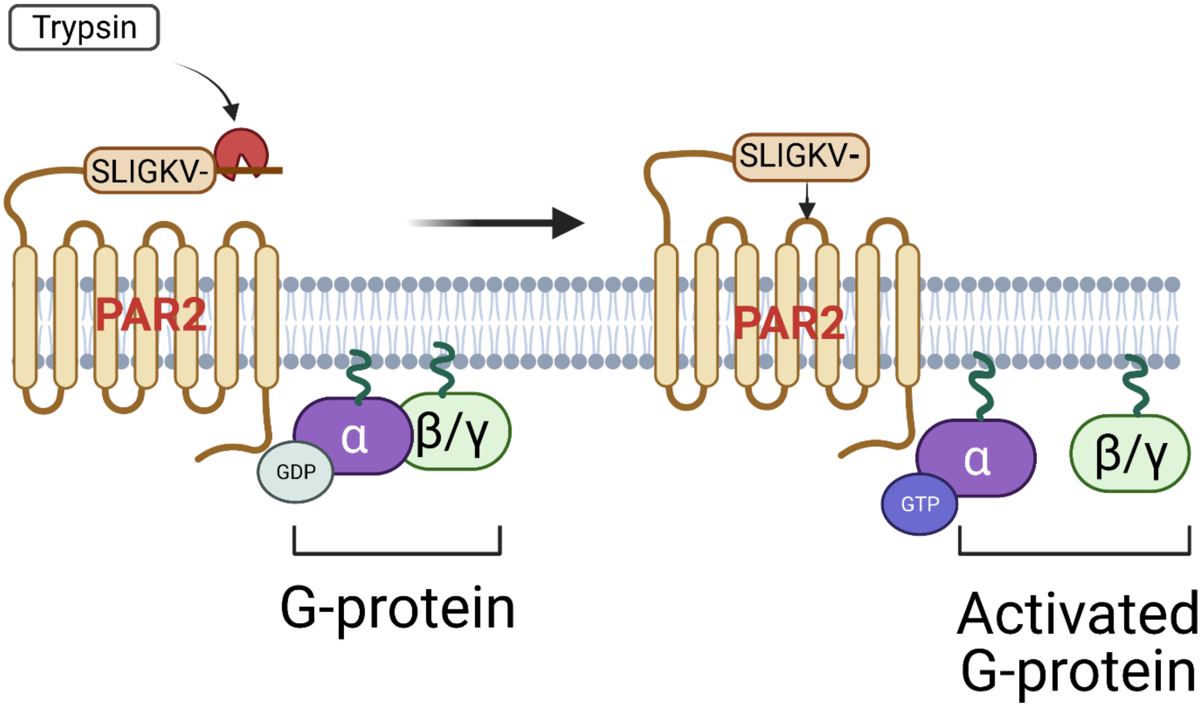

Figure 7. Activation of PAR2.

PAR2 is widely expressed in many cell types, including, but not limited to, endothelial and smooth muscle cells in the cardiovascular, immune, and central nervous systems[50,51]. Physiologically, PAR2 is mainly involved in inflammation, cell migration, and the functioning of tissue metabolism[52]. Abnormal functions of PAR2, have been linked to various cancers[45,49]. In cancer cells such as those found in breast and prostate cancer, PAR2 has been shown to significantly promote proliferation and metastasis[50,51]. As well, there is a 16-fold increase in abnormal expression level of PAR2 in lung cancer, with other cancers also demonstrating an elevated expression level of PAR2[2]. It is important to note that the expression level of PAR2 is positively correlated with cancer staging and progression[2]. Therefore, blocking PAR2 activity is proposed to provide excellent benefits for the treatment of certain diseases[50]. The physiological functions of PAR2 activation have been widely studied by using PAR2 knockout models (Table 1), indicating that inhibiting the function of PAR2 could have potential diagnostic and therapeutic applications for these human diseases[43,53].

Table 1. Summary of PAR2 related disease models and effect of PAR2 knockout (KO).

Mouse disease model	**Physiological effect of PAR2 KO**
Cancer nociception	Inhibited Cancer-induced allodynia
Bone cancer-induced hyperalgesia	Reduced mechanical allodynia and thermal hyperalgesia
Mammary tumour	Delayed development and metastasis of tumour
Prostate cancer	attenuate to tumor cell migration and metastasis
Lung cancer	Contribute to attenuate cancer cell apoptosis

1.6 Known Ligand Targeting PAR2

Since the discovery of PAR2 in the 1990s, a great number of basic studies have been performed on the development of effective PAR2 selective ligands[54]. In recent years, researchers also looked other PAR2-related details, including discerning its physiological pathways, and the development of PAR2-selective ligands[55]. To date, there have been peptide, small molecule, and antibody antagonists of PAR2 reported in the literature[53]. In the last decade, there has been increasing interest in the development of PAR2 small molecule antagonists due to their generally higher stability and better pharmacokinetic properties compared with peptides, including greater membrane permeability (which can improve oral bioavailability)[56].

In designing a novel PAR2-targeting small molecule antagonist, the literature on PAR2-specific ligands in the past decade was reviewed. A few small molecule PAR2 antagonists were reported between 2010 and 2020, each with a molecular weight between 200 to 600 (Figure 8)[53,56].

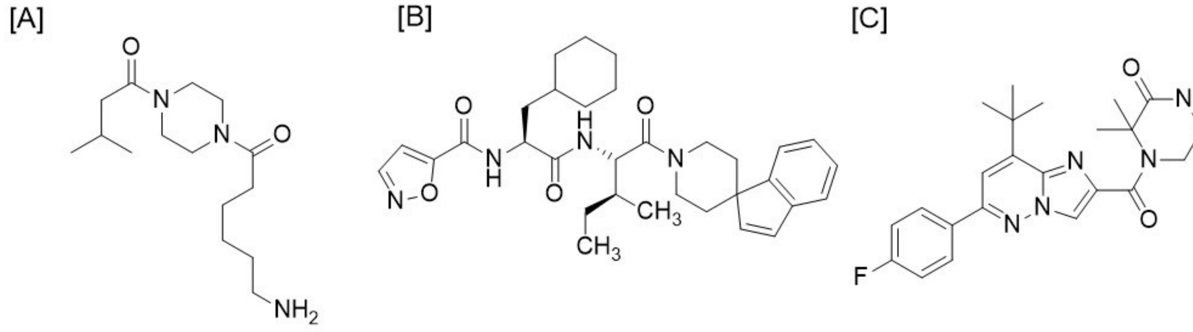

ENMD1068
IC50 of 5mM

GB88
IC50 of 2uM

I-191
IC50 of 1.1nM

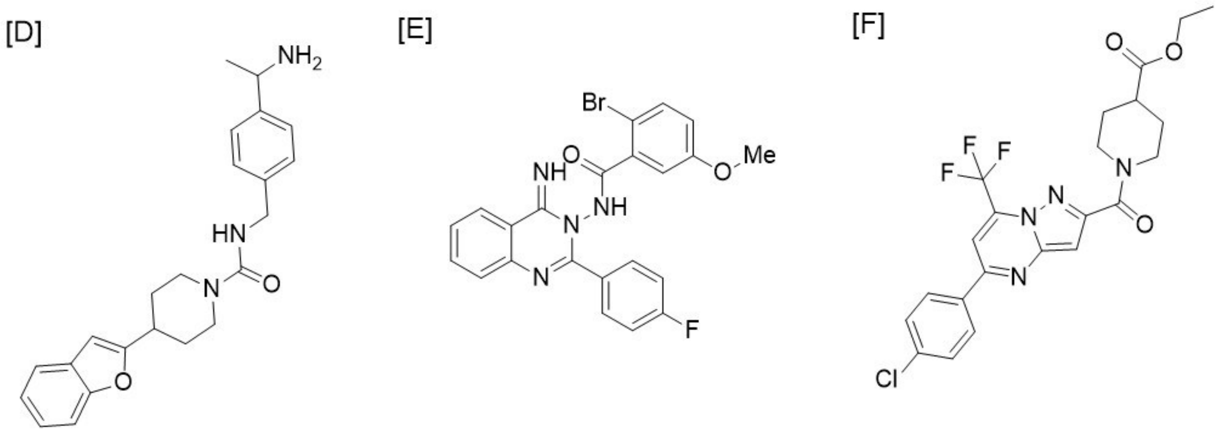

Piperidine Compound
Proximate Ltd.
IC50 <5nM

Quinazoline Compound
Neopharma Co. Ltd.
IC50 of 9nM

Imidazopyridazine Compound
Vertex Pharm
IC50 of 0.01nM

Figure 8. PAR2 antagonists reported in literature.

ENMD1068 (compound A) is a weak antagonist at millimolar concentrations[57]. Compound A targets the cleavage site of tethered ligands, which effectively inhibits receptor activation in vivo and in vitro, and has good PAR2 selectivity[57]. However, it requires a relatively high concentration, reflective of low receptor affinity[51,57]. GB88 (compound B) is a novel and potent small molecule antagonist[56]. In preventing agonist-induced intracellular calcium release, compound B was 1000-Fold more potent than compound A in human monocyte-derived macrophages[57]. As well, compound B has been shown to reduce inflammation in a rat model of colitis[57]. However, compound B only blocks certain PAR2-stimulated signaling pathways, such as inhibiting PAR2-activated Calcium ion (Ca^{2+}) mobilization with an IC_{50} of 2 μM, but does not block mitogen-activated protein kinase (MAPK) activation, which is important to the migration of cancer cell via MAPK mediated cell adhesion[58]. I-191 (compound C) is another potent PAR2 antagonist that inhibits multiple PAR2-induced signaling pathways and PAR2-mediated downstream functional responses[50]. Unlike compound B (also an agonist in stimulating other activation), compound C is a full antagonist[50]. Particularly, compound C inhibits cytokine-related caspase cleavage through extracellular signal-regulated kinase (ERK)½, and forskolin-induced cyclic adenosine monophosphate (cAMP) accumulation in human colon adenocarcinoma grade II (HT29) cells, showing valuable characteristics in dealing with cancer cells[45,50]. As calcium signalling has been shown to play an important role in the development of many diseases[13,53]. compound D, E, and F were primarily investigated for their inhibition of calcium release induced by known PAR2 agonists in a variety of cultured human cell types. Especially in malignant tumours, abnormal levels of calcium signalling are associated with cancer proliferation, metastasis, and aggressiveness[53]. Compound D and F have been shown to elicit responses in rodent models of human diseases, with possible therapeutic applications in inflammatory diseases, pain, and cancers[59,60].

In addition to antagonists, there are also several PAR2 agonists that have been studied and reported in the recent literature (Figure 9). Small molecule PAR2 agonists AC-55541 (compound G), AC-98170 (compound H) and AC-264613 (compound I) were discovered through the screening of a chemical library[61]. These agonists activate PAR2 for cell proliferation, calcium ion (Ca^{2+}) mobilization and hydrolysis of phosphatidylinositol in human HEK293 cells[54]. Particularly, compound H was reported as a full agonist in PAR2-dependent Ca^{2+} signalling, and demonstrated good stability, but modifications will need to be made to improve its solubility[62,63]. Compound I does not motivate the release of $Ca2^+$ at 1μM[62]. GB110 (compound J) is a peptidomimetic agonist, and was reported as a potent and selective PAR2 agonist; compound B was derived from this agonist[63]. Unlike compound G-I, the use of compound J has been evaluated in different disease models in small animals. For example, in a study, compound J induced inflammatory effects, causing joint swelling and synovial hyperemia in WT mice[64].

[G]

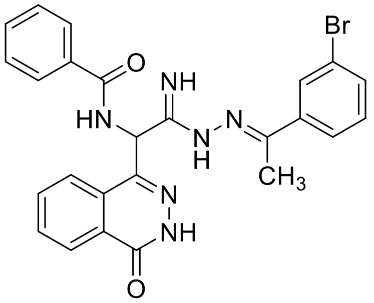

AC-55541

EC_{50} of 0.2um

[H]

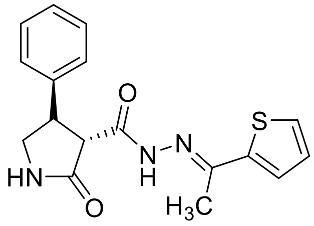

AC-98170

EC_{50} of 0.4um

[I]

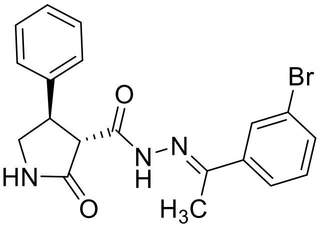

AC-264613

EC_{50} of 0.3um

[J]

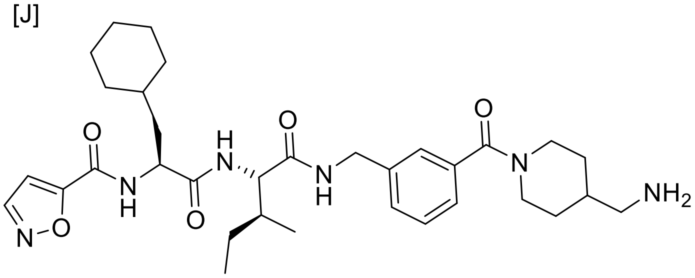

GB 110

EC_{50} of 0.28um

Figure 9. Structure of PAR2 agonists.

1.7 Labeling Strategy

Fluorine (F), due to its unique physical and chemical properties can serve as a bio-isostere of hydrogen, carbonyl, sulfonyl, and cyanide groups[65]. In drug design, fluorine is usually introduced into small molecules to block sites prone to oxidative metabolism, thus improving the metabolic stability of compounds and prolonging the action time of drugs in vivo[66]. The substitution of fluorine helps improve the lipophilicity of compounds, promote membrane penetration, reduces the production of active metabolites, avoids the inhibition of metabolic enzymes, and improves their potency and bioavailability[65,67]. Fluorine 18 (^{18}F) is a fluorine radioisotope that is significant due to its half-life ($t_{1/2}$ =109.8 minutes) and positron-emitting properties (branching ratio-97% β^{+} decay, positron range, max positron energy-635keV)[19], along with high specific activity and ease of large scale production[22]. ^{18}F allows direct or indirect introduction into an interesting molecule by nucleophilic or electrophilic substitutions reactions[22]. Based on all the reasons, ^{18}F become a favourable tracer used in PET radiopharmaceuticals in both clinical and preclinical reasrach[12,66]. A site-specific and one-step radiolabelling method that introduces [^{18}F] into molecules has been discovered, called Spirocyclic Iodonium Ylide (SCIDY) technology (Figure 10)[68].

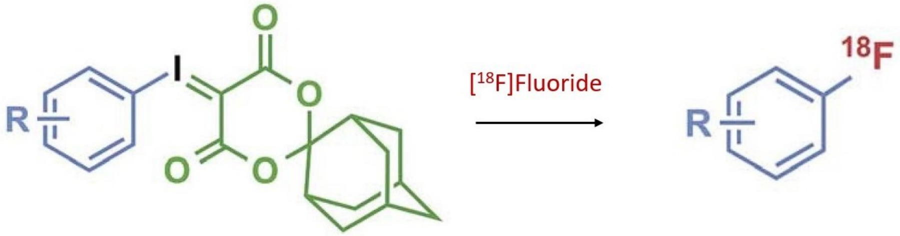

Figure 10. Direct radio-Fluorination of aromatic ring.

SCIDY technology was discovered in 2014, and it has several advantages, including not requiring a catalyst metal, single-step labelling, and broad compatibility functional group[68–70]. Therefore, this technology will be used for the proposed radiolabelling in this thesis.

1.8 Purpose of Thesis

The work of this thesis focuses on the development and evaluation of a novel PAR2 antagonist as a potential PET imaging agent for cancer. More specifically, my objective was to prepare a small array of PAR2 antagonist based upon a lead compound, AZ3451. A library of the first generation of AZ3451 derivatives has been designed and synthesized. Derivatives will be fully characterized by mass spectrometry, ^{1}H-NMR. All compounds have greater than 95% purity as confirmed by HPLC. Collaborator Dr. Rithwik Ramachandran at Western University (UWO) will perform functional assays to evaluate all compounds for the therapeutic potential. Long-term objective will involve radioligand binding assay for candidate compound, and the candidate will be selected for radiolabelling. The proposed strategy for radiolabelling with fluorine-18 will be explored. Finally, lead imaging agent will then be evaluated *in vitro* and *in vivo* studies using small animal models of cancer.

Chapter Two

Design and synthesis of small molecule ligands targeting PAR2 as potential diagnostic and therapeutic agents.

2.1 Introduction

Currently, [^{18}F]FDG is the primary PET agent used for diagnosis and staging of cancer. However, [^{18}F]FDG is not always the best option for certain cancers as specificity is not always high enough[71]. Protease-activated receptors 2 (PAR2) is naturally expressed in many tissues, and the activation of PAR2 is implicated in a wide range of diseases[45]. In cancer cells, the abnormal function of PAR2 has been reported to be associated with cell metastasis, migration, and proliferation[52,54]. To date, no studies about radioligands targeting PAR2 have been published aside from another MSc thesis from Western University. Therefore, this thesis is focused on the design and synthesis of small molecule ligands targeting PAR2 for the purpose of the discovery of potential diagnostic imaging and therapeutic agents for cancers.

Most of the PAR2 antagonists reported are either weak antagonists (ENMD1068), partial antagonists (GB88), or have poor selectivity for PAR2 (Compound F)[50]. AZ3451 was reported by Cheng *et al.* as a novel, potent, and selective PAR2 antagonist (Figure 11)[44]. The mechanism of antagonism by AZ3451 is not fully explored; the most plausible mechanism is that this ligand restricts the conformational rearrangement of helical bundle upon PAR2 activation[44].

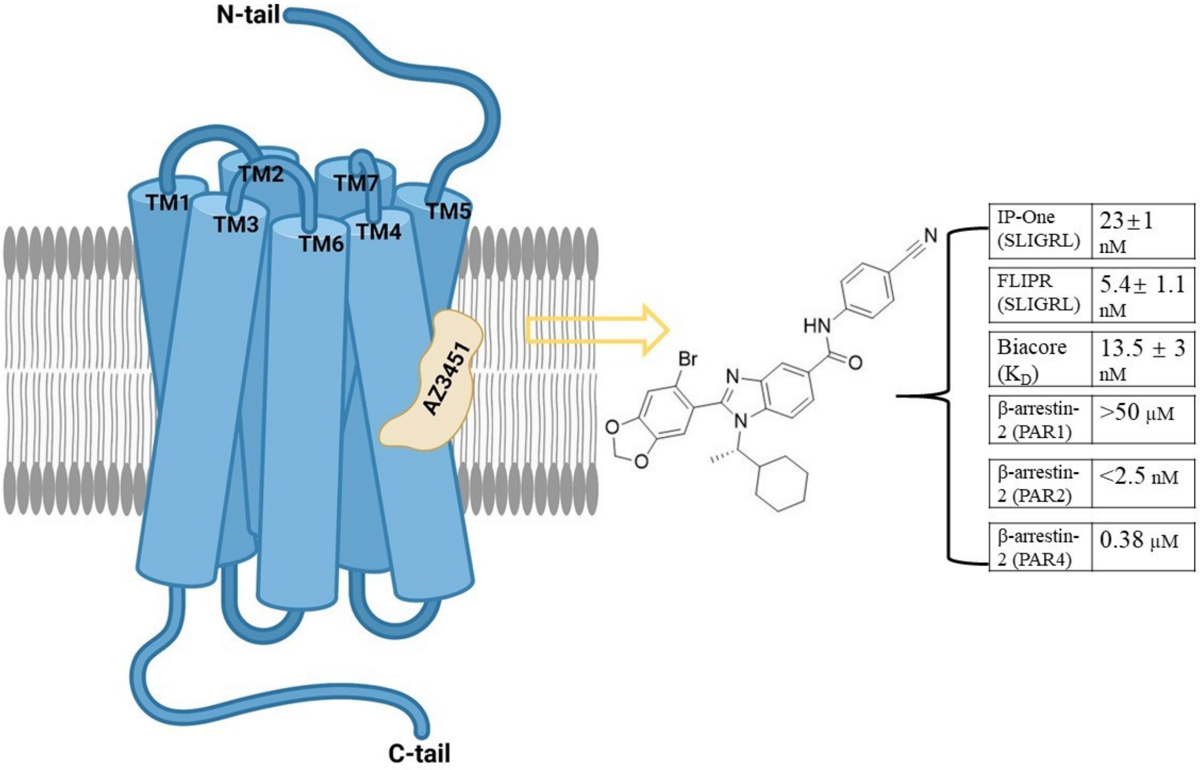

IP-One (SLIGRL)	23±1 nM
FLIPR (SLIGRL)	5.4± 1.1 nM
Biacore (K_D)	13.5 ± 3 nM
β-arrestin-2 (PAR1)	>50 μM
β-arrestin-2 (PAR2)	<2.5 nM
β-arrestin-2 (PAR4)	0.38 μM

Figure 11. Interplay of antagonist AZ3451 (orange) with PAR2, and pharmacology and binding affinity of AZ3451.

Crystallographic studies indicate that AZ3451 binds to an allosteric site outside the helical bundle of PAR2[44,72]. From the perspective of innovative drug research and development, targeting protein allosteric sites offers an extremely attractive prospect for the emergence of novel drug targets[73]. Allosteric sites tend to have fewer side effects as residues of the allosteric binding sites tend to be less conserved among receptor subtypes, thus offer significantly better subtype selectivity[72,74]. Allosteric sites, however, can be more prone to drug resistance due to mutations at the allosteric sites[37,41].

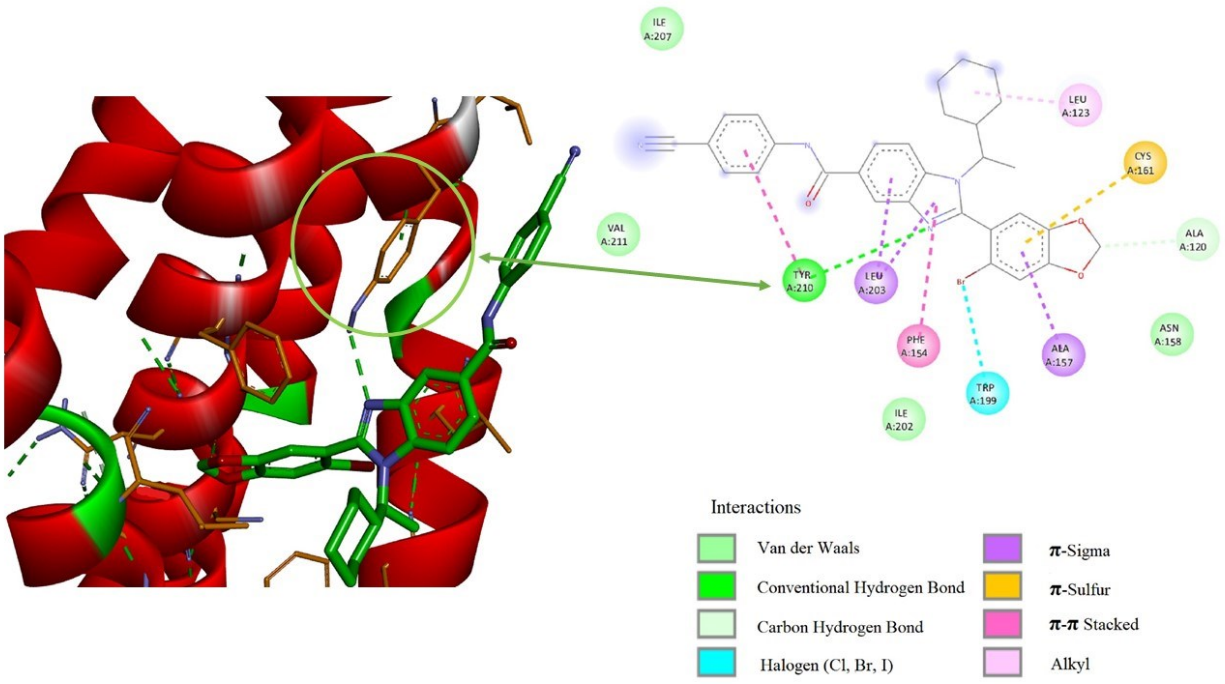
ILE A:207
LEU A:123
CYS A:161
VAL A:211
ALA A:120
TYR A:210
LEU A:203
ASN A:158
PHE A:154
ALA A:157
TRP A:199
ILE A:202
Br
Interactions
Van der Waals
Conventional Hydrogen Bond
Carbon Hydrogen Bond
Halogen (Cl, Br, I)
π-Sigma
π-Sulfur
π-π Stacked
Alkyl

Figure 12. AZ3451 - PAR2 interactions in three-D and two-D diagram. AZ3451 interactions with different functional group within the binding pocket in PAR2.

The pharmacology of AZ3451 can be better understood examining its allosteric binding interactions (Figure 12). There were hydrophobic interactions found between the 1,3-benzodioxole moiety and residues Ala120, Leu123, Phe154, Ala157, Cys161, Trp199, and Ile202[44]. These interactions help AZ3451 fit in the hydrophobic pocket[44]. Importantly, the aromatic ring of the benzonitrile moiety interacts with Try210 through π-stacking interactions, greatly contributing to the stability of AZ3451 within the allosteric binding pocket[44]. Other important interactions are the hydrogen bonding interaction (3.4 Å) between Tyr210 and the benzimidazole nitrogen and another hydrophobic interaction between the cyclohexyl group and residue Leu123[44]. AZ3451 has excellent selectivity for PAR2 over the other three PAR members. For example, the residues of PAR2 that form interactions with the 1,3-benzodioxole moiety are Ala120, Leu123, Phe154, Ala157, (Gly157 in wild type), Cys161, Trp199, and Ile202, while the residue Cys184 in PAR1, instead of Gly157 in PAR2, induces steric repulsion to the 1,3-benzodioxole moiety[44]. Furthermore, there is a weak hydrogen bonding interaction between residue Tyr210 and N_1 of the benzimidazole moiety for PAR2. However, residue Tyr210 is not conserved in PAR1(Leu238), PAR3(Phe229), and PAR4 (Thr212)[44].

Moreover, the pharmacology and binding data (Figure 11) showed that AZ3451 has high potency (23 ± 1 nM) and is highly selective for PAR2 from various assays reported by Cheng *et al.*[44]. The IP-One assay was performed to measure the production of inositol 1,4,5-triphosphate (IP3), which signals the activation of Gq-protein upon ligand binding[44,75]. SLIGRL is a receptor-activating peptide that mimics the substrate sequence (SLIGKV) of the tethered ligand of PAR2[76]. After the peptide agonist (SLIGRL) activates the receptor, mobilization of calcium ions was measured using the Fluorescent Imaging Plate Reader (FLIPR) technique[77]. AZ3451 showed great inhibition in both two assays. K_D, the equilibrium dissociation constant, represents the strength of the interaction between a ligand and its receptor[40]. AZ3451 also exhibited high binding affinity (13.5 ± 3 nM) and selectivity for PAR2 (2.5 nM) in β-arrestin-2 assays[78]. Based on all the properties of AZ3451, it was chosen as the starting point of our medicinal chemistry effort toward the design and the synthesis of new antagonists for PAR2.

2.2 Ligand Design.

In drug design, a structural moiety of a starting compound is replaced by other groups with the goal to improve the properties of the molecule (e.g., binding affinity, functional activity, ADMET, etc.)[79]. The crystal structure of the AZ3451-PAR2 complex shows that the aromatic ring of the benzonitrile moiety interacts with Try210 through π-π stacking interactions. However, this benzonitrile is solvent exposed and can be readily modified through amide bind coupling in the last step. Therefore, the benzonitrile group can be seen as an access point to introduce new functional groups with variable properties. For example, replacement by larger aromatic rings may enhance π-π stacking interactions with Tyr210, heterocycle replacement may improve the lipophilicity of the molecule, and the addition of fluorine may boost the binding affinity and provide fluorine-bearing cold compounds for PET imaging agent development[80]. Our first round of structural optimization will focus on the R group as shown in Figure 13.

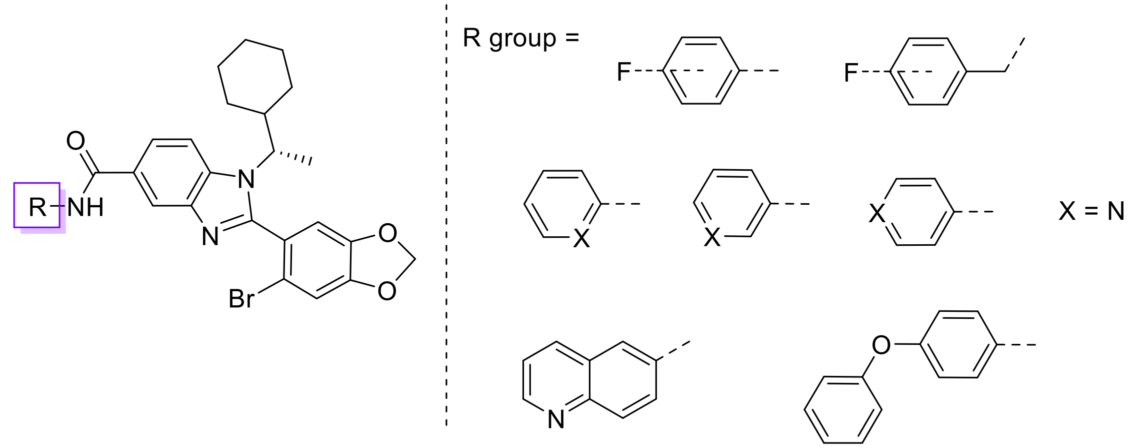

Figure 13. Ligand design of AZ3451 analogues with R group.

Fluorine (F) is an important element in medicinal chemistry[81]. Fluorination introduces fluorine atoms into a compound to increase lipophilicity, which favours hydrophobic binding sites within the membrane[82]. In the view of pharmacology, since the carbon-fluorine bond is stable, fluorine substituents protect the aromatic ring, fluorinated compounds can delay metabolism of the drugs in the body[67]. Therefore, adding F to bioactive organic compounds can improve lipophilicity, promote membrane penetration, and increase bioavailability[67,83]. In this thesis, fluorine will be introduced with the expectation of improving the binding affinity of the compounds. For example, the fluorine atom will be introduced to the ortho, meta, and para position on the aromatic ring

(Figure 13). This will be helpful for the exploration of the structure-activity relationship (SAR) when obtaining the IC_{50} value for each compound[84]. The addition of the CH_2 group in n-fluoro-methylbenzene increases the length of the carbon chain, possibly strengthen π-π stacking interactions with Tyr210.

Heterocyclic compounds can participate in a variety of molecular interactions, including acting as hydrogen bond donors or acceptors and exhibiting van der Waals forces and hydrophobic interactions; these enable heterocyclic compounds to bind to the receptor in a number of ways[85]. The introduction of heterocycles to bioactive compounds can provide a useful functional group, that can be modified to optimize solubility, lipophilicity, and polarity[85,86]. In addition, heterocycles come in a variety of shapes and sizes, allowing them to match the different binding pockets of receptors[86]. Heterocyclic aromatic compounds, such as pyridine, have been introduced in this thesis. In contrast to a benzene ring, pyridine is a unique aromatic ring. As the lone pair of its nitrogen atom is not overlapped with the π-system of the aromatic ring, it contributes to the basicity of pyridine[87]. Due to this weak basicity, pyridine can be used for improving the water solubility of drugs[86,87]. The nitrogen atom of pyridine also contains three positions for substitution: ortho-, meta, and para. This can enhance the structural diversity of the compound and is useful for exploration of the SAR. Moreover, 2-nitropyridines are relatively easy to radiolabel with ^{18}F and could provide an easy PET imaging agent to develop.

Furthermore, by adding a bulky group to the ligand, like n-biphenyl and n-phenoxy phenyl, the metabolic stability of ligand may be increased. This is because the bulky groups are used as a shield, which is a known steric hindrance[88]. This effect is used to control the selectivity of ligands, potentially enhancing ligand-receptor interactions and avoiding side effects[79,88]. To sum up, a wide range of diverse building blocks have been designed and introduced to the ligand in the R position. (Shown in Chapter 2.33).

2.3 Results and Discussion

2.3.1 Organic Synthesis of AZ3451

Our first goal was to synthesize AZ3451 by using multi-step organic synthesis procedures (shown in Scheme 1).

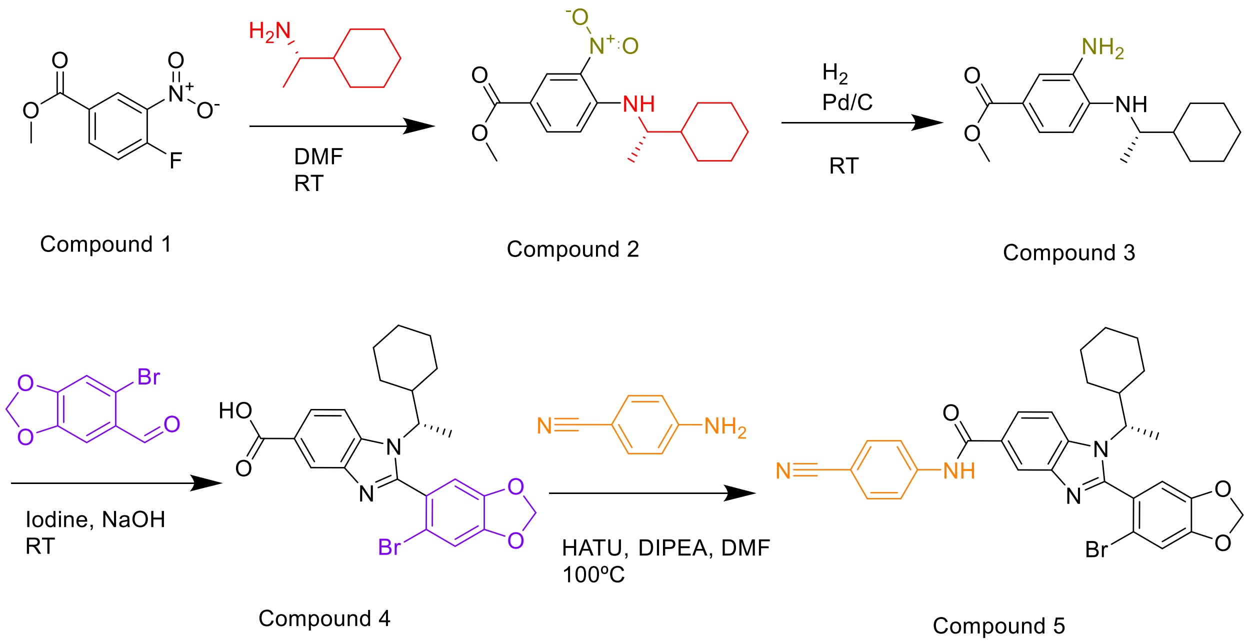

DMF
RT
H2
Pd/C
RT
Iodine, NaOH
RT
HATU, DIPEA, DMF
100ºC
Compound 1
Compound 2
Compound 3
Compound 4
Compound 5

Scheme 1. The reported synthetic scheme for AZ3451.

The synthetic procedures were based on journal article by Cheng *et al.* with some small modifications[44]; the detailed methodology can be found in **Chapter 4** (Experimental Procedure**)**. The first reaction was a nucleophilic aromatic substitution reaction. Compound 1 reacted with 1-cyclohexylethanamine in DMF to make compound 2 (^{1}H-NMR in Appendix 2). 1-

cyclohexylethanamine acted as a nucleophile to attack the aromatic ring at the position of the fluorine atom in compound 1, displacing the fluorine as a leaving group. The second step is a reduction reaction. The purified compound 2 was treated with excess hydrogen gas with a palladium on carbon catalyst to reduce the nitro group to a primary amine group giving compound 3 (^{1}H-NMR in Appendix 2). The third step was an iodine - mediated cyclization reaction and ester hydrolysis. The mechanism of the former has not been fully explored yet, but a proposal from the literature is shown in Scheme 2[89]. Condensation of a benzaldehyde forms an imine. Then iodine-mediated cyclization of the intermediate generates a plausible iodo-species[89]. Finally, the subsequent elimination of one molecule of HI promoted by a base produces the benzimidazole framework.

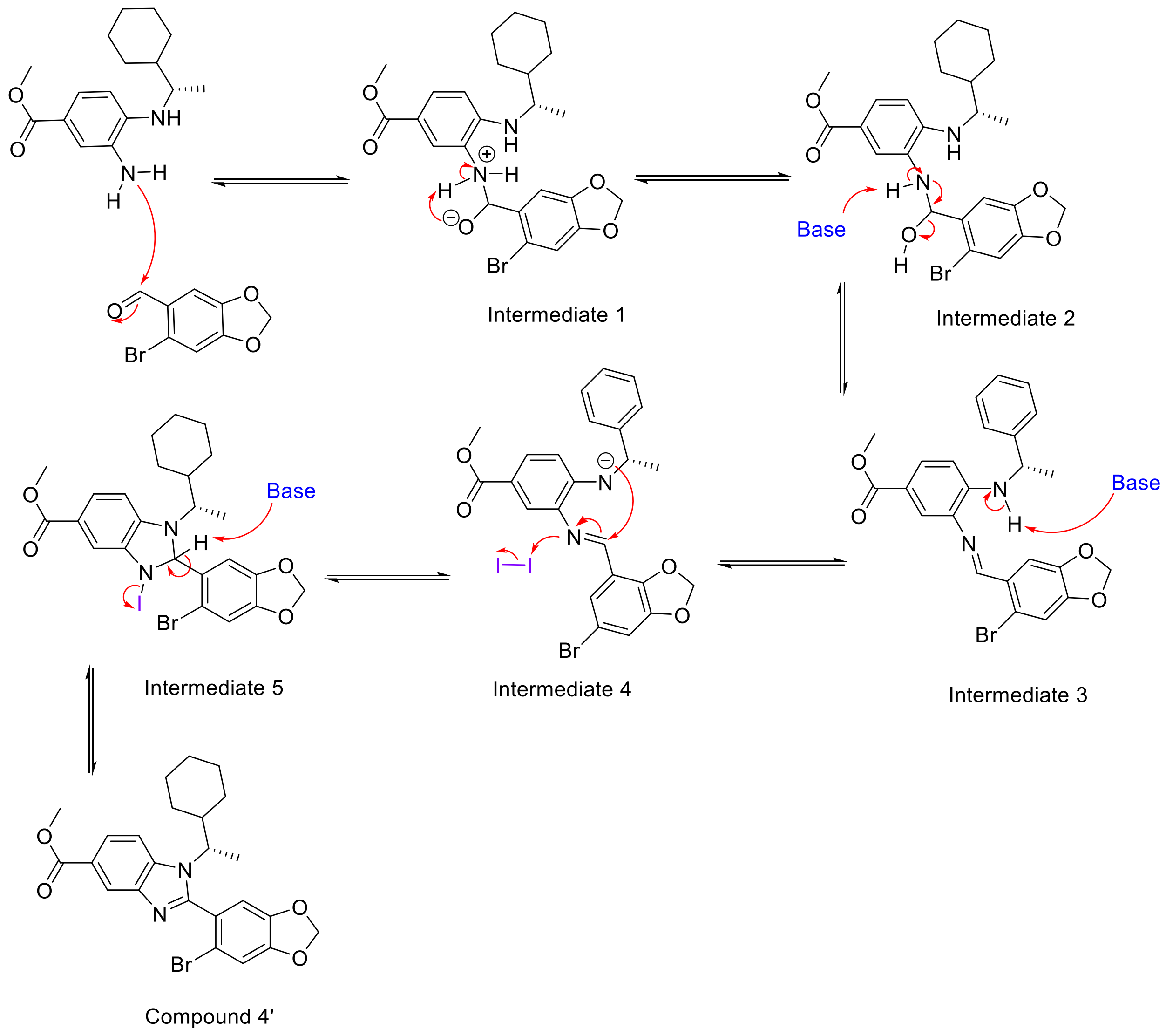
Intermediate 1
Intermediate 2
Intermediate 3
Intermediate 4
Intermediate 5
Compound 4'
Base
I—I
Br

Scheme 2. Proposed mechanism of Iodine-mediated Cyclization[89,90].

The iodine - mediated cyclization reaction proceeded quickly without any issues. However, the amount of ester hydrolysis depended on the reaction time (Figure 14 A). In the first several attempts following the reaction conditions and time from the literature, the resulting main product was compound 4’ intermediate, the ester product. One possible reason is that the ester needs a longer time to be hydrolyzed to the carboxylic acid. Extending the time from one hour to two hours gave a mixture of ester and carboxylic acid which was confirmed by thin layer chromatography (TLC), while extending the time to five hours exclusively gave only the carboxylic acid (Figure

14 B).

A)

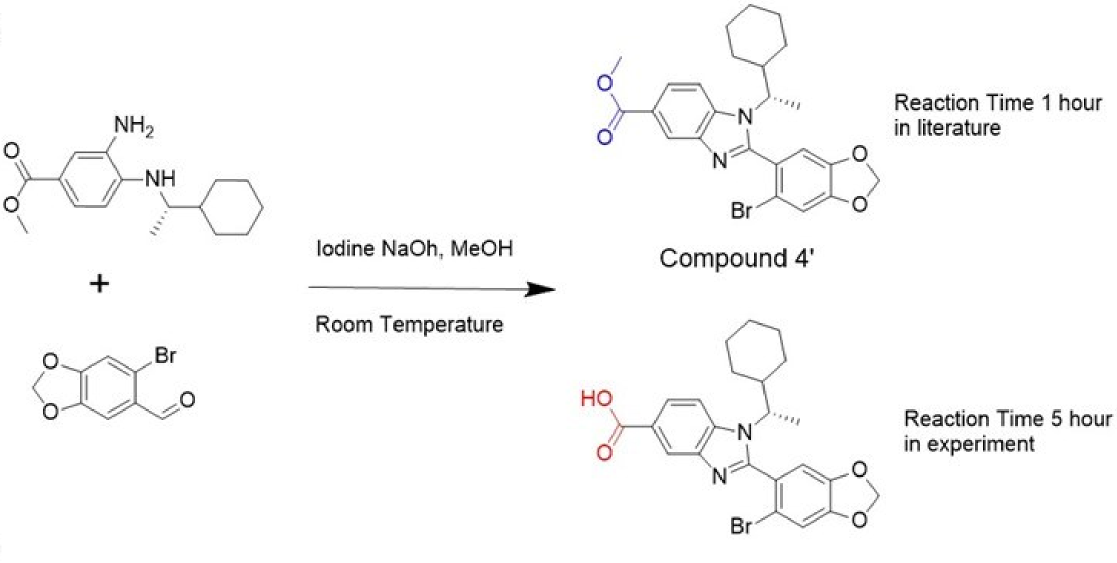

Reaction Time 1 hour in literature

Compound 4'

Reaction Time 5 hour in experiment

Compound 4

B)

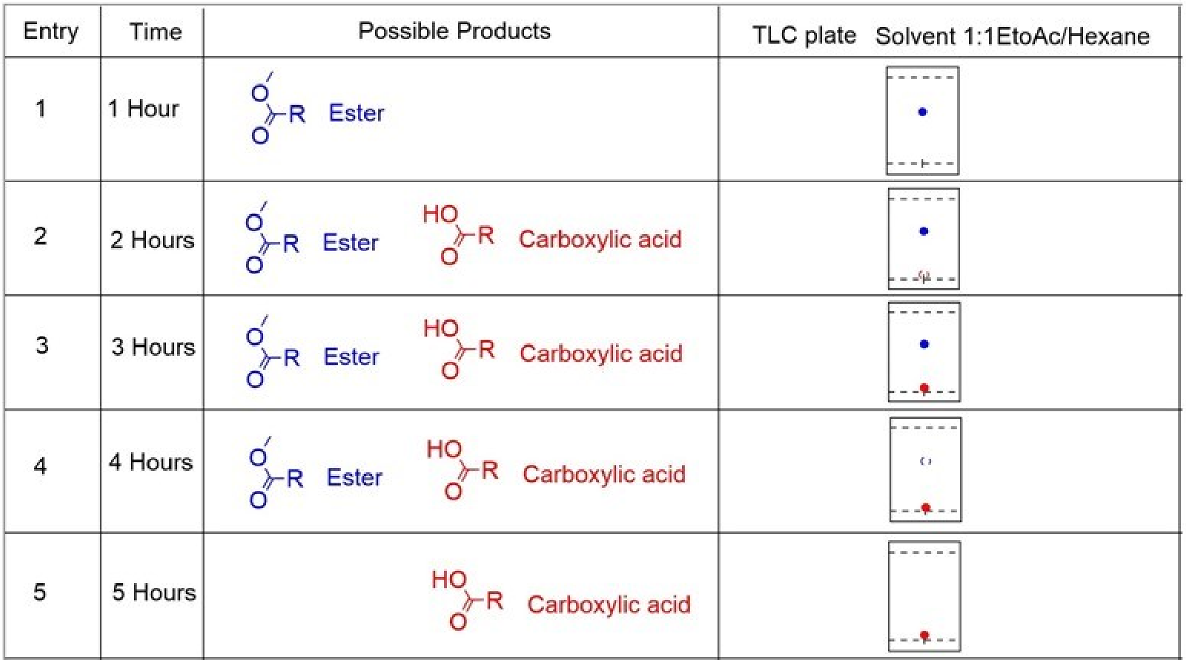

Entry	Time	Possible Products		TLC plate Solvent 1:1EtoAc/Hexane
1	1 Hour	Ester		
2	2 Hours	Ester	Carboxylic acid	
3	3 Hours	Ester	Carboxylic acid	
4	4 Hours	Ester	Carboxylic acid	
5	5 Hours		Carboxylic acid	

Figure 14. A) Scheme of the third step. B) Results of TLC of third step from 1 hour to 5 hours.

The ester and carboxylic acid products were isolated, and their structures were confirmed by proton-nuclear magnetic resonance (^{1}H-NMR) shown in Figure 15. The ester has a peak at 3.9ppm, indicating the presence of a methyl group, while there is no peak at 3.9ppm for the carboxylic acid. The high-performance liquid chromatography (HPLC), mass spectrometry (MS) and ^{1}H-NMR spectroscopy data for compound 4 can be found in **Appendix 2**.

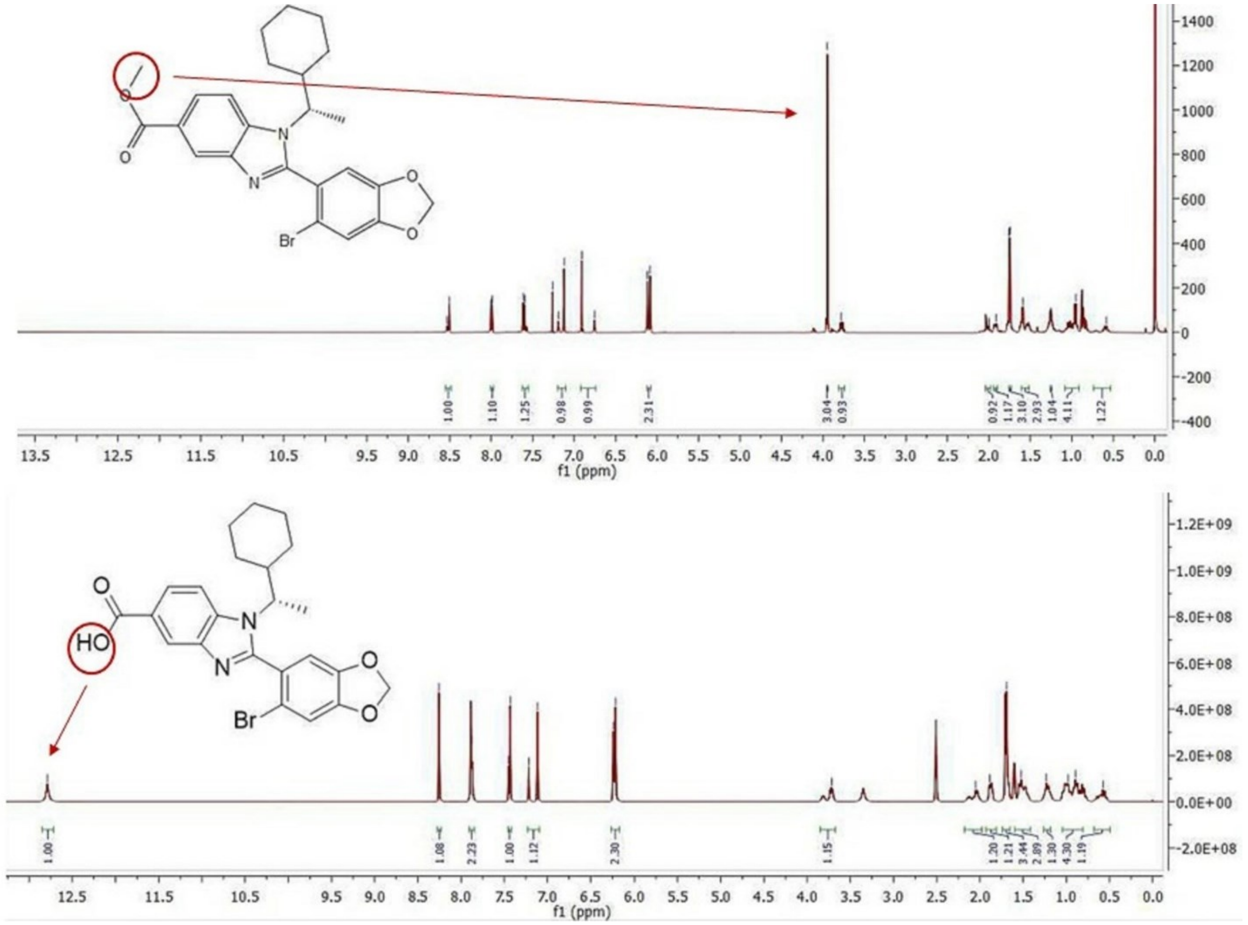

Figure 15. The spectra of ^{1}H-NMR for the reaction at the first hour (ester) and the fifth hour (carboxylic acid).

The fourth step reacted the carboxylic acid intermediate with the amino group of 4-aminobenzonitrile to generate an amide bond for the final product. In this last step, following the reaction conditions provided in the literature, did not successfully yield the desired product after several attempts. In the literature, the organic solvent used was dichloromethane (DCM) with a reaction time of more than 24 hours at room temperature. The last 3 hours were done at 80 °C under reflux. It was suspected that long reaction time and heating might affect the reactivity of 1-[Bis(dimethylamino)methylene]-1H-1,2,3-triazolo[4,5-b] pyridinium 3-oxid hexafluorophosphate (HATU). Therefore, in the improved method for the fourth step, carboxylic acid, compound 4, from the previous step was added into the flask with HATU and N, N-Diisopropylethylamine (DIPEA) and stirred for 1 hour at room temperature to activate the carboxylic acid group, making it more electrophilic. After 1 hour, the carboxylic acid was fully activated, and so 4-aminobenzonitrile was added into the reaction mixture. The solution was stirred for another 8 hours at 100 °C to get the final product. The detailed steps are presented in the **Experimental Procedure Chapter**. Based on the ^{1}H-NMR spectrum (Figure 16) and MS (**in Appendix 3**), it was confirmed that the desired product, AZ3451, was synthesized.

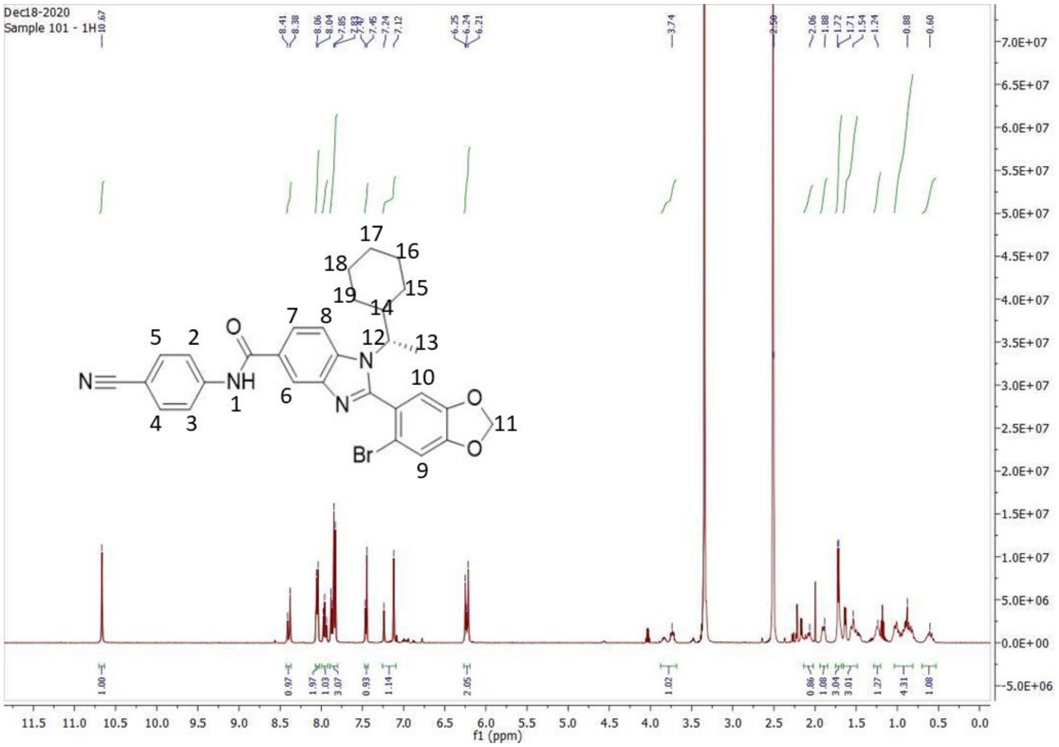

Figure 16. The spectrum of ^{1}H-NMR for AZ3451.

2.32 Conformational isomer of AZ3451

As shown in Figure 16, multiple peaks were detected at 6.21-6.25ppm. These peaks have an integration of 2 which corresponds to the CH_2 group in the 1,3-benzodioxole substituent (carbon

11 in Figure 16). However, the peak should be a singlet based on the structure. Unfortunately, the characterization of AZ3451 was not described very clearly in the literature, and hence, a molecular modelling study was done to discover a possible explanation. This showed that the carbon-carbon bond between the imidazole and aromatic ring of 1,3-benzodioxole cannot freely rotate by 180 degrees[91]. Also, steric hindrance from the methyl group (connected to the methylcyclohexane) affects the protons in the carbon atom connected to the two oxygen atoms in 1,3-benzodioxole (Figure 17).

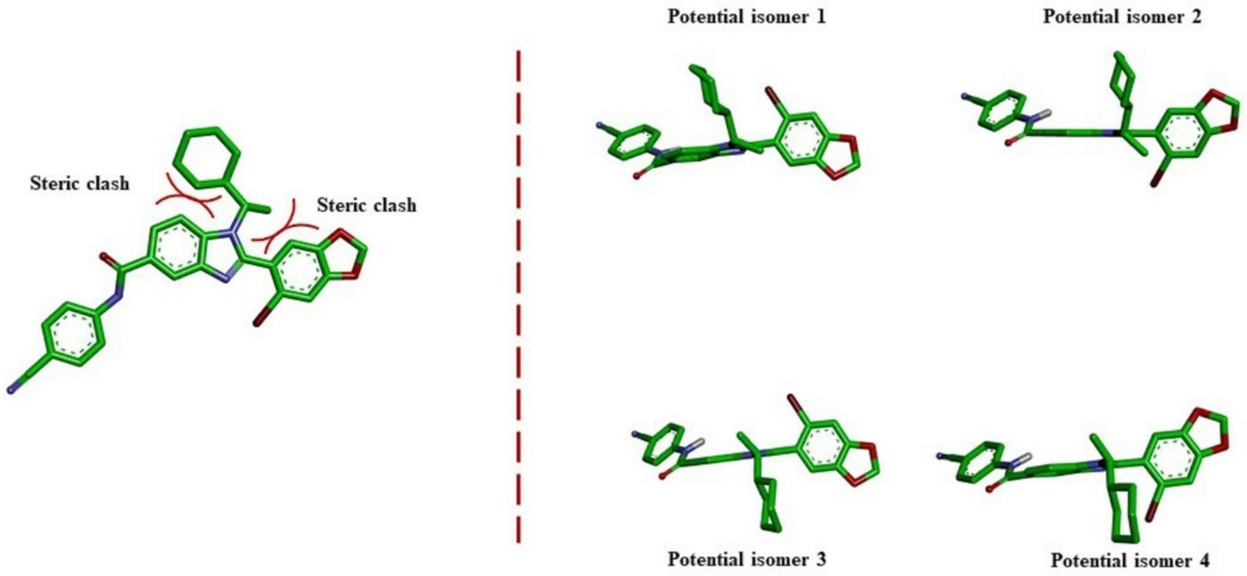

Potential isomer 1

Potential isomer 2

Potential isomer 3

Potential isomer 4

Figure 17. Structure of AZ3451 and 4 types of potential conformational isomer.

It was determined that the CH_2 group in the 1,3-benzodioxole of carboxylic acid compound 4 showed the same pattern (Figure 18). Since the building block of 1,3-benzodioxole was introduced into the compound in the cyclization step, it was suspected that conformational isomers were formed during the iodine-mediated cyclization (Scheme 2). A variable temperature NMR (VT-NMR) study was performed. The results of compound 4 and analogs 12a showed that the multiple peaks merged into one single peak at higher temperatures, indicating conformational isomerism (Figure 19 A and B).

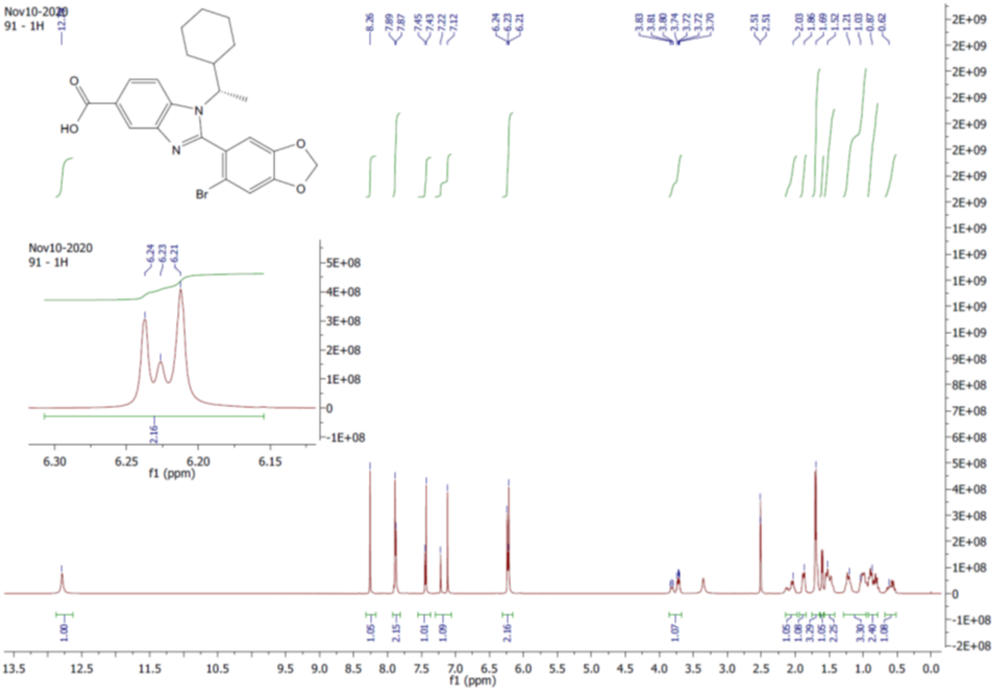

Figure 18. The spectrum of ^{1}H-NMR of carboxylic acid compound 4.

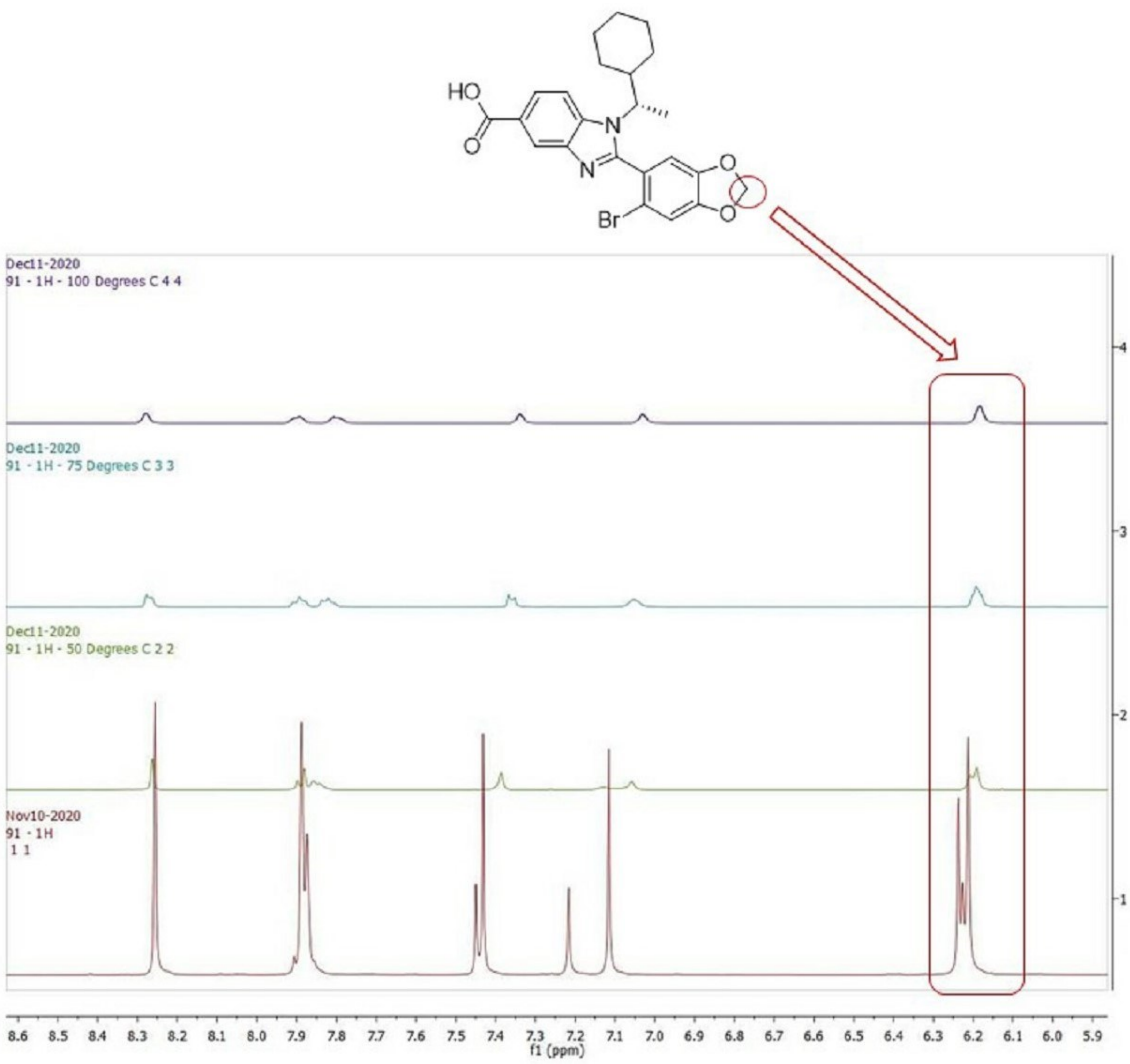

Figure 19 A)**.** The spectrum of ^{1}H-NMR for carboxylic acid compound 4 at 25°C, 50°C, 75°C and 100°C.

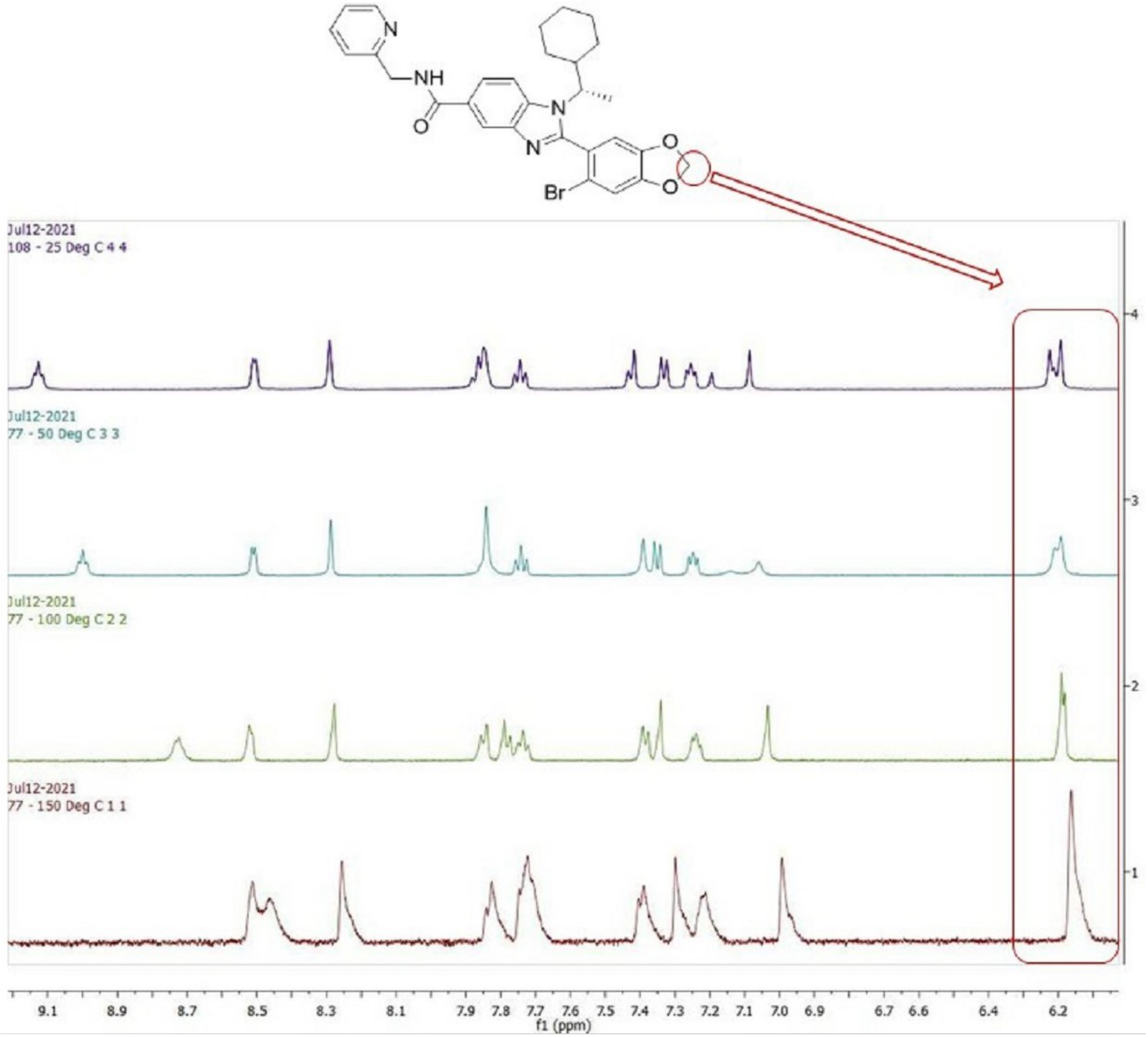

Figure 19 B) The spectrum of ^{1}H-NMR for 12a at 25°C, 50°C, 100°C and 150°C.

2.33 Organic synthesis of AZ3451 Analogues

Although AZ3451 is of particular interest due to its already high potency and selectivity, the development of AZ3451 analogues with modified functional groups could potentially yield novel ligands with enhanced binding to PAR2. As shown in Figure 12, the benzonitrile group of AZ3451 does not have strong interaction with the receptor. Therefore, the benzonitrile group can be seen as a breakthrough point that introduces an aromatic substituent, so that the analogues could form stronger interactions with the receptor. A total of 18 analogues with different substituents in the R position have been designed and synthesized (Figure 20). Their synthesis is like that of AZ3451, with detailed experimental procedures can be found in **Experimental Procedure Chapter**. The structures of these 18 analogues can be found in **Appendix A**.

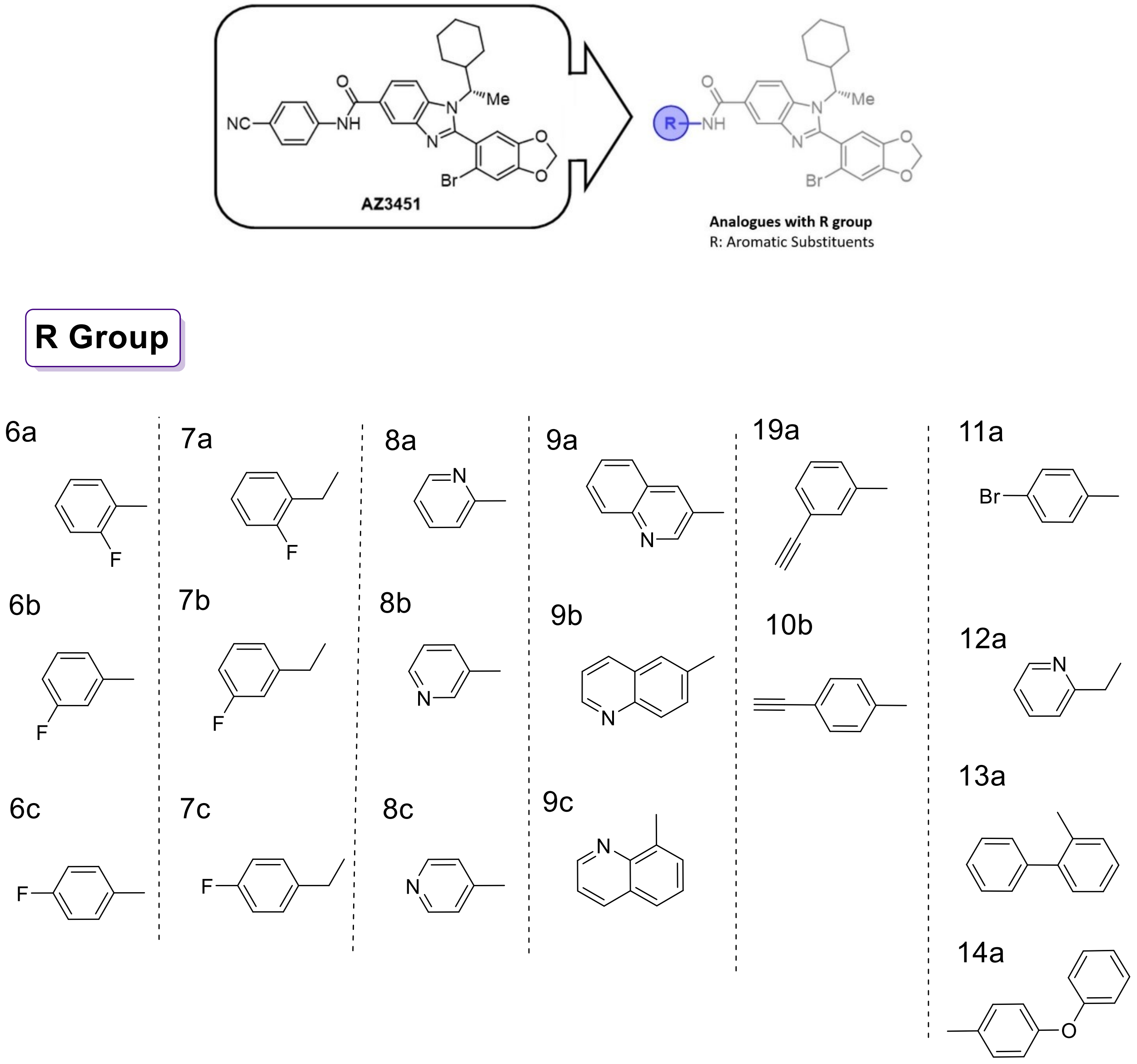
AZ3451
Analogues with R group
R: Aromatic Substituents
R Group
6a
7a
8a
9a
19a
11a
6b
7b
8b
9b
10b
12a
6c
7c
8c
9c
13a
14a

Figure 20. AZ3451 analogues with R-group.

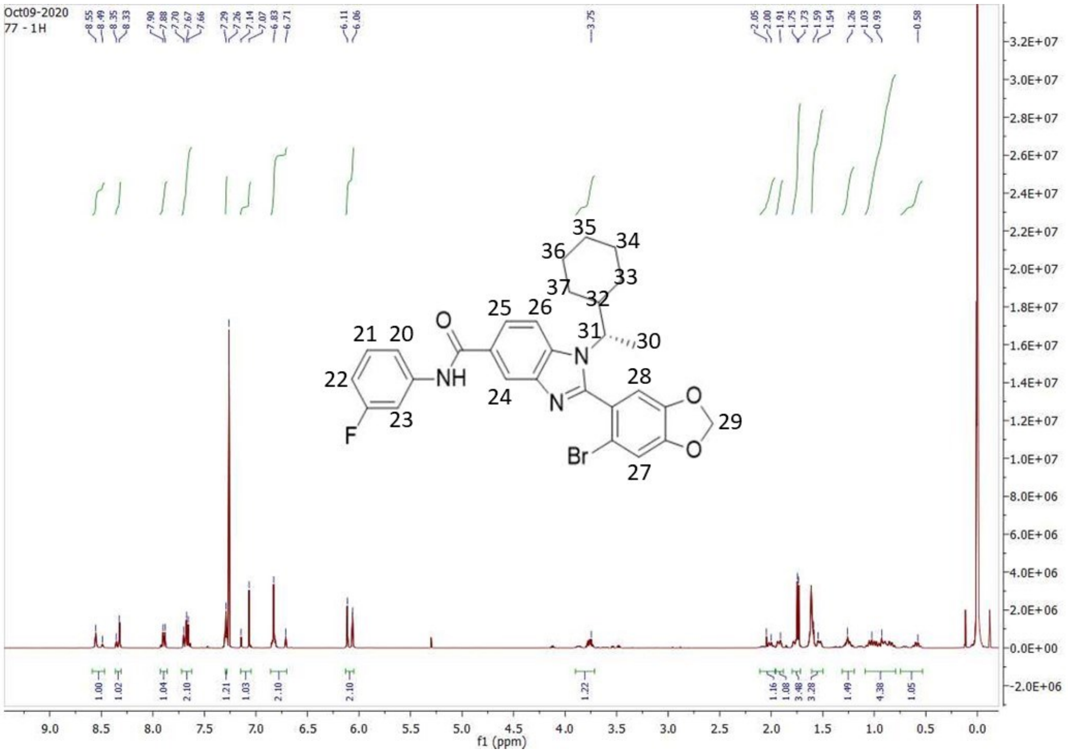

Figure 21. The spectrum of ^{1}H-NMR of compound 6b.

The ^{1}H-NMR spectrum of the compound 6b as an example is shown in Figure 21. The peaks at chemical shifts of 7.70 ppm, 7.67 ppm, 7.29 ppm and 6.83 ppm correspond to the four proton atoms in the aromatic ring of the fluorobenzene moiety (carbon numbers 20, 21, 22, and 23). The signals at chemical shifts of 8.55 ppm, 8.35 ppm and 7.90 ppm correspond to the three proton atoms in the aromatic ring of the benzimidazole (carbon numbers 24, 25, and 26). The signals at chemical shifts of 7.07 ppm and 6.83 ppm correspond to the two hydrogen atoms in the aromatic ring of the 1,3-benzodioxole (carbon numbers 27 and 28). The signals at 6.11-6.06 ppm correspond to the hydrogen atoms between the two oxygen atoms of the 1,3-benzodioxole (carbon number 29). The signals at 3.75 ppm corresponds to the hydrogen atom between the imidazole and cyclohexane rings (carbon number 31). The protons with a chemical shift of 1.75 ppm correspond to the methyl group adjacent to the cyclohexyl ring (carbon number 30). The remaining protons with chemical shifts between 2.05 ppm to 0.58 ppm correspond to the protons on the cyclohexyl ring (carbon number 32-37).

The purities of 14 analogues were tested by HPLC using a solvent system of water and acetonitrile (Table 2). All 14 of these analogues met the 95% purity requirement, and the rest of the analogues are waiting for further purification. The structures of all AZ3451 analogues can be found in **Appendix 1**. The data and spectra from MS, HPLC, and ^{1}H-NMR for all AZ3451 analogues are available in the **Experimental Procedure Chapter** and in **Appendix 3**.

Table 2. Purities of 14 analogues.

Compound	Purity	Compound	Purity
6a	99%	8b	95%
6b	98%	8c	99%
6c	99%	10a	97%
7a	99%	11a	98%
7b	98%	12a	98%
7c	97%	13a	99%
8a	98%	14a	98%

2.4 Molecular Docking

Molecular docking is a computational method for searching the preferred binding conformation and orientation of the ligand with its receptor and predicts the binding affinity of the ligand-receptor complex (Figure 22)[92]. Molecular docking is an important tool in drug design and is highly useful for identifying a lead compound in drug development[17].

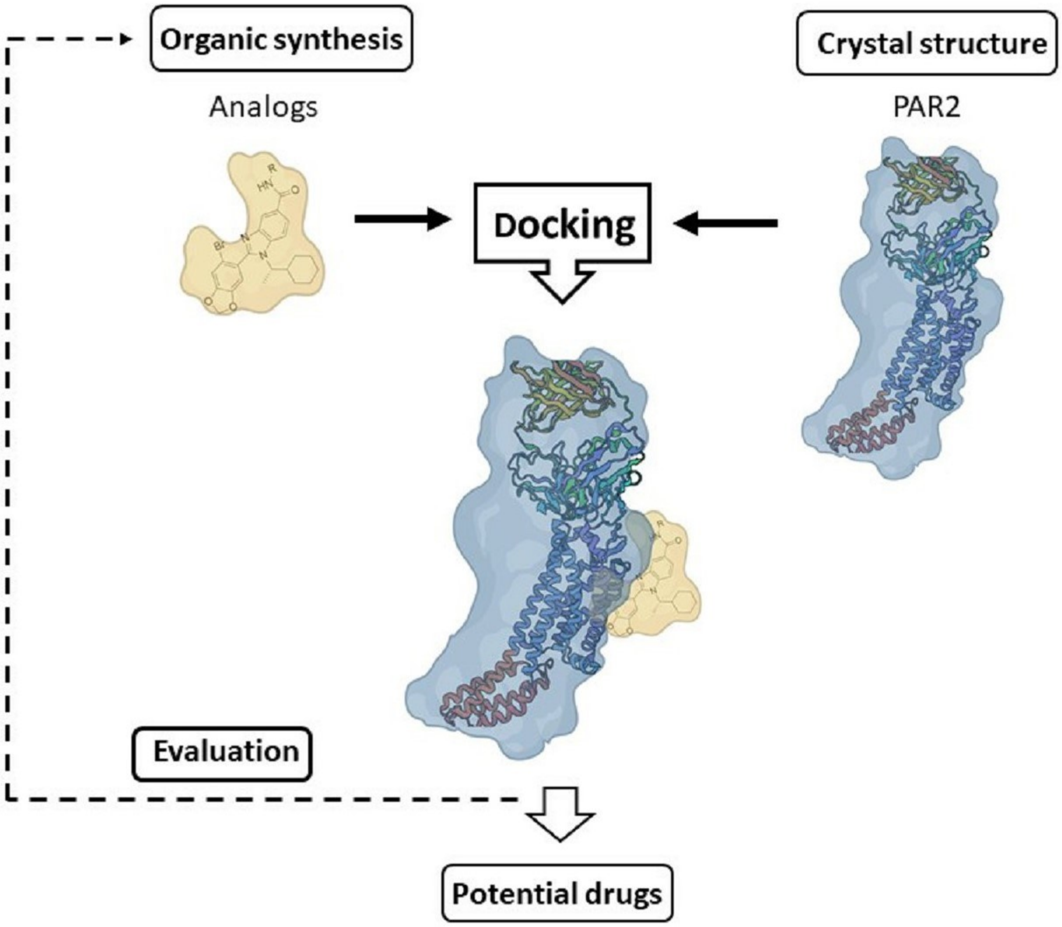
Organic synthesis
Analogs
Crystal structure
PAR2
Docking
Evaluation
Potential drugs

Figure 22. The diagram of molecular docking between a ligand and its target protein. The ligand (analogs) is docked onto the receptor (PAR2) and interactions are checked; the scoring function generates a value depending on the best selected ligand. The evaluation will be performed to improve the organic synthesis of the ligand.

A molecular docking study is often used to seek ideas to optimize parent compounds. The strength of ligand-protein interaction can be estimated by binding energy due to the energy released upon binding[93,94]. A favorable interaction gives a negative value[94], therefore, the lower value means better binding. Molecular docking was performed to predict the binding free energy using Auto Dock vina (molecular modeling simulation software). The docking pose with the most similar binding mode to that of AZ3451 in the crystal structure and high binding affinity was selected. The estimated binding free energies are listed in Table 3.

Table 3. Binding affinity of the reference compound (AZ3451), and the analogues.

Compound	**AZ3451**	**6a**	**7a**	**8a**	**9a**	**10a**	**11a**	**12a**	**13a**
Bind free energy(Kcal/mol)	-7.7	-6.8	-8.2	-6.7	-8.3	-7.8	-6.9	-8.0	-8.1

The predicted binding modes of the analogues in PAR2 are shown in Figure 23, Figure 24, and Figure 25; the left-hand side of Figure 23, Figure 24, and Figure 25 shows the 3-D binding modes of these analogues in PAR2. And the right-hand side is the 2-D diagram of detailed interactions. All the analogues have similar binding modes as compared to AZ3451. Specifically, the interactions between 1,3-benzodioxole moiety and Ala120, Ala157, Cys161 are retained[44]. The benzimidazole moiety interacts with Leu123, Tyr 210, Phe154, and the hydrogen bonding interaction is found between the imidazole ring and Tyr210[44]. The cyclohexyl ring interacts with Leu123, and the pi-pi stacking interactions between the aromatic ring that connected to the amide bond and Tyr210 is retained[44]. Interestingly, the analogues 7a and 12a with additional CH_2 group, and analogues 9a and 13a with bulky group has lower binding free energies, indicating that they may have a higher binding affinity with PAR2.

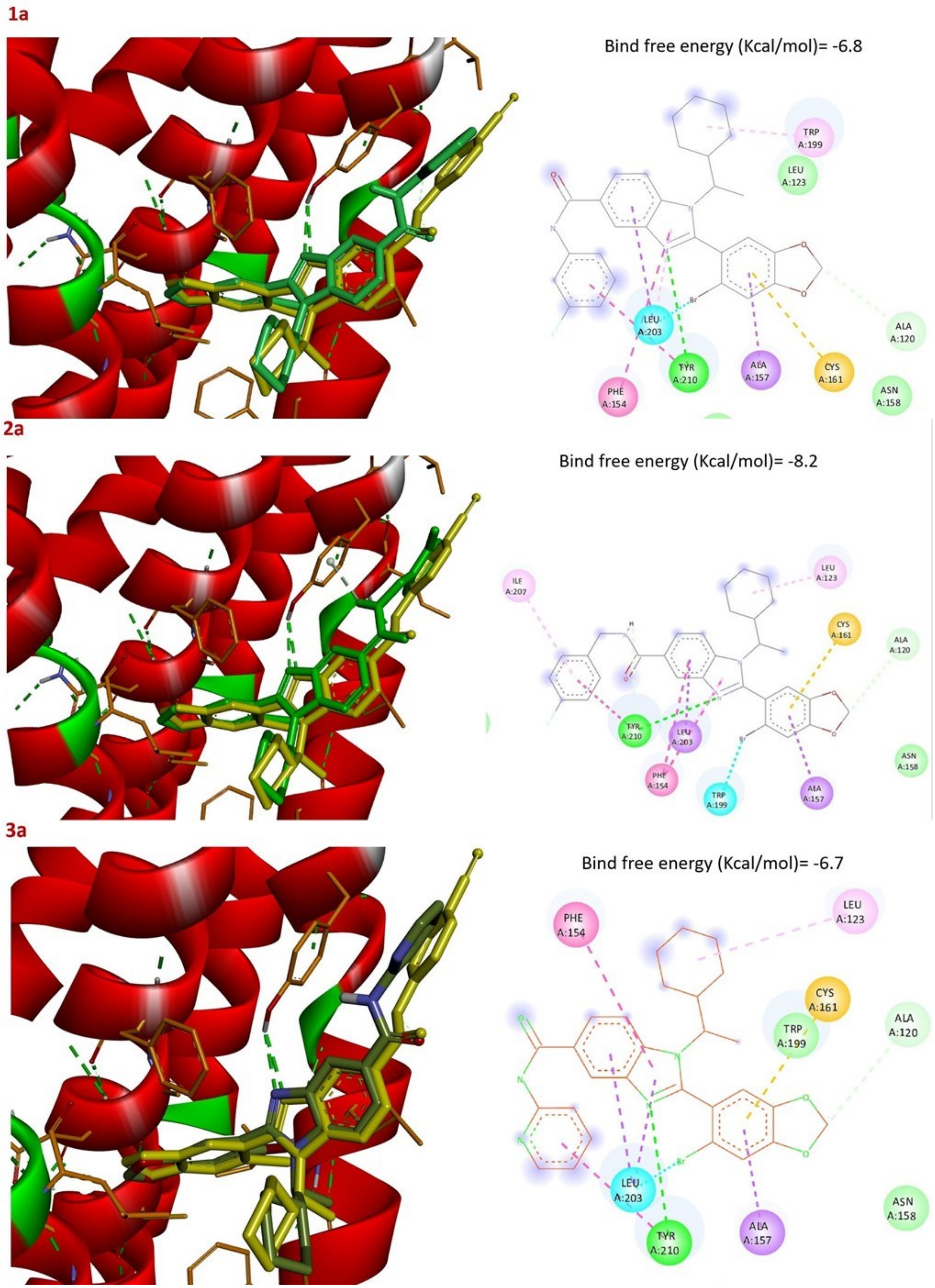
1a
Bind free energy (Kcal/mol)= -6.8
TRP A:199
LEU A:123
LEU A:203
TYR A:210
PHE A:154
ALA A:157
CYS A:161
ALA A:120
ASN A:158
2a
Bind free energy (Kcal/mol)= -8.2
ILE A:207
LEU A:123
CYS A:161
ALA A:120
TYR A:210
LEU A:203
PHE A:154
TRP A:199
ALA A:157
ASN A:158
3a
Bind free energy (Kcal/mol)= -6.7
PHE A:154
LEU A:123
CYS A:161
TRP A:199
ALA A:120
LEU A:203
TYR A:210
ALA A:157
ASN A:158

Figure 23. Ligand-receptor interaction for analogues 6a-8a. AZ3451 is shown in yellow stick, analogues 6a-8a are shown as green sticks.

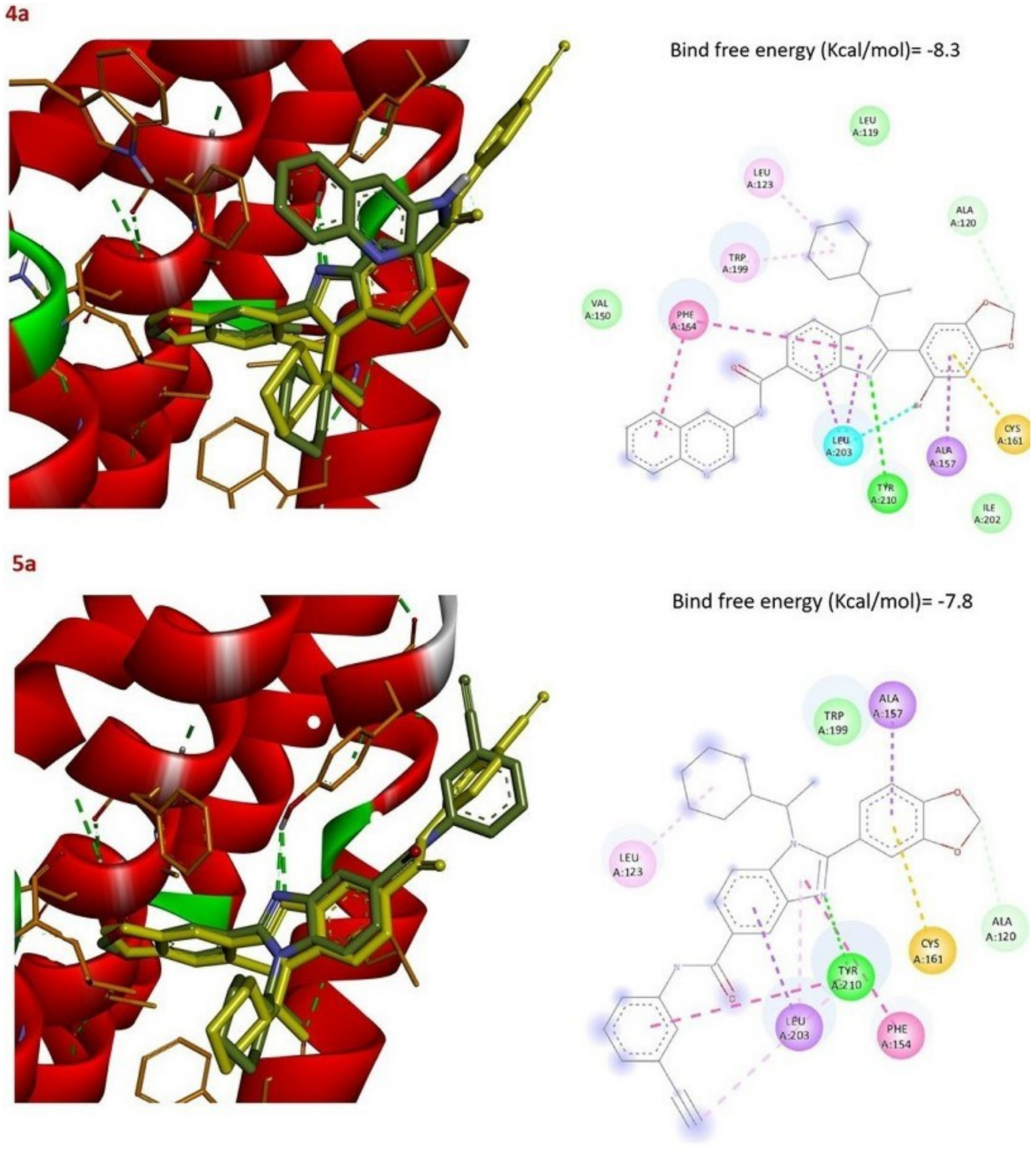
4a
Bind free energy (Kcal/mol)= -8.3
LEU A:119
LEU A:123
ALA A:120
TRP A:199
VAL A:150
PHE A:154
LEU A:203
CYS A:161
ALA A:157
TYR A:210
ILE A:202
5a
Bind free energy (Kcal/mol)= -7.8
TRP A:199
ALA A:157
LEU A:123
ALA A:120
CYS A:161
TYR A:210
LEU A:203
PHE A:154

Figure 24. Ligand-receptor interactions for analogues 9a-10a. AZ3451 is shown in yellow stick. Analogues 9a-10a are shown as green sticks.

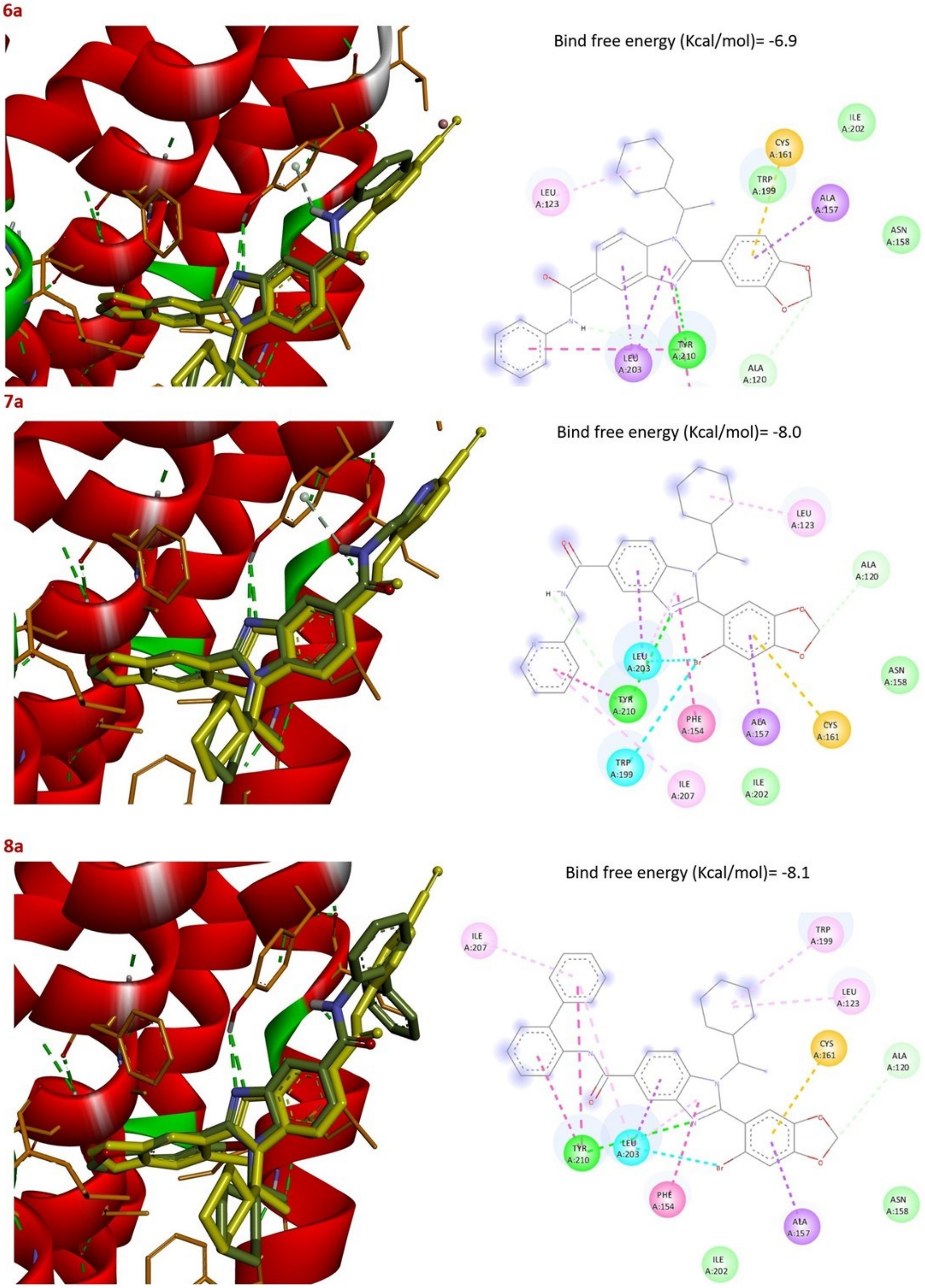
6a
Bind free energy (Kcal/mol)= -6.9
LEU A:123
CYS A:161
ILE A:202
TRP A:199
ALA A:157
ASN A:158
LEU A:203
TYR A:210
ALA A:120
7a
Bind free energy (Kcal/mol)= -8.0
LEU A:123
ALA A:120
LEU A:203
ASN A:158
TYR A:210
PHE A:154
ALA A:157
CYS A:161
TRP A:199
ILE A:207
ILE A:202
Br
8a
Bind free energy (Kcal/mol)= -8.1
ILE A:207
TRP A:199
LEU A:123
CYS A:161
ALA A:120
TYR A:210
LEU A:203
PHE A:154
ALA A:157
ASN A:158
ILE A:202
Br

Figure 25. Ligand-receptor interactions for analogues 11a-13a. AZ3451 is shown in yellow stick. Analogues 11a-13a are shown as green sticks.

2.5 Discussion of compound 8c.

Compound 8c (building block with 4-Aminopyridine) was reported as a novel and potent PAR2 antagonist on December 17, 2020 as it had been already made in the Hou lab[72]. AZ2623 is a heterocycle with a nitrogen atom in the para-position of the aromatic ring (Figure 26).

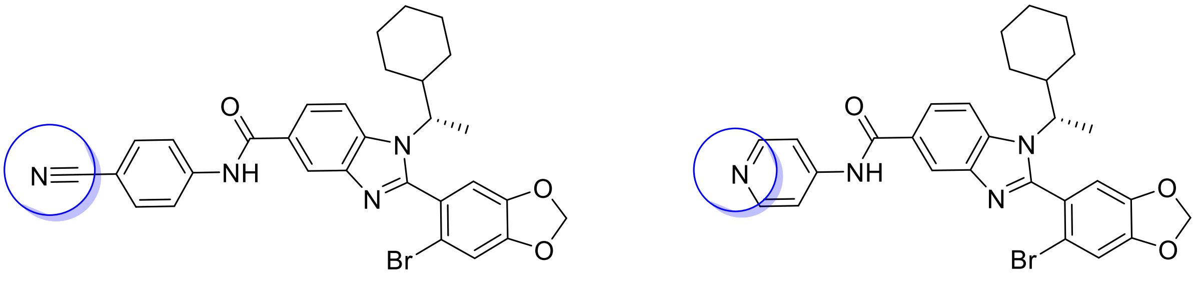

AZ3451 AZ2623

Figure 26. Structure of AZ3451 and AZ2623, with their similarity highlighted in the blue circle.

Compared to AZ3451, which has a nitrile group at the para-position of the aromatic ring, AZ2623 has very similar potency (Table 4)[72]. AZ2623 showed slightly better antagonism activity in Ca^{2+} mobilisation assays using human PAR2 and rat PAR2, and this compound also shows a good inhibition of the inositol phosphate signalling cascade[72]. PAR2 is known to activate phosphorylated extracellular-regulated kinase ½ and stimulate β-arrestin-2 recruitment[72]. AZ2623 shows a better ability to attenuate those two signalling pathways, which are activated by PAR2.

Table 4. *In vitro* pharmacology of AZ3451 and AZ2623 from Kennedy et al[72]. Data are presented as mean pIC_{50} ± standard error measurement with the number of independent measurements in parentheses.

Compounds	**Ca2+ flux (human PAR2)**	**Ca2+ flux (rats PAR2)**	**IP1 (human PAR2)**	**pERK1/2 (human PAR2)**	**β-arrestin (human PAR2)**
AZ3451	8.6 ± 0.1 (n=30)	8.5 ± 0.1 (n=12)	7.65 ± 0.02 (n=122)	6.44 ± 0.03 (n=3)	7.06 ± 0.04 (n=3)
AZ2623	8.3 ± 0.1 (n=26)	8.3 ± 0.1 (n=12)	7.09 ± 0.02 (n=106)	6.1 ± 0.1 (n=3)	6.31 ± 0.04 (n=3)

2.6 Other series of AZ3451 analogues.

2.61 The design and synthesis of the second series of AZ3451 analogue.

In addition, based on the previous set of structural modifications done with aromatic substituents connected to the amide bond, another set of AZ3451 analogues was designed, but the synthesis has not yet been completed (Scheme 3). The main modifications for this series were at the 1,3-benzodioxole with a bromine substituent that has been exchanged by a benzene ring with bromine substituent. Making this part of the molecule more hydrophobic, may potentially improve its binding interactions with PAR2. Unfortunately, due to time constraints, this scheme has only been completed to the first three steps. The ^{1}H-NMR data for compound 6 can be found in the **Experimental Procedures Chapter**, and MS and ^{1}H-NMR spectra for compound 6 can be found in **Appendix 4**.

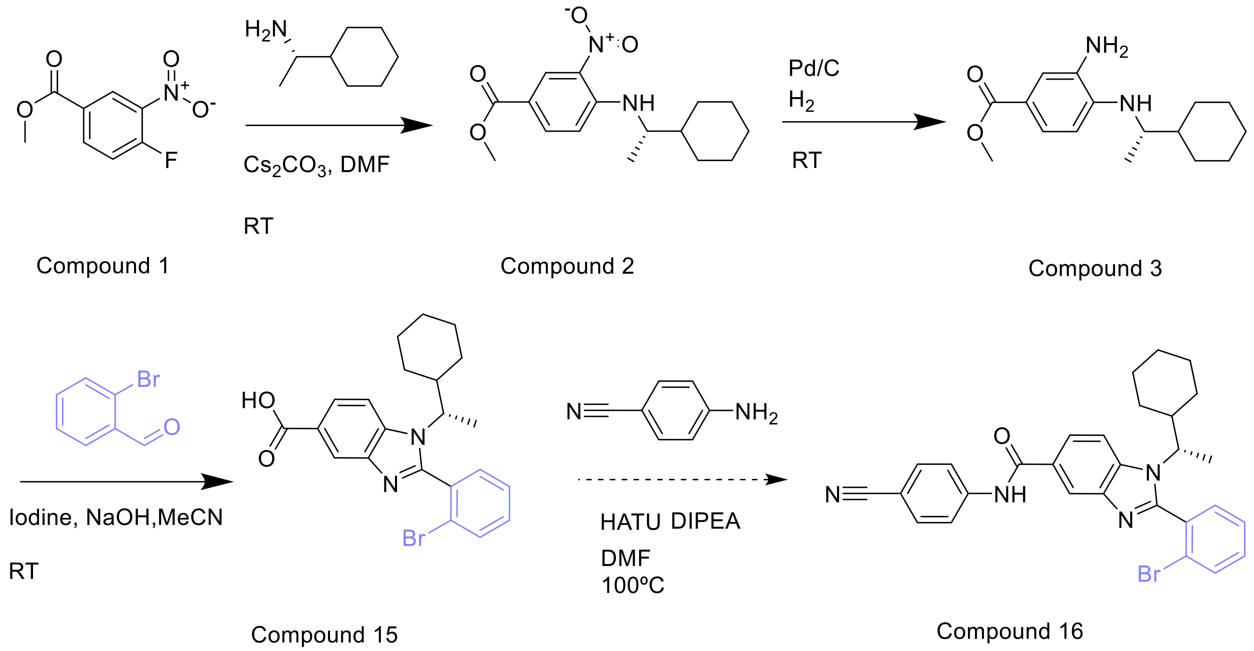
H2N
Cs2CO3, DMF
RT
Pd/C
H2
RT
Compound 1
Compound 2
Compound 3
Br
Iodine, NaOH,MeCN
RT
HO
N≡
NH2
HATU DIPEA
DMF
100ºC
Compound 15
Compound 16

Scheme 3. The proposed synthetic scheme for the second series of analogues.

2.62 The design and synthesis of the third series of AZ3451 analogue.

A third series of AZ3451 analogues has been designed (Scheme 4). The modification in this scheme is that (S)-(+)-1-cyclohexylethanamine was replaced by 4-fluorobenzylamine. The main idea of this aromatic ring replacement is that the aromatic ring may enhance the π-π stacking interactions with residues in the binding pocket. However, only the first two steps of this synthesis have been performed due to time constraints.

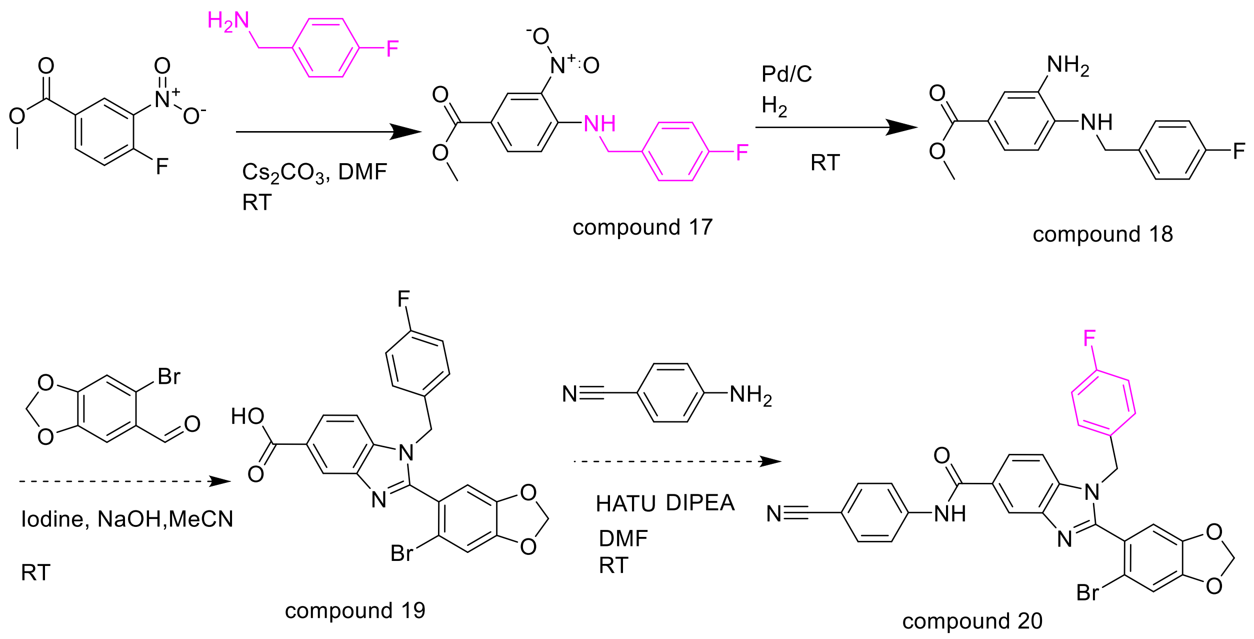
H2N
F
Cs2CO3, DMF
RT
Pd/C
H2
RT
compound 17
compound 18
Iodine, NaOH,MeCN
RT
compound 19
HATU DIPEA
DMF
RT
compound 20

Scheme 4. The proposed synthetic scheme for the third series of analogues.

The synthesis of compound 11 (Scheme 4) will be continued; since (S)-(+)-1-cyclohexylethanamine was replaced by 4-fluorobenzylamine, compound 20 also could be used to determine the presence of conformational isomers (Figure 27).

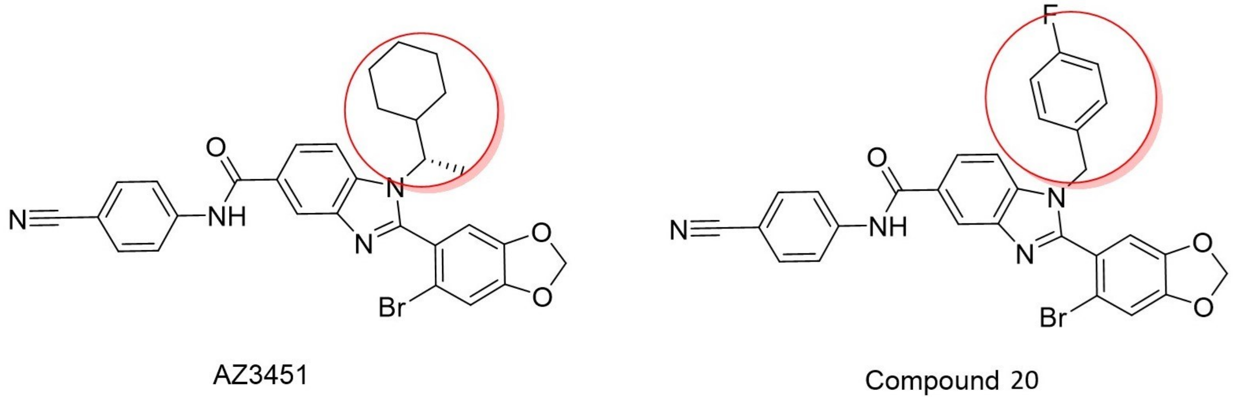
AZ3451

Compound 20

Figure 27. Structure of AZ3451 and compound 20.

Chapter Three

3.1 Conclusion

Cancer remains a public health threat both in Canada and world wide[4]. With the search for better methods for the diagnosis and treatment of cancer remains an active area of research. Although there are several ways to diagnose cancer in the clinic, many are not target-specific and therefore are limited in utility. For example, [^{18}F]FDG, the most commonly used PET tracer, is not a target-specific radiotracer and is limited to certain cancers like prostate, lung, and breast[30,95]. Therefore, an urgent need exists to develop novel PET radiotracers that are target specific.

PAR2 is a member of the GPCR family of proteins and is known to be involved in many diseases[55,96]. More specifically, PAR2 is highly implicated in lung and breast cancers[52]. There are currently no PET radiotracers that are approved for PAR2 imaging[97], however, in recent literature, AZ3451 has been reported as a highly effective and selective PAR2 antagonist; this antagonist was used as the starting point in this thesis. This project involved the design, synthesis, and evaluation of analogues of AZ3451. A candidate compound to be radiolabeled with ^{18}F to prepare a novel PET imaging agent that targets PAR2.

To develop the library of analogues, a four-step synthesis scheme was designed and completed, and a three-step radiolabelling scheme was proposed. A total of 18 compounds were synthesized and characterized by mass spectrometry and ^{1}H-NMR. The significance of this research project is that the novel compounds synthesized have potential for the treatment of PAR2-related diseases, while the putative radioligands have potential for non-invasive cancer diagnosis through targeting PAR2.

3.2 Future Work

3.21 Organic Synthesis

Additional synthesis is required to expand the library of AZ3451 analogues. For our first round of structural optimization, rapid library expansion will be achieved through the introduction of additional building blocks and the incorporation of more halogens like chlorine and iodine. Once the binding affinity data has been obtained for the first round of AZ3451 analogues, it will be used to direct the design of second and third generation of AZ3451 analogues.

3.22 Biology Assay

Collaborators from UWO will evaluate the library of analogues for binding affinity to PAR2. All binding affinity data will be used to select a candidate for radiolabeling and direct the design of future AZ3451 analogues. Intracellular calcium release assay will be performed to determine the binding affinities of AZ3451 analogues; PAR2 couples to subtypes of G-proteins, like G_q-protein, and calcium release assay is a cell-based second messenger assay that determine the Ca^{2+} flux associated with G_q-protein activation or inhibition[75]. Changes in intracellular Ca^{2+} concentration can be measured after the analogues bind to PAR2[59,98] along with β-arrestin-2 recruitment assay to test the binding affinity of the analogues[99]. There are two types of β-arrestin, short-term interaction between PAR2 of the arrestins indicates a preference for β-arrestin-2[78]. Arrestins can desensitize PARs by arresting the G-protein signaling pathway, and can also acts as scaffold proteins involved in endosomal trafficking and signaling modulation[78]. Endocytosis and intracellular trafficking of PAR2 are important to sustain its physiological functions in cell[78,99]. Therefore, the PAR2-arrestin interaction can be used as a measurement of ligand binding.

3.23 Radiolabel Approach

After the binding affinity data has been obtained for the library of AZ3451 analogues, ^{18}F will be introduced into the selected candidate compound to make it an imaging agent for PET[22]. The synthesis must be designed with the half-life of ^{18}F in mind[69]. The conditions used to prepare the "cold" compounds required several hours to react[22,69]. To maximum the radiochemical yield (RCY), it is important to introduce the radionuclide as late in the synthesis as possible[68,69]. Scheme 5 shows the proposed multi-step radiolabelling procedure to prepare the AZ3451-derived ^{18}F-radiolabelled ligand.

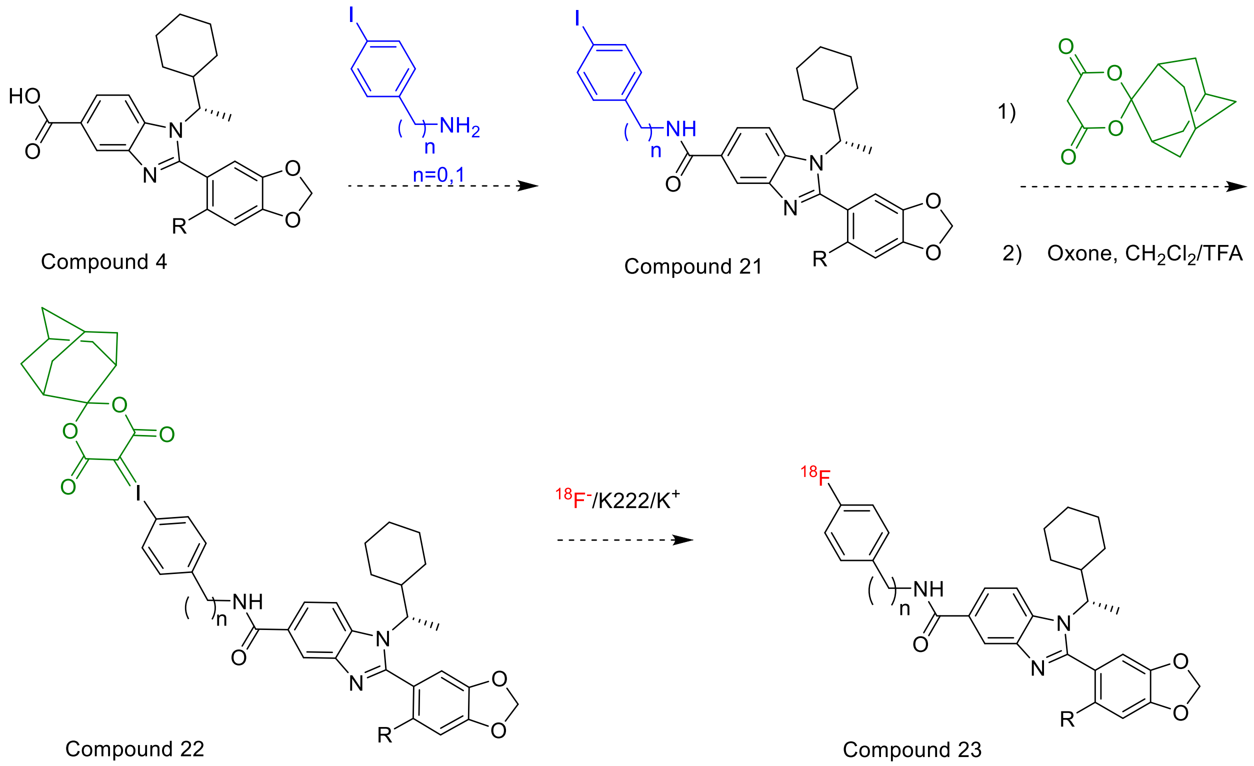
HO
O
N
N
O
O
R
Compound 4
I
NH2
n
n=0,1
I
NH
n
O
N
N
O
O
R
Compound 21
1)
O
O
O
O
2) Oxone, CH2Cl2/TFA
O
O
O
O
I
NH
n
O
N
N
O
O
R
Compound 22
18F-/K222/K+
18F
NH
n
O
N
N
O
O
R
Compound 23

Scheme 5. Proposed radiolabelling scheme for AZ3451-derived ligand.

This synthetic scheme was created with three main steps. As mentioned in Chapter 1.7, SCIDY technology that involves iodonium-mediated arene radio-fluorination will be used in the radio synthesis[70]. Therefore, in the first step in this synthesis involves the amidation of compound 4 to produce compound 12. After this reaction, the next step will be to introduce SCIDY to compound 8 to produce a spiro-iodine (III)-based precursor (compound 13)[70]. Lastly, this precursor will undergo radio-fluorination, in which compound 13 will react with nucleophilic ^{18}F to yield compound 14 (radiotracer). Eventually, a successful ^{18}F-radioligand is a useful tool that could highlight PAR2 expression both *in vitro* and *in vivo* with potential clinical applications in cancer, such as breast cancer and lung cancer.

Chapter Four

Experimental Procedures

All reagents are available and were obtained from Sigma-Aldrich, Fisher Scientific, and Oakwood Chemicals. The purity of the compounds was analysed using analytical HPLC (Agilent Technologies 1200 series) equipped with a C18 column (3.0 x 150 mm 4-micron), and UV detector set to 365nm. HPLC data was processed using Project HPLC testing. Compound purity was measures as the area under the curve (AUC) for the desire product over the total AUC for all peaks and reported as a percentage. The results are summarized in the Results and Discussion section. NMR spectra were obtained on a 500Hz Bruker NMR Instrument Chloroform-d or DMSO-d6 with the chemical shifts referenced to solvent signals.

Types of flash silica gel column chromatography. Type #A: flash silica gel column chromatography with an elution gradient 1:3 EtOAc : Hexane. Column length=400mm, column diameter=26mm. Silica gel length: 120mm. Type #B: flash silica gel column chromatography with an elution gradient 1:1 EtOAc : Hexane. . Column length=400mm, column diameter=26mm. Silica gel length: 140mm. Type #C: flash silica gel column chromatography with an elution gradient 1:50 MeOH: DCM. . Column length=600mm, column diameter=15mm. Silica gel length: 200mm. Type #D: flash silica gel column chromatography with an elution gradient 1:100 MeOH: DCM. Column length=400mm, column diameter=26mm. Silica gel length: 220mm.

Synthesis of (S)-methyl 4-((1-cyclohexylethyl) amino)-3-nitrobenzoate. (Compound 2)

To a 100mL round-bottom flask equipped with a stir bar was measured and added methyl 4-fluoro-3-nitrobenzoate (1000mg, 5.02mmol), and caesium carbonate (3271.1mg, 10.04mmol). To this reaction mixture, (S)-cyclohexyl ethylamine (766.13mg, 6.024mmol) was added via a syringe.

DMF (10mL) was measured and added to the round-bottomed flask, which was then sealed with a rubber septum and allowed to stir for two hours at room temperature. The resulting orange/yellow-colour mixture was then checked by TLC 1:3 EtOAc : hexane. The reaction mixture was diluted with 100mL of EtOAc and extracted with 200mL of saturated NH_4Cl solution. The aqueous layer was separated, extracted 2 times with EtOAC. The combined organic layers were dried over Na_2SO_4 and filtered. The solvent was then removed under reduced pressure by rotary evaporation. The crude product was then prepared for flash silica gel chromatography. Column Awas used to elute the purified product, (S)-methyl 4-((1-cyclohexylethyl) amino)-3-nitrobenzoate. A 1401 mg (91% yield) of pure product was obtained. ^1H NMR (500 MHz, $CDCl_3$) δ 8.83 (s, 1H), 8.48 (d, 1H), 8.01 (m, 1H), 3.90 (s, 3H), 2.01 (m, 1H), 1.55 (m, 3H), 1.47 (m, 1H), 1.15(m, 9H), 0.64 (m, 1H) MS m/z: for Chemical Formula: $C_{16}H_{22}N_2O_4$ [M + H]+ 307.12 (calcd.) 306.4 (found.)

Synthesis of (S)-methyl 3-amino-4-((1-cyclohexylethyl) aminobenzoate. (Compound 3)

(S)-methyl 4-((1-cyclohexylethyl) amino)-3-nitrobenzoate (1401mg, 4.57 mmol) was added to a 250mL round-bottom flask. Pd/C catalyst (Palladium content 10%, 40mg, 0.37mmol) was added into the flask via spatula along with a stir bar. A 1:1 EtOAc: MeOH solution (12mL) was added to the flask, and then sealed with a rubber septum. The air within the flask was removed under vacuum and refilled twice with H_2 by H_2-filled balloon. With the H_2-filled balloon still attached, the reaction was then allowed to progress for 8 hours at room temperature while stirring. The reaction was checked for completion by TLC (1:3 EtOAc: Hexane), and then filtered through a layer of diatomaceous earth washed with high volumes of EtOAc. The resulting light grey colour liquid was then concentrated under pressure by rotary evaporation and further dried in a desiccator to afford the desired product as a light green solid. 1262mg (97% yield) was obtained and this product was used directly without further purification in the next step. ^{1}H NMR (500 MHz, $CDCl_3$) δ 7.57 (m, 1H), 7.41 (s, 1H), 6.55 (s, 1H), 3.87 (s, 3H), 2.04 (m, 1H), 1.35 (m, 3H), 1.51 (m, 1H), 1.13 (m, 9H), 0.67 (m, 1H) MS m/z: for Chemical Formula: $C_{16}H_{24}N_2O_2$ [M + H]+ 276.18 (calcd.) 275.9 (found.)

Synthesis of (S)-2-(6-bromobenzo[d] [1,3] dioxol-5-yl)-1-(1-cyclohexylethyl)-1H-benzo[d]imidazole-5-carboxylic acid. (Compound 4)

To a 250mL round-bottomed flask was added (S)-methyl 3-amino-4-((1-cyclohexylethyl) aminobenzoate (1262mg, 4.45mmol) and iodine (2259.2mg, 8.9mmol). Sodium hydroxide pellets (1779.4 mg, 44.5mmol) were then added to the flask, followed by the addition of 6-bromobenzo-d-1,3-dioxole-5-carbaldehyde (823.3mg, 4.45mmol) via spatula. A stir bar was added to the flask and then acetonitrile (12mL). The round-bottom flask was sealed with a rubber septum. The flask was flushed with Argon. After sonication, the flask was set onto a stir plate for 6 hours at room temperature under argon gas. This reaction was checked by TLC (1:3 EtOAc: Hexane and 1:1 EtOAc: Hexane). The reaction mixture was a smooth, shaded brown sand-like solution. The reaction mixture was acidified to pH 2-3 using a 2M HCl solution. The crude product was concentrated via rotary evaporation to yield an oil-like dark/brown product stuck to the flask. The residue was redissolved in EtOAc (100mL, sonicated) and poured into a 500mL separatory funnel. Saturated NaCl solution (150mL) was added, followed by distilled water (100mL). Three extractions of aqueous layers were performed, adding 30mL of EtOAc each time. The combined organic layers were dried over Na_2SO_4, filtered, washed using EtOAc, and concentrated under reduced pressure by rotary evaporation. The sample was then prepared for a flash silica chromatography column. The crude product in silica was then added to the column and was washed with hexane. Column A was initially used, which was switched to column B. A 1902mg (81% yield) was obtained. ^{1}H NMR (500 MHz, DMSO) δ 12.79 (s, 1H), 8.26 (s, 1H), 7.90 – 7.86 (m, 2H), 7.44 (d, 1H), 7.12 (s, 1H), 6.26 – 6.19 (m, 2H), 3.75 (m, 1H), 2.16 – 1.99 (m, 1H), 1.87 (m, 1H), 1.70 (m, 3H), 1.62 – 1.42 (m, 3H), 1.29 – 1.13 (m, 1H), 1.07 – 0.75 (m, 4H), 0.68 – 0.49 (m, 1H). MS m/z: for Chemical Formula: $C_{23}H_{23}BrN_2O_4$ [M + H]+ 470.08 (calcd.) 471.0 (found.)

General synthetic method for AZ3451 and its derivatives.

To a 100mL round bottom flask was added compound 4 (100 mg, 206 μmol), HATU (158 mg, 412 μmol), DIPEA (53.2 mg, 2.5μL, 0.412 mmol), and DMF (2 mL). This was stirred at ambient temperature for 1 hour followed by addition of the specific amine. The reaction was then heated to 100 °C and monitored by TLC.

The reaction mixture diluted with 200ml of DI water and 100ml of saturated NaCl solution in a 500ml separatory funnel. The aqueous layer was washed twice with EtOAc (60 mL). The combined organic layers were dried over Na_2SO_4, filtered, and concentrated under reduced pressure by rotary evaporation. A crude mixture was obtained and prepared for a flash silica chromatography.

Synthesis of (S)-2-(6-bromobenzo[d] [1,3] dioxol-5-yl)-N-(4-cyanophenyl)-1-(1-cyclohexylethyl)-1Hbenzo[d]imidazole-5-carboxamide (Compound 5 - AZ3451).

4-Aminobenzonitrile (36.5mg, 0.412mmol) was added into the flask then heated to 100°C for 12 hours. The TLC solvent system was 1:1 EtOAc: Hexane and 1:12 MeOH: DCM plus one drop of NH_4OH. A brown, oil-like crude product was obtained and purified first with an eluting solvent of 1:3 EtOAc: Hexane, which was switched to 1:1 EtOAc: Hexane as the final eluent.

Further purification by flash silica gel column with DCM. This purification process in fume hood all the time. The chromatography column was set up using wet loading with DCM. The crude product in silica was then added to the column and was washed with DCM. An initial column C was used, and the column solvent system was changed to column D. A light brown solid produc-48.8mg (41% yield) was obtained. ^1H NMR (500 MHz, DMSO) δ 10.67 (s, 1H), 8.42 – 8.36 (m, 1H), 8.08 – 8.02 (m, 2H), 7.96 (m, 1H), 7.86 (m, 3H), 7.46 (m, 1H), 7.25 – 7.10 (m, 1H), 6.26 – 6.20 (m, 2H), 3.87 – 3.68 (m, 1H), 2.14 – 2.03 (m, 1H), 1.90 (m, 1H), 1.72 (m, 3H), 1.63 (dm 1H), 1.58 – 1.43 (m, 2H), 1.26 (m, 1H), 1.07 – 0.76 (m, 4H), 0.59 (m, 1H). MS m/z: for Chemical Formula: $C_{30}H_{27}BrN_4O_3$ [M + H]+ 570.13 (calcd.) 571.3 (found.)

Synthesis of (S)-2-(6-bromobenzo-1,3-dioxol-5-yl)-1-(1-cyclohexylethyl)-N-(2-fluorophenyl)-1H-benzo[d]imidazole-5-carboxamide. (Compound 6a)

The method similar for the preparation of AZ3451 was used except the building block (R group) is 2-Fluoroaniline (35.2mg, 0.420mmol). And the reaction time was changed to 7 hours. Purification of the crude product by flash silica chromatography with an elution gradient 1:1 EtOAc: Hexane and further purification by column C. A colorless solid product-66mg (54.6%) was obtained. ^1H NMR (500 MHz, $CDCl_3$) δ 8.53 (m, 1H), 8.33 (m, 1H), 8.22 (m, 1H), 7.94 (m, 1H), 7.69 (m, 1H), 7.20 (m, 1H), 7.17 – 7.11 (m, 1H), 7.09 (m, 1H), 6.85 (m, 1H), 6.12 (m, 2H), 3.84 (m, 1H), 2.06 (m, 1H), 1.94 (m, 1H), 1.78 (m, 3H), 1.68 – 1.51 (m, 3H), 1.40 – 1.15 (m, 1H), 1.11 – 0.80 (m, 4H), 0.78 – 0.55 (m, 1H). MS m/z: for Chemical Formula: $C_{29}H_{27}BrFN_3O_3$ [M +

H]+ 563.12 (calcd.) 564.1 (found.) Purity testing by HPLC (65%-95% Acetonitrile 10 minutes) t_R = 6.254 minutes. Purity=99%.

Synthesis of (S)-2-(6-bromobenzo-1,3-dioxol-5-yl)-1-(1-cyclohexylethyl)-N-(3-fluorophenyl)-1H-benzo[d]imidazole-5-carboxamide. (Compound 6b)

The method similar for the preparation of AZ3451 was used except replacing the building blocks (R group) with 3-Fluoroaniline (39mg, 0.421mmol). And the reaction time for reflux is change to 6 hours. Purification with similar method by the crude product was purified by column B and further purification by column C. A colorless solid product-75mg (64.6%) was obtained. ^{1}H NMR (500 MHz, $CDCl_3$) δ 8.55 (m, 1H), 8.33 (m, 1H), 7.90 – 7.88 (m, 1H), 7.70 – 7.66 (m, 2H), 7.29 (m, 1H), 7.07 (m, 1H), 6.83 – 6.71 (m, 2H), 6.09 (d, 2H), 3.80 (m, 1H), 2.11 – 1.97 (m, 1H), 1.92 (d, 1H), 1.80 – 1.71 (m, 3H), 1.63 – 1.50 (m, 3H), 1.31 – 1.20 (m, 1H), 1.09 – 0.79 (m, 4H), 0.74 – 0.53 (m, 1H). MS m/z: for Chemical Formula: $C_{29}H_{27}BrFN_3O_3$ [M + H]+ 563.12 (calcd.) 564.14 (found.) Purity testing by HPLC (Acquisition method - 65%-95% Acetonitrile 10 minutes) t_R = 5.006 minutes. Purity=99%.

Synthesis of (S)-2-(6-bromobenzo-1,3-dioxol-5-yl)-1-(1-cyclohexylethyl)-N-(4-fluorophenyl)-1H-benzo[d]imidazole-5-carboxamide. (Compound 6c)

The method similar for the preparation of AZ3451 was used except replacing the building block with (R group) 4-Fluoroaniline (36.5mg, 0.412mmol). Purification with similar method by the crude product was purified by column B and further purification by column C. A light-yellow solid product-50mg (43.6%) was obtained. ^{1}H NMR (500 MHz, $CDCl_3$) δ 9.46 (m, 1H), 8.48 (m, 1H), 7.91 (m, 1H), 7.68 – 7.62 (m, 2H), 7.60 (m, 1H), 7.02 – 6.93 (m, 2H), 6.70 – 6.56 (m, 1H), 6.08 – 5.98 (d, 2H), 3.85 – 3.64 (m, 1H), 1.98 (m, 1H), 1.89 (m, 1H), 1.71 (m, 3H), 1.62 – 1.46 (m, 3H), 1.41 – 1.18 (m, 1H), 1.13 – 0.74 (m, 4H), 0.71 – 0.47 (m, 1H). MS m/z: for Chemical Formula: $C_{29}H_{27}BrFN_3O_3$ [M + H]+ 563.12 (calcd.) 566.1 (found.) Purity testing by HPLC (Acquisition method - 75%-95% Acetonitrile 10 minutes) t_R = 2.980 minutes. Purity=99%.

Synthesis of (S)-2-(6-bromobenzo-1,3-dioxol-5-yl)-1-(1-cyclohexylethyl)-N-(2-fluorobenzyl)-1H-benzo[d]imidazole-5-carboxamide. (Compound 7a)

The method similar for the preparation of AZ3451 was used except replacing the building block (R group) with 2-Fluorobenzylamine (53mg, 0.41mmol). And purification with similar method by the crude product was purified by column A and further purification by column C. A white solid product-65mg (56.5%) was obtained. ^{1}H NMR (500 MHz, $CDCl_3$) δ 8.18 (m, 1H), 7.83 (m, 1H), 7.61 (m, 1H), 7.44 (m, 1H), 7.19 – 6.99 (m, 3H), 6.97 – 6.86 (m, 1H), 6.77 (m, 1H), 6.10 (d, 2H), 4.73 (m, 2H), 3.90 – 3.69 (m, 1H), 2.03 (m, 1H), 1.92 (m, 1H), 1.75 (m, 3H), 1.57 (m, 3H), 1.22 (m, 1H), 1.09 – 0.78 (m, 4H), 0.73 – 0.52 (m, 1H). MS m/z: for Chemical Formula: $C_{30}H_{29}BrFN_3O_3$ [M + H]+ 577.14 (calcd.) 578.04 (found.)

Synthesis of (S)-2-(6-bromobenzo-1,3-dioxol-5-yl)-1-(1-cyclohexylethyl)-N-(3-fluorobenzyl)-1H-benzo[d]imidazole-5-carboxamide. (Compound 7b)

The method similar for the preparation of AZ3451 was used except replacing the building block (R group) with 3-Fluorobenzylamine (55mg, 0.411mmol). And the reaction time for reflux is change to 6 hours. Purification with similar method by column A and further purification by

column C. A white solid product-70mg (58.8%) was obtained. ^{1}H NMR (500 MHz, CDCl$_3$) δ 8.20 (m, 1H), 7.86 (m, 1H), 7.62 (m, 1H), 7.32 – 7.25 (m, 1H), 7.19 – 7.04 (m, 2H), 6.96 (m, 1H), 6.88 (s, 1H), 6.84 – 6.71 (m, 1H), 6.10 (d, 2H), 4.72 – 4.63 (d, 2H), 3.90 – 3.70 (m, 1H), 2.04 (m, 1H), 1.92 (m, 1H), 1.76 (m, 3H), 1.58 (m, 3H), 1.42 – 1.19 (m, 1H), 1.10 – 0.79 (m, 4H), 0.64 (m, 1H). MS m/z: for Chemical Formula: $C_{30}H_{29}BrFN_3O_3$ [M + H]+ 577.14 (calcd.) 583.15 (found.) Purity testing by HPLC (Acquisition method - 75%-95% Acetonitrile 10 minutes) t_R = 2.254 minutes. Purity=99%.

Synthesis of (S)-2-(6-bromobenzo-1,3-dioxol-5-yl)-1-(1-cyclohexylethyl)-N-(4-fluorobenzyl)-1H-benzo[d]imidazole-5-carboxamide. (Compound 7c)

The method similar for the preparation of AZ3451 was used except replacing the building block (R group) with 4-Fluorobenzylamine (53mg, 0.41mmol). And the reaction time for reflux is change to 6 hours. Purification with similar method by the crude product was purified by column A and further purification by column C. A light-brown solid product-78mg (64%) was obtained. ^{1}H NMR (500 MHz, CDCl$_3$) δ 8.17 (m, 1H), 7.84 (m, 1H), 7.61 (m, 1H), 7.33 (m, 2H), 7.14 (m, 1H), 7.01 (m, 2H), 6.89 – 6.70 (m, 1H), 6.09 (d, 2H), 4.64 (d, 2H), 3.90 – 3.71 (m, 1H), 2.03 (m, 1H), 1.92 (m, 1H), 1.75 (m, 3H), 1.64 – 1.49 (m, 3H), 1.24 (m, 1H), 1.17 – 0.78 (m, 4H), 0.63 (m, 1H). MS m/z: for Chemical Formula: $C_{30}H_{29}BrFN_3O_3$ [M + H]+ 577.14 (calcd.) 578.0 (found.) Purity testing by HPLC (Acquisition method - 65%-95% Acetonitrile 10 minutes) t_R = 3.935 minutes. Purity=99%.

Synthesis of (S)-2-(6-bromobenzo-1,3-dioxol-5-yl)-1-(1-cyclohexylethyl)-N-(pyridin-2-yl)-1H-benzo[d]imidazole-5-carboxamide. (Compound 8a)

The method similar for the preparation of AZ3451 was used except replacing the building block (R group) 2-Aminopyridine (53.2mg, 0.412mmol). And the reaction time for reflux is change to 10 hours. Purification with similar method by the crude product was purified by column B and further purification by column C. A light-brown solid product-33mg (29%) was obtained. ^{1}H NMR (500 MHz, $CDCl_3$) δ 8.79 (m, 1H), 8.44 (m, 1H), 8.41 – 8.36 (m, 1H), 8.30 (m, 1H), 7.94 – 7.89 (m, 1H), 7.77 (m, 1H), 7.67 (m, 1H), 7.17 (m, 1H), 6.96 (m, 1H), 6.10 (d, 2H), 3.93 – 3.76 (m, 1H), 2.15 – 2.00 (m, 1H), 1.94 (m, 1H), 1.77 (m, 3H), 1.69 – 1.51 (m, 3H), 1.38 – 1.17 (m, 1H), 1.10 – 0.81 (m, 4H), 0.79 – 0.56 (m, 1H). MS m/z: for Chemical Formula: $C_{28}H_{27}BrN_4O_3$ [M + H]+ 546.13 (calcd.) 547.0 (found.)

Synthesis of (S)-2-(6-bromobenzo-1,3-dioxol-5-yl)-1-(1-cyclohexylethyl)-N-(pyridin-3-yl)-1H-benzo[d]imidazole-5-carboxamide. (Compound 8b)

The method similar for the preparation of compound 8a was used except replacing the building block (R group) with 3-Aminopyridine (53mg, 0.41mmol). And the reaction time for reflux is change to 9 hours. Purification with similar method by the crude product was purified by column B and further purification by column C. A brown solid product-53mg (47.3%) was obtained. ^{1}H NMR (500 MHz, $CDCl_3$) δ 8.84 (m, 1H), 8.45 (m, 1H), 8.38 (m, 1H), 8.30 (m, 1H), 8.32 (m, 1H), 7.91 (m, 1H), 7.77 (m, 1H), 7.70 (m, 1H) 7.27 (m, 1H), 6.93 (m, 1H), 6.13 (d, 2H), 3.78 (m, 1H), 2.03 (m, 1H), 1.93 (m, 1H), 1.77 (m, 3H), 1.63 (m, 3H), 1.25 (m, 1H), 1.10 – 0.81 (m, 4H), 0.79 – 0.56 (m, 1H). MS m/z: for Chemical Formula: $C_{28}H_{27}BrN_4O_3$ [M + H]+ 546.13 (calcd.) 547.0 (found.) MS m/z: for Chemical Formula: $C_{28}H_{27}BrN_4O_3$ [M + H]+ 546.13 (calcd.) 547.3 (found.)

Synthesis of (S)-2-(6-bromobenzo-1,3-dioxol-5-yl)-1-(1-cyclohexylethyl)-N-(pyridin-4-yl)-1H-benzo[d]imidazole-5-carboxamide. (Compound 8c)

The method similar for the preparation of compound 8a was used except replacing the building block (R group) with 4-Aminopyridine (54mg, 0.411mmol). And the reaction time for reflux is change to 11 hours. Purification with similar method by the crude product was purified by column B and further purification by column D. A brown solid product-60mg (53.5%) was obtained. ^{1}H NMR (500 MHz, $CDCl_3$) δ 10.14 (m, 1H), 8.59 (m, 1H), 8.44 (m, 2H), 7.91 (m, 1H), 7.68 (m, 1H), 7.60 (m, 1H) 6.95 (m, 1H), 6.63 (m, 1H), 6.04 (d, 2H), 3.69 (m, 1H), 1.97 (m, 1H), 1.87 (m, 1H), 1.65 (m, 3H), 1.53 (m, 3H), 1.22 (m, 1H), 1.02 – 0.78 (m, 4H), 0.78 – 0.52 (m, 1H). MS m/z: for Chemical Formula: $C_{28}H_{27}BrN_4O_3$ [M + H]+ 546.13 (calcd.) 547.0 (found.) MS m/z: for Chemical Formula: $C_{28}H_{27}BrN_4O_3$ [M + H]+ 546.13 (calcd.) 547.3 (found.)MS m/z: for Chemical Formula: $C_{28}H_{27}BrN_4O_3$ [M + H]+ 546.13 (calcd.) 548.3 (found.) Purity testing by HPLC (Acquisition method - 75%-95% Acetonitrile 10 minutes) t_R = 2.134 minutes. Purity=98%.

Synthesis of (S)-2-(6-bromobenzo-1,3-dioxol-5-yl)-1-(1-cyclohexylethyl)-N-(quinolin-3-yl)-1H-benzo[d]imidazole-5-carboxamide. (Compound 9a)

The method similar for the preparation of AZ3451 was used except replacing the building block (R group) with 3-aminoquinoline (44.6mg, 0.31mmol). And the reaction time for reflux is change to 8 hours. Purification with similar method by the crude product was purified by column B and further purification by column C. A brown solid product-60mg (48.7%) was obtained. ^{1}H NMR (500 MHz, $CDCl_3$) δ 11.04 – 10.62 (m, 1H), 9.07 (m, 1H), 8.89 (s, 1H), 8.79 (m, 1H), 8.06 (d, 1H), 7.98 (d, 1H), 7.83 (t, 1H), 7.66 – 7.57 (m, 1H), 7.54 (t, 1H), 6.79 (m, 1H), 6.54 (m, 1H), 5.74 (m, 1H), 5.31 – 4.88 (m, 1H), 3.82 – 3.55 (m, 1H), 2.00 (m, 1H), 1.86 (m, 2H), 1.73 (m, 1H), 1.64 – 1.46 (m, 4H), 1.32 – 1.14 (m, 1H), 1.11 – 0.89 (m, 3H), 0.84 – 0.68 (m, 1H), 0.57 (m, 1H). MS m/z: for Chemical Formula: $C_{32}H_{29}BrN_4O_3$ [M + H]+ 596.14 (calcd.) 597.1 (found.) Purity testing by HPLC (Acquisition method - 65%-95% Acetonitrile 10 minutes) t_R = 3.909 minutes. Purity=99%.

Synthesis of (S)-2-(6-bromobenzo-1,3-dioxol-5-yl)-1-(1-cyclohexylethyl)-N-(quinolin-6-yl)-1H-benzo[d]imidazole-5-carboxamide. (Compound 9b)

The method similar for the preparation of compound 9a was used except replacing the building block (R group) with 6-aminoquinoline (45mg, 0.32mmol). And the reaction time for reflux is change to 8 hours. Purification with similar method by the crude product was purified by column B and further purification by column C. A brown solid product-75mg (60.9%) was obtained. ^1H NMR (500 MHz, $CDCl_3$) δ 10.27 (m, 1H), 8.84 (s, 1H), 8.68 (m, 1H), 8.50 (m, 1H), 8.15 (m, 1H), 7.99 (m, 1H), 7.87 (m, 1H), 7.60 (m, 1H), 7.41 – 7.34 (m, 1H), 6.80 (m, 1H), 6.60 – 6.47 (m, 1H), 5.90 – 5.81 (m, 1H), 5.45 (m, 1H), 3.82 – 3.59 (m, 1H), 2.09 – 1.92 (m, 1H), 1.87 (m, 1H), 1.69 (m, 3H), 1.60 – 1.45 (m, 3H), 1.21 (m, 1H), 1.11 – 0.72 (m, 4H), 0.69 – 0.44 (m, 1H). MS m/z: for Chemical Formula: $C_{32}H_{29}BrN_4O_3$ [M + H]+ 596.14 (calcd.) 597.2 (found.) Purity testing by HPLC (Acquisition method - 65%-95% Acetonitrile 10 minutes) t_R = 2.625 minutes. Purity=99%.

Synthesis of (S)-2-(6-bromobenzo-1,3-dioxol-5-yl)-1-(1-cyclohexylethyl)-N-(quinolin-8-yl)-1H-benzo[d]imidazole-5-carboxamide. (Compound 9c)

The method similar for the preparation of compound 9a was used except replacing the building block (R group) with 8-aminoquinoline (45.6mg, 0.311mmol). And the reaction time for reflux is change to 8 hours. Purification with similar method by the crude product was purified by column and further purification by column D. A light-brown solid product-93mg (68.9%) was obtained. ^{1}H NMR (500 MHz, $CDCl_3$) δ 10.94 (m, 1H), 8.97 (m, 1H), 8.84 (s, 1H), 8.60 (m, 1H), 8.19 (m, 1H), 8.10 (m, 1H), 7.73 (m, 1H), 7.61 (m, 1H), 7.54 (m, 1H), 7.19 (m, 1H), 6.87 (m, 1H), 6.13 (m, 2H), 3.95 – 3.77 (m, 1H), 2.10 (m, 1H), 1.96 (m, 1H), 1.79 (m, 3H), 1.70 – 1.52 (m, 3H), 1.41 – 1.19 (m, 1H), 1.12 – 0.80 (m, 4H), 0.78 – 0.58 (m, 1H). MS m/z: for Chemical Formula: $C_{32}H_{29}BrN_4O_3$ [M + H]+ 596.14 (calcd.) 599.1 (found.) Purity testing by HPLC (Acquisition method - 75%-95% Acetonitrile 10 minutes) t_R = 8.675 minutes. Purity=94%.

Synthesis of (S)-2-(6-bromobenzo-1,3-dioxol-5-yl)-1-(1-cyclohexylethyl)-N-(3-ethynylphenyl)-1H-benzo[d]imidazole-5-carboxamide. (Compound 10a)

The method similar for the preparation of AZ3451 was used except replacing the building block (R group) with 3-ethynyaniline (35.6mg, 0.312mmol). And the reaction time for reflux is change to 6 hours. Purification with similar method by the crude product was purified by column B and further purification by column C. A light-yellow solid product-68mg (59.6%) was obtained. ^{1}H NMR (500 MHz, $CDCl_3$) δ 9.14 (m, 1H), 8.45 (m, 1H), 7.95 – 7.85 (m, 2H), 7.69 (m, 1H), 7.62 (m, 1H), 7.23 (m, 1H), 7.06 – 6.95 (m, 1H), 6.74 – 6.62 (m, 1H), 6.11 – 6.01 (d, 2H), 3.87 – 3.67 (m, 1H), 3.07 (s, 1H), 2.09 (m, 1H), 1.86 (m, 1H), 1.73 (m, 3H), 1.62 – 1.47 (m, 3H), 1.30 – 1.16 (m, 1H), 1.13 – 0.76 (m, 4H), 0.62 (m, 1H). MS m/z: for Chemical Formula: $C_{31}H_{28}BrN_3O_3$ [M + H]+ 569.13 (calcd.) 570.0 (found.) Purity testing by HPLC (Acquisition method - 75%-95% Acetonitrile 10 minutes) t_R = 2.980 minutes. Purity=96%.

Synthesis of (S)-2-(6-bromobenzo-1,3-dioxol-5-yl)-1-(1-cyclohexylethyl)-N-(4-ethynylphenyl)-1H-benzo[d]imidazole-5-carboxamide. (Compound 10b)

The method similar for the preparation of compound 10a was used except replacing the building block (R group) by 4-ethynyaniline (42.6mg, 0.301mmol). Purification with similar method by the crude product was purified by column B and further purification by column C. A light-yellow solid product-70mg (60.6%) was obtained. ^{1}H NMR (500 MHz, $CDCl_3$) δ 9.57 (m, 1H), 8.49 (m, 1H), 7.92 (m, 1H), 7.69 (m, 1H), 7.59 (m, 1H), 7.42 (m, 2H), 7.03 – 6.90 (m, 1H), 6.63 (m, 1H), 6.06 (d, 2H), 3.85 – 3.63 (m, 1H), 3.06 (s, 1H), 2.09 – 1.86 (m, 1H), 1.74 (m, 1H), 1.66 (m, 3H), 1.63 – 1.47 (m, 3H), 1.29 – 1.17 (m, 1H), 1.11 – 0.75 (m, 4H), 0.70 – 0.48 (m, 1H). MS m/z: for Chemical Formula: $C_{31}H_{28}BrN_3O_3$ [M + H]+ 569.13 (calcd.) 570.0 (found.)

Synthesis of (S)-2-(6-bromobenzo-1,3-dioxol-5-yl)-N-(4-bromophenyl)-1-(1-cyclohexylethyl)-1H-benzo[d]imidazole-5-carboxamide. (Compound 11a)

The method similar for the preparation of AZ3451 was used except replacing the building block (R group) by 4-Bromoaniline (82.6mg, 0.477mmol). And the reaction time for reflux is change to 7 hours. Purification with similar method by the crude product was purified by column B and further purification by column C. A white-yellow solid product-50mg (43.6%) was obtained. ^{1}H NMR (500 MHz, $CDCl_3$) δ 9.76 (m, 1H), 8.53 (m, 1H), 7.91 (m, 1H), 7.60 (m, 2H), 7.38 (m, 2H), 7.00 – 6.89 (m, 1H), 6.65 – 6.52 (m, 1H), 6.05 (d, 2H), 3.85 – 3.61 (m, 1H), 2.08 – 1.93 (m, 1H), 1.88 (m, 1H), 1.70 (m, 3H), 1.62 – 1.45 (m, 3H), 1.31 – 1.16 (m, 1H), 1.11 – 0.74 (m, 4H), 0.72 – 0.48 (m, 1H). MS m/z: for Chemical Formula: $C_{29}H_{27}Br_2N_3O_3$ [M + H]+ 623.04 (calcd.) 626.3

(found.) Purity testing by HPLC (Acquisition method - 65%-95% Acetonitrile 10 minutes) t_R = 6.740 minutes. Purity=98%.

Synthesis of (S)-2-(6-bromobenzo-1,3-dioxol-5-yl)-1-(1-cyclohexylethyl)-N-(pyridin-2-ylmethyl)-1H-benzo[d]imidazole-5-carboxamide. (Compound 12a)

The method similar for the preparation of AZ3451 was used except replacing the building block (R group) by 2-(Amino methyl) pyridine (33.6mg, 0.309mmol). And the reaction time for reflux is change to 6 hours. Purification with similar method by the crude product was purified by column B and further purification by column C. A light-yellow solid product-74.8mg (63.7%) was obtained. ^{1}H NMR (500 MHz, $CDCl_3$) δ 8.56 (m, 1H), 8.32 (m, 1H), 7.90 (m, 1H), 7.74 (m, 1H), 7.71 – 7.60 (m, 2H), 7.35 (m, 1H), 7.19 (m, 1H), 6.84 (m, 1H), 6.11 (d, 2H), 4.81 (m, 2H), 3.90 – 3.73 (m, 1H), 2.05 (m, 1H), 1.93 (m, 1H), 1.76 (m, 3H), 1.57 (m, 3H), 1.23 (m, 1H), 1.10 – 0.79 (m, 4H), 0.75 – 0.52 (m, 1H). MS m/z: for Chemical Formula: $C_{29}H_{29}BrN_4O_3$ [M + H]+ 560.14 (calcd.) 561.4 (found.) Purity testing by HPLC (Acquisition method - 50%-95% Acetonitrile 10 minutes) t_R = 2.103 minutes. Purity=99%.

Synthesis of (S)-N-([1,1'-biphenyl]-2-yl)-2-(6-bromobenzo-1,3-dioxol-5-yl)-1-(1-cyclohexylethyl)-1H-benzo[d]imidazole-5-carboxamide. (Compound 13a)

The method similar for the preparation of AZ3451 was used except replacing the building block (R group) by 2-Aminobiphenyl (52.6mg, 0.31mmol). And the reaction time for reflux is change to 6 hours. Purification with similar method by the crude product was purified by column B and further purification by column C. A light-grey solid product-67mg (52.3%) was obtained. ^{1}H NMR (500 MHz, $CDCl_3$) δ 8.59 (m, 1H), 8.12 (s, 1H), 7.93 (m, 1H), 7.76 (m, 1H), 7.59 (m, 1H), 7.53

(m, 2H), 7.49 – 7.40 (m, 3H), 7.30 (m, 1H), 7.24 – 7.18 (m, 1H), 7.08 (m, 1H), 6.81 (m, 1H), 6.10 (d, 2H), 3.88 – 3.71 (m, 1H), 1.96 (m, 2H), 1.75 (m, 3H), 1.37 – 1.20 (m, 4H), 1.09 – 0.78 (m, 4H), 0.73 – 0.51 (m, 1H). MS m/z: for Chemical Formula: $C_{35}H_{32}BrN_3O_3$ [M + H]+ 621.16 (calcd.) 622.22 (found.) Purity testing by HPLC (Acquisition method - 65%-95% Acetonitrile 10 minutes) t_R = 6.361 minutes. Purity=95%.

Synthesis of (S)-2-(6-bromobenzo-1,3-dioxol-5-yl)-1-(1-cyclohexylethyl)-N-(4-phenoxyphenyl)-1H-benzo[d]imidazole-5-carboxamide. (Compound 14a)

The method similar for the preparation of AZ3451 was used except replacing the building block (R group) by 4-phenoxyaniline(43.6mg, 0.3mmol) . And the reaction time for reflux is change to 5 hours. Purification with similar method by the column B and further purification by column C. A brown solid product-91mg (57%) was obtained. ^1H NMR (500 MHz, $CDCl_3$) δ 9.23 (m, 1H), 8.45 (m, 1H), 7.92 (m, 1H), 7.66 (m, 2H), 7.61 (m, 1H), 7.33 (m, 2H), 7.08 (m, 1H), 6.99 (m, 4H), 6.75 – 6.61 (m, 1H), 6.06 (d, 2H), 3.76 (m, 1H), 2.09 – 1.95 (m, 1H), 1.90 (m, 1H), 1.72 (m, 3H), 1.64 – 1.46 (m, 3H), 1.29 – 1.17 (m, 1H), 1.13 – 0.76 (m, 4H), 0.71 – 0.47 (m, 1H). MS m/z: for Chemical Formula: $C_{35}H_{32}BrN_3O_4$ [M + H]+ 637.16 (calcd.) 638.2 (found.) Purity testing by HPLC (Acquisition method - 75%-95% Acetonitrile 10 minutes) t_R = 4.832 minutes. Purity=98%.

Synthesis of (S)-2-(2-bromophenyl)-1-(1-cyclohexylethyl)-1H-benzoimidazole-5-carboxylic acid. (Compound 15)

The method similar for the preparation of compound 4 in Scheme1, except that 6-bromobenzo-d-1,3-dioxole-5-carbaldehyde was replaced by 2-Bromobenzaldehyde to made compound 13 in

Scheme 6. Purification with similar method by the crude product was purified by flash silica chromatography with an elution gradient 1:3 EtOAc: Hexane. And then, the column solvent system was changed to 1:1 EtOAc: Hexane. A dark-brown solid product 1034mg (85%) was obtained. ^{1}H NMR (500 MHz, $CDCl_3$) δ 8.67 (m, 1H), 8.09 (m, 1H), 7.78 (m, 1H), 7.65 (m, 1H), 7.52 – 7.47 (m, 2H), 7.43 – 7.40 (m, 1H), 3.90 – 3.69 (m, 1H), 2.03 (m, 1H), 1.97 (m, 1H), 1.78 (m, 3H), 1.65 – 1.58 (m, 3H), 1.26 – 1.18 (m, 1H), 0.95 – 0.78 (m, 4H), 0.73 – 0.50 (m, 1H). MS m/z: for Chemical Formula: $C_{22}H_{23}BrN_2O_2$ [M + H]+ 426.00 (calcd.) 427.7 (found.)

References

1. Blasberg RG. Molecular imaging and cancer. *Mol Cancer Ther*. 2003;2(3):335-343.

2. Wang J, Rizvi SMA, Madigan MC, et al. Characterization of Benign and Malignant Prostate Epithelial tHoechst 33342 Side Populations. *Prostate*. 2007;67(April):1384-1396. doi:10.1002/pros

3. Miller KD, Nogueira L, Mariotto AB, et al. Cancer treatment and survivorship statistics, 2019. *CA Cancer J Clin*. 2019;69(5):363-385. doi:10.3322/caac.21565

4. Advanced U, Cancer M, Cancer MA, et al. Advanced and Metastatic Cancer Understanding Advanced and Metastatic Cancer. Published online 2016:1-26.

5. Gaudette LA, Illing EM, Hill GB. Canadian Cancer Statistics 1991. *Health Rep*. 1991;3(2):107-135.

6. Rosling H. Lung Cancer Statistics [video]. 2009;2010(888):2-5. http://www.gapminder.org/videos/lung-cancer-statistics/

7. Miller JM. Breast cancer statistics. *Mayo Clin Proc*. 1980;55(9):585.

8. Hristova L, Hakama M. Effect of screening for cancer in the Nordic countries on deaths, cost and quality of life up to the year 2017. *Acta Oncol Suppl*. 1997;36(9). doi:10.1080/0284186x.1997.11835453

9. Brawley OW, Kramer BS. Cancer screening in theory and in practice. *J Clin Oncol*. 2005;23(2):293-300. doi:10.1200/JCO.2005.06.107

10. Forbes JF. Multimodality treatment of cancer. *Aust N Z J Surg*. 1982;52(4):341-346. doi:10.1111/j.1445-2197.1982.tb06005.x

11. Kircher MF, Hricak H, Larson SM. Molecular imaging for personalized cancer care. *Mol Oncol*. 2012;6(2):182-195. doi:10.1016/j.molonc.2012.02.005

12. Holland JP, Liang SH, Rotstein BH, et al. Alternative approaches for PET radiotracer development in Alzheimer's disease: Imaging beyond plaque. *J Label Compd Radiopharm*. 2014;57(4):323-331. doi:10.1002/jlcr.3158

13. James ML, Gambhir SS. A molecular imaging primer: Modalities, imaging agents, and applications. *Physiol Rev*. 2012;92(2):897-965. doi:10.1152/physrev.00049.2010

14. Gambhir SS. Molecular imaging of cancer with positron emission tomography. *Nat Rev Cancer*. 2002;2(9):683-693. doi:10.1038/nrc882

15. Blahd WH. Ben Cassen and the development of the rectilinear scanner. *Semin Nucl Med*. 1996;26(3):165-170. doi:10.1016/S0001-2998(96)80021-3

16. Kraus VB. Biomarkers as drug development tools: Discovery, validation, qualification and use. *Nat Rev Rheumatol*. 2018;14(6):354-362. doi:10.1038/s41584-018-0005-9

17. Shoichet BK, McGovern SL, Wei B, Irwin JJ. Lead discovery using molecular docking. *Curr Opin Chem Biol*. 2002;6(4):439-446. doi:10.1016/S1367-5931(02)00339-3

18. Hughes JP, Rees SS, Kalindjian SB, Philpott KL. Principles of early drug discovery. *Br J Pharmacol*. 2011;162(6):1239-1249. doi:10.1111/j.1476-5381.2010.01127.x

19. Thompson S, Kilbourn MR, Scott PJH. Radiochemistry, PET imaging, and the internet of chemical things. *ACS Cent Sci*. 2016;2(8):497-505. doi:10.1021/acscentsci.6b00178

20. Chen K, Chen X. Positron emission tomography imaging of cancer biology: Current status and future prospects. *Semin Oncol*. 2011;38(1):70-86.

doi:10.1053/j.seminoncol.2010.11.005

21. Chen DL, Schuster DP. Imaging pulmonary inflammation with positron emission tomography: A biomarker for drug development. *Mol Pharm*. 2006;3(5):488-495. doi:10.1021/mp060050w

22. Jacobson O, Kiesewetter DO, Chen X. Fluorine-18 radiochemistry, labeling strategies and synthetic routes. *Bioconjug Chem*. 2015;26(1):1-18. doi:10.1021/bc500475e

23. Alauddin MM. Positron emission tomography (PET) imaging with. *Am J Nucl Med Mol Imaging*. 2012;2(1):55-76.

24. Miller PW, Long NJ, Vilar R, Gee AD. Synthesis of11C, 18F, 15O, and 13N radiolabels for positron emission tomography. *Angew Chemie - Int Ed*. 2008;47(47):8998-9033. doi:10.1002/anie.200800222

25. Production and use of PET radioisotopes Teacher resource. 2019;(August).

26. Piel M, Vernaleken I, Rösch F. Positron emission tomography in CNS drug discovery and drug monitoring. *J Med Chem*. 2014;57(22):9232-9258. doi:10.1021/jm5001858

27. Phelps ME. Positron emission tomography provides molecular imaging of biological processes. *Proc Natl Acad Sci U S A*. 2000;97(16):9226-9233. doi:10.1073/pnas.97.16.9226

28. Hovhannisyan N, Dhilly M, Guillouet S, Leporrier M, Barré L. Comparative Analysis between [18F]Fludarabine-PET and [18F]FDG-PET in a Murine Model of Inflammation. *Mol Pharm*. 2016;13(6):2136-2139. doi:10.1021/acs.molpharmaceut.6b00050

29. Gallamini A, Zwarthoed C, Borra A. Positron emission tomography (PET) in oncology.

Cancers (Basel). 2014;6(4):1821-1889. doi:10.3390/cancers6041821

30. Hofman MS, Hicks RJ. How We Read Oncologic FDG PET/CT. *Cancer Imaging*. 2016;16(1):1-14. doi:10.1186/s40644-016-0091-3

31. Pet F, Pet F, Fdg- T, et al. Imaging : Molecular or Molecular Imaging : A Tool for Developing Central Nervous. :31-32.

32. Dang C V. Links between metabolism and cancer. *Genes Dev*. 2012;26(9):877-890. doi:10.1101/gad.189365.112

33. Liberti M V., Locasale JW. Correction to: "The Warburg Effect: How Does it Benefit Cancer Cells?". [Trends in Biochemical Sciences, 41 (2016) 211]. *Trends Biochem Sci*. 2016;41(3):287. doi:10.1016/j.tibs.2016.01.004

34. Lind P, Igerc I, Beyer T, Reinprecht P, Hausegger K. Advantages and limitations of FDG PET in the follow-up of breast cancer. *Eur J Nucl Med Mol Imaging*. 2004;31(SUPPL. 1). doi:10.1007/s00259-004-1535-8

35. Rosenbaum DM, Rasmussen SGF, Kobilka BK. The structure and function of G-protein-coupled receptors. *Nature*. 2009;459(7245):356-363. doi:10.1038/nature08144

36. Sriram K, Insel PA. G protein-coupled receptors as targets for approved drugs: How many targets and how many drugs? *Mol Pharmacol*. 2018;93(4):251-258. doi:10.1124/mol.117.111062

37. Jeffrey Conn P, Christopoulos A, Lindsley CW. Allosteric modulators of GPCRs: A novel approach for the treatment of CNS disorders. *Nat Rev Drug Discov*. 2009;8(1):41-54. doi:10.1038/nrd2760

38. Cherezov V, Rosenbaum DM, Hanson MA, et al. High-resolution crystal structure of an engineered human β2-adrenergic G protein-coupled receptor. *Science (80-)*. 2007;318(5854):1258-1265. doi:10.1126/science.1150577

39. Lesarge JC. Scholarship @ Western Design , Synthesis , and Evaluation of Novel Protease-Activated Receptor 2 (PAR2) -Targeting Imaging Agents for Cancer Keywords. 2018;2.

40. Digby GJ, Lober RM, Sethi PR, Lambert NA. Some G protein heterotrimers physically dissociate in living cells. *Proc Natl Acad Sci U S A*. 2006;103(47):17789-17794. doi:10.1073/pnas.0607116103

41. Trzaskowski B, Latek D, Yuan S, Ghoshdastider U, Debinski A, Filipek S. Action of Molecular Switches in GPCRs - Theoretical and Experimental Studies. *Curr Med Chem*. 2012;19(8):1090-1109. doi:10.2174/092986712799320556

42. Luttrell LM, Lefkowitz RJ. The role of β-arrestins in the termination and transduction of G-protein-coupled receptor signals. *J Cell Sci*. 2002;115(3):455-465.

43. Ramachandran R, Noorbakhsh F, Defea K, Hollenberg MD. Targeting proteinase-activated receptors: Therapeutic potential and challenges. *Nat Rev Drug Discov*. 2012;11(1):69-86. doi:10.1038/nrd3615

44. Cheng RKY, Fiez-Vandal C, Schlenker O, et al. Structural insight into allosteric modulation of protease-activated receptor 2. *Nature*. 2017;545(7652):112-115. doi:10.1038/nature22309

45. Hamilton JR, Trejo J. Challenges and opportunities in protease-activated receptor drug

development. *Annu Rev Pharmacol Toxicol*. 2017;57(September 2016):349-373. doi:10.1146/annurev-pharmtox-011613-140016

46. Bonaca MP, Scirica BM, Creager MA, et al. Vorapaxar in patients with peripheral artery disease results from TRA2°P-TIMI 50. *Circulation*. 2013;127(14):1522-1529. doi:10.1161/CIRCULATIONAHA.112.000679

47. Abdulsattar Y, Ternas T, Garcia D. Vorapaxar: Targeting a novel antiplatelet pathway. *P T*. 2011;36(9):564-568.

48. Bunnett N, Defea K, Hamilton J, Hollenberg MD, Ramachandran R. Proteinase-activated receptors (version 2019 . 4) in the IUPHAR / BPS Guide to Pharmacology Database. Published online 2019:1-8.

49. Adams MN, Ramachandran R, Yau MK, et al. Structure, function and pathophysiology of protease activated receptors. *Pharmacol Ther*. 2011;130(3):248-282. doi:10.1016/j.pharmthera.2011.01.003

50. Jiang Y, Yau MK, Lim J, et al. A potent antagonist of protease-Activated receptor 2 that inhibits multiple signaling functions in human cancer cells s. *J Pharmacol Exp Ther*. 2018;364(2):246-257. doi:10.1124/jpet.117.245027

51. Kelso EB, Lockhart JC, Hembrough T, et al. Therapeutic promise of proteinase-activated receptor-2 antagonism in joint inflammation. *J Pharmacol Exp Ther*. 2006;316(3):1017-1024. doi:10.1124/jpet.105.093807

52. Ungefroren H, Witte D, Rauch BH, et al. Proteinase-activated receptor 2 may drive cancer progression by facilitating TGF-β signaling. *Int J Mol Sci*. 2017;18(11).

doi:10.3390/ijms18112494

53. Yau MK, Lim J, Liu L, Fairlie DP. Protease activated receptor 2 (PAR2) modulators: A patent review (2010-2015). *Expert Opin Ther Pat*. 2016;26(4):471-483. doi:10.1517/13543776.2016.1154540

54. Yau MK, Liu L, Fairlie DP. Toward drugs for protease-activated receptor 2 (PAR2). *J Med Chem*. 2013;56(19):7477-7497. doi:10.1021/jm400638v

55. Kagota S, Maruyama K, McGuire JJ. Characterization and Functions of Protease-Activated Receptor 2 in Obesity, Diabetes, and Metabolic Syndrome: A Systematic Review. *Biomed Res Int*. 2016;2016. doi:10.1155/2016/3130496

56. Suen JY, Cotterell A, Lohman RJ, et al. Pathway-selective antagonism of proteinase activated receptor 2. *Br J Pharmacol*. 2014;171(17):4112-4124. doi:10.1111/bph.12757

57. Lohman R, Cotterell AJ, Barry GD, et al. An antagonist of human protease activated receptor-2 attenuates PAR2 signaling, macrophage activation, mast cell degranulation, and collagen-induced arthritis in rats. *FASEB J*. 2012;26(7):2877-2887. doi:10.1096/fj.11-201004

58. Pan SL, Tao KY, Guh JH, et al. The p38 mitogen-activated protein kinase pathway plays a critical role in PAR2-induced endothelial IL-8 production and leukocyte adhesion. *Shock*. 2008;30(5):496-502. doi:10.1097/SHK.0b013e3181673233

59. Cui C, Merritt R, Fu L, Pan Z. Targeting calcium signaling in cancer therapy. *Acta Pharm Sin B*. 2017;7(1):3-17. doi:10.1016/j.apsb.2016.11.001

60. Bong AHL, Monteith GR. Calcium signaling and the therapeutic targeting of cancer cells.

Biochim Biophys Acta - Mol Cell Res. 2018;1865(11):1786-1794. doi:10.1016/j.bbamcr.2018.05.015

61. Agonists SP-, Lund BW, Bertozzi SM, et al. Discovery of Potent and Selective Small-Molecule PAR-2 Agonists. Published online 2008:5490-5493.

62. Suen JY, Barry GD, Lohman RJ, et al. Modulating human proteinase activated receptor 2 with a novel antagonist (GB88) and agonist (GB110). *Br J Pharmacol*. 2012;165(5):1413-1423. doi:10.1111/j.1476-5381.2011.01610.x

63. Barry GD, Suen JY, Le GT, Cotterell A, Reid RC, Fairlie DP. Novel agonists and antagonists for human protease activated receptor 2. *J Med Chem*. 2010;53(20):7428-7440. doi:10.1021/jm100984y

64. Heuberger DM, Schuepbach RA. Correction to: Protease-activated receptors (PARs): Mechanisms of action and potential therapeutic modulators in PAR-driven inflammatory diseases (Thrombosis Journal (2019) 17: 4 DOI: 10.1186/s12959-019-0194-8). *Thromb J*. 2019;17(1):1-24. doi:10.1186/s12959-019-0212-x

65. Meanwell NA. Fluorine and Fluorinated Motifs in the Design and Application of Bioisosteres for Drug Design. *J Med Chem*. 2018;61(14):5822-5880. doi:10.1021/acs.jmedchem.7b01788

66. Liao GJ, Clark AS, Schubert EK, Mankoff DA. 18F-fluoroestradiol PET: Current status and potential future clinical applications. *J Nucl Med*. 2016;57(8):1269-1275. doi:10.2967/jnumed.116.175596

67. Johnson BM, Shu YZ, Zhuo X, Meanwell NA. Metabolic and Pharmaceutical Aspects of

Fluorinated Compounds. *J Med Chem*. 2020;63(12):6315-6386. doi:10.1021/acs.jmedchem.9b01877

68. Rotstein BH, Stephenson NA, Vasdev N, Liang SH. Spirocyclic hypervalent iodine(III)-mediated radiofluorination of non-activated and hindered aromatics. *Nat Commun*. 2014;5(May):1-7. doi:10.1038/ncomms5365

69. Rotstein BH, Wang L, Liu RY, et al. Mechanistic studies and radiofluorination of structurally diverse pharmaceuticals with spirocyclic iodonium(III) ylides. *Chem Sci*. 2016;7(7):4407-4417. doi:10.1039/c6sc00197a

70. Liang SH, Wang L, Stephenson NA, Rotstein BH, Vasdev N. Facile 18 F labeling of non-activated arenes via a spirocyclic iodonium(III) ylide method and its application in the synthesis of the mGluR 5 PET radiopharmaceutical [18 F]FPEB. *Nat Protoc*. 2019;14(5):1530-1545. doi:10.1038/s41596-019-0149-3

71. Salminen E, Hogg A, Binns D, Frydenberg M, Hicks R. Investigations with FDG-PET scanning in prostate cancer show limited value for clinical practice. *Acta Oncol (Madr)*. 2002;41(5):425-429. doi:10.1080/028418602320405005

72. Kennedy AJ, Sundström L, Geschwindner S, et al. Protease-activated receptor-2 ligands reveal orthosteric and allosteric mechanisms of receptor inhibition. *Commun Biol*. 2020;3(1). doi:10.1038/s42003-020-01504-0

73. Lu S, He X, Ni D, Zhang J. Allosteric Modulator Discovery: From Serendipity to Structure-Based Design. *J Med Chem*. 2019;62(14):6405-6421. doi:10.1021/acs.jmedchem.8b01749

74. Wiesmann C, Barr KJ, Kung J, et al. Allosteric inhibition of protein tyrosine phosphatase 1B. *Nat Struct Mol Biol*. 2004;11(8):730-737. doi:10.1038/nsmb803

75. Trinquet E, Bouhelal R, Dietz M. Monitoring Gq-coupled receptor response through inositol phosphate quantification with the IP-One assay. *Expert Opin Drug Discov*. 2011;6(10):981-994. doi:10.1517/17460441.2011.608658

76. Gardell LR, Ma JN, Seitzberg JG, et al. Identification and characterization of novel small-molecule protease-activated receptor 2 agonists. *J Pharmacol Exp Ther*. 2008;327(3):799-808. doi:10.1124/jpet.108.142570

77. Harvey JH, Van Rijn RM, Whistler JL. A FLIPR assay for evaluating agonists and antagonists of GPCR heterodimers. *Methods Mol Biol*. 2013;995(5):43-54. doi:10.1007/978-1-62703-345-9_4

78. Spillmann M, Thurner L, Romantini N, et al. New insights into arrestin recruitment to GPCRs. *Int J Mol Sci*. 2020;21(14):1-14. doi:10.3390/ijms21144949

79. Harrold MW, Zavod RM. Basic Concepts in Medicinal Chemistry. *Drug Dev Ind Pharm*. 2014;40(7):988-988. doi:10.3109/03639045.2013.789908

80. Cai L, Lu S, Pike VW. Chemistry with [18F]fluoride ion. *European J Org Chem*. 2008;(17):2853-2873. doi:10.1002/ejoc.200800114

81. Yerien DE, Bonesi S, Postigo A. Fluorination methods in drug discovery. *Org Biomol Chem*. 2016;14(36):8398-8427. doi:10.1039/c6ob00764c

82. Swinson J. Fluorine - A vital element in the medicine chest. *Pharmaceuticals*. Published online 2005:26-30.

83. Purser S, Moore PR, Swallow S, Gouverneur V. Fluorine in medicinal chemistry. *Chem Soc Rev*. 2008;37(2):320-330. doi:10.1039/b610213c

84. Guha R. On exploring structure-activity relationships. *Methods Mol Biol*. 2013;993:81-94. doi:10.1007/978-1-62703-342-8_6

85. Heravi MM, Zadsirjan V. Prescribed drugs containing nitrogen heterocycles: an overview. *RSC Adv*. 2020;10(72):44247-44311. doi:10.1039/d0ra09198g

86. Jampilek J. Heterocycles in medicinal chemistry. *Molecules*. 2019;24(21):10-13. doi:10.3390/molecules24213839

87. Rodríguez E, Arqués JL, Rodríguez R, et al. We are IntechOpen , the world ' s leading publisher of Open Access books Built by scientists , for scientists TOP 1 %. *Intech*. 1989;32(tourism):137-144. https://www.intechopen.com/books/advanced-biometric-technologies/liveness-detection-in-biometrics

88. Banert K, Seifert J. Steric hindrance classified: Treatment of isothiocyanatoallene with secondary amines bearing bulky substituents to generate 2-aminothiazoles. *Org Chem Front*. 2019;6(20):3517-3522. doi:10.1039/c9qo00312f

89. Hu Z, Zhao T, Wang M, Wu J, Yu W, Chang J. I2-Mediated Intramolecular C-H Amidation for the Synthesis of N-Substituted Benzimidazoles. *J Org Chem*. 2017;82(6):3152-3158. doi:10.1021/acs.joc.7b00142

90. cyclization-mechanism.pdf.

91. Hou J, Kovacs MS, Dhanvantari S, Luyt LG. Development of Candidates for Positron Emission Tomography (PET) Imaging of Ghrelin Receptor in Disease: Design, Synthesis,

and Evaluation of Fluorine-Bearing Quinazolinone Derivatives. *J Med Chem*. 2018;61(3):1261-1275. doi:10.1021/acs.jmedchem.7b01754

92. Meng X-Y, Zhang H-X, Mezei M, Cui M. Molecular Docking: A Powerful Approach for Structure-Based Drug Discovery. *Curr Comput Aided-Drug Des*. 2012;7(2):146-157. doi:10.2174/157340911795677602

93. de Ruyck J, Brysbaert G, Blossey R, Lensink MF. Molecular docking as a popular tool in drug design, an in silico travel. *Adv Appl Bioinforma Chem*. 2016;9(1):1-11. doi:10.2147/AABC.S105289

94. Jarmoskaite I, Alsadhan I, Vaidyanathan PP, Herschlag D. How to measure and evaluate binding affinities. *Elife*. 2020;9:1-34. doi:10.7554/ELIFE.57264

95. Yu X, Li X, Song X, et al. Advantages and disadvantages of F-18 fluorodeoxyglucose positron emission tomography/computed tomography in carcinoma of unknown primary. *Oncol Lett*. 2016;12(5):3785-3792. doi:10.3892/ol.2016.5203

96. Lindner JR, Kahn ML, Coughlin SR, et al. Delayed Onset of Inflammation in Protease-Activated Receptor-2-Deficient Mice. *J Immunol*. 2000;165(11):6504-6510. doi:10.4049/jimmunol.165.11.6504

97. Majewski MW, Gandhi DM, Rosas R, Kodali R, Arnold LA, Dockendorff C. Design and Evaluation of Heterobivalent PAR1-PAR2 Ligands as Antagonists of Calcium Mobilization. *ACS Med Chem Lett*. 2019;10(1):121-126. doi:10.1021/acsmedchemlett.8b00538

98. Pierre O, Fouchard M, Buscaglia P, et al. Calcium Increase and Substance P Release

Induced by the Neurotoxin Brevetoxin-1 in Sensory Neurons: Involvement of PAR2 Activation through Both Cathepsin S and Canonical Signaling. *Cells*. 2020;9(12). doi:10.3390/cells9122704

99. Namkung Y, Le Gouill C, Lukashova V, et al. Monitoring G protein-coupled receptor and β-arrestin trafficking in live cells using enhanced bystander BRET. *Nat Commun*. 2016;7. doi:10.1038/ncomms12178

Appendix 1: Structures of AZ3451 Analogues.

(6a)

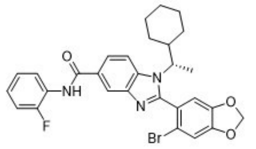
O
NH
F
N
N
Br
O
O

(6b)

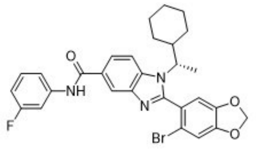
O
NH
F
N
N
Br
O
O

(6c)

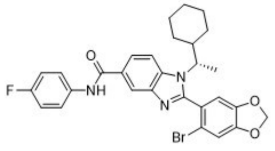
O
F
NH
N
N
Br
O
O

(7a)

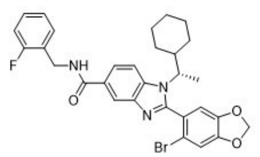
F
NH
O
N
N
Br
O
O

(7b)

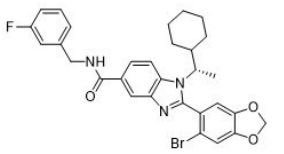
F
NH
O
N
N
Br
O
O

(7c)

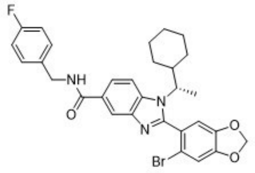
F
NH
O
N
N
Br
O
O

(8a)

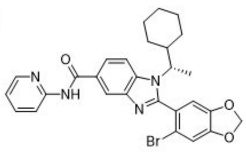
O
N
NH
N
N
Br
O
O

(8b)

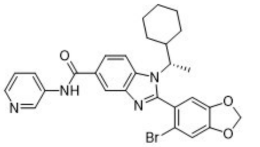
O
NH
N
N
N
Br
O
O

(8c)

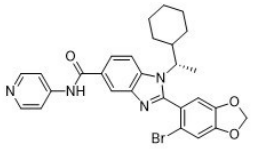
O
N
NH
N
N
Br
O
O

(9a)

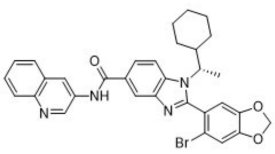
O
NH
N
N
N
Br
O
O

(9b)

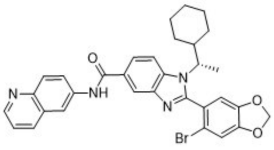
O
N
NH
N
N
Br
O
O

(9c)

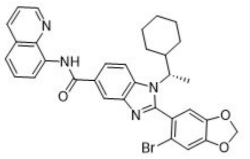
N
NH
O
N
N
Br
O
O

(10a)

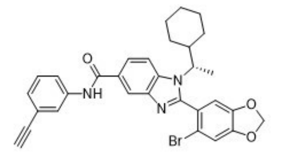

(10b)

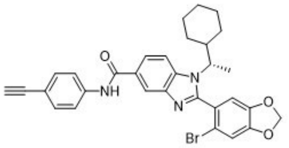

(11a)

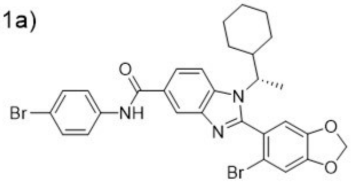
O
Br
NH
N
N
Br
O
O

(12a)

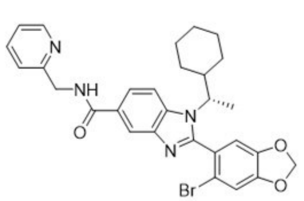
N
NH
O
N
N
Br
O
O

(13a)

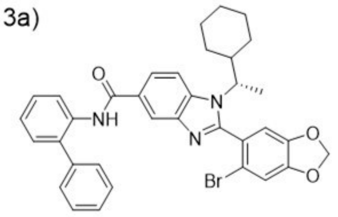

(14a)

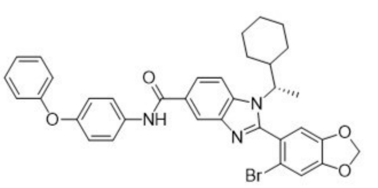
O
O
NH
N
N
Br
O
O

Appendix 2:

^{1}H-NMR spectra for compound 2

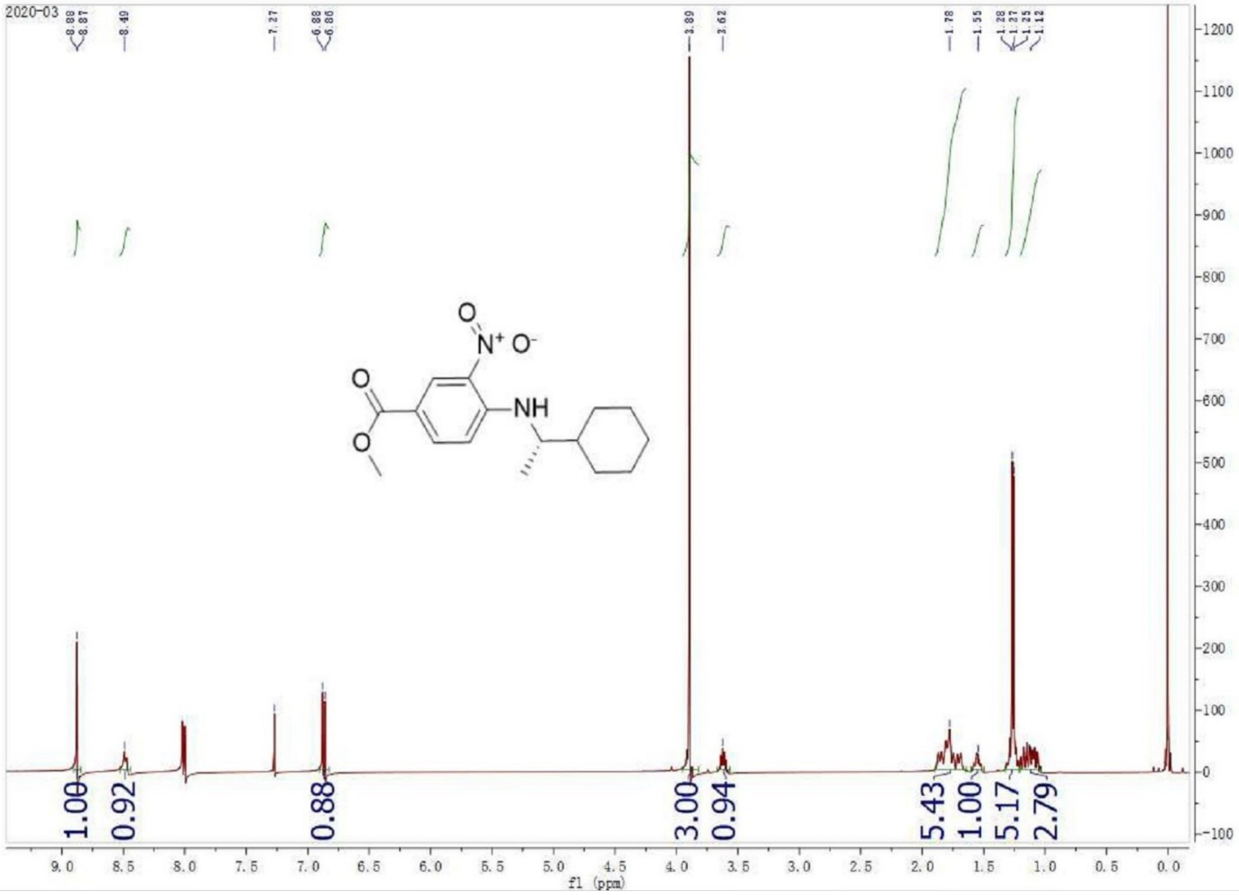

^{1}H-NMR spectra for compound 3

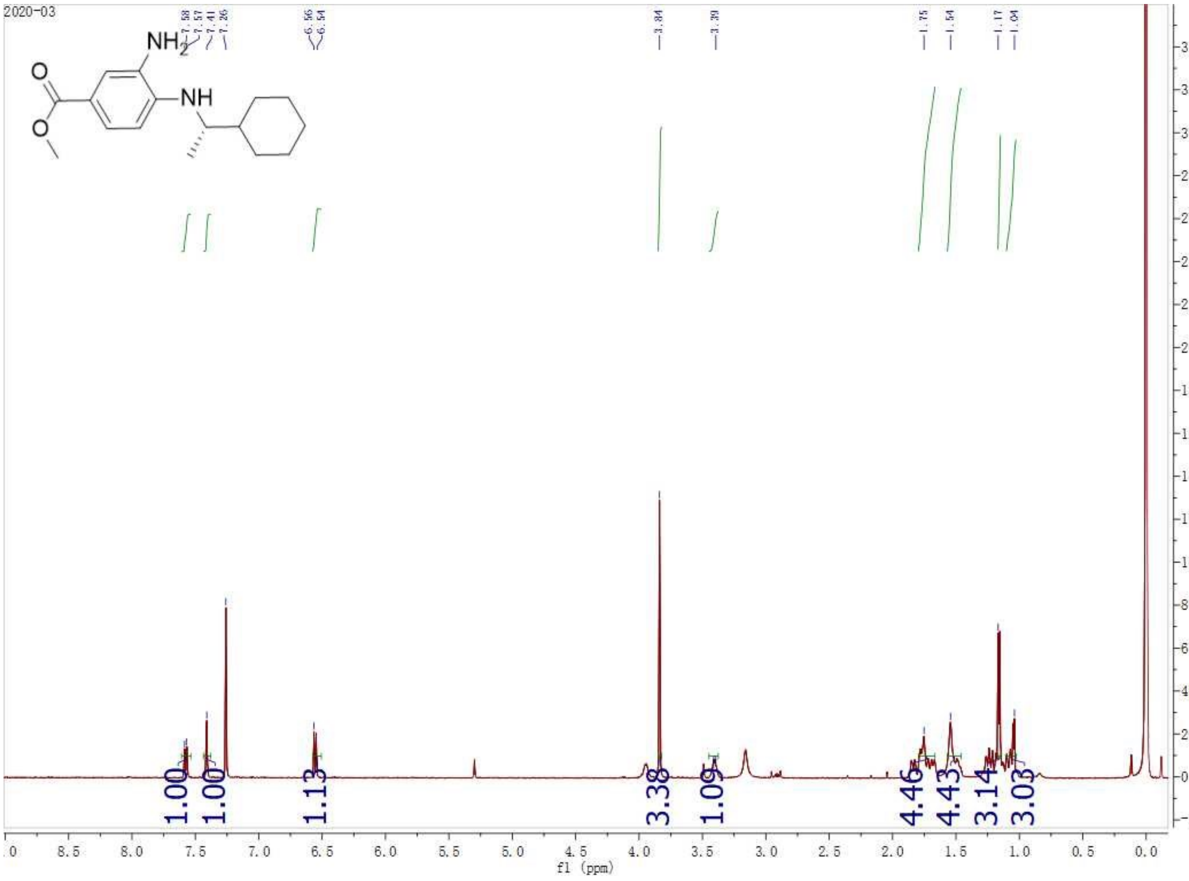

Characterization Data (Mass Spectroscopy, HPLC, and ^{1}H-NMR) for compound 4 (Carboxylic compound) and Compound 5 (AZ3451)

Compound 4. (S)-2-(6-bromobenzo[d] [1,3] dioxol-5-yl)-1-(1-cyclohexylethyl)-1H-benzo[d]imidazole-5-carboxylic acid.

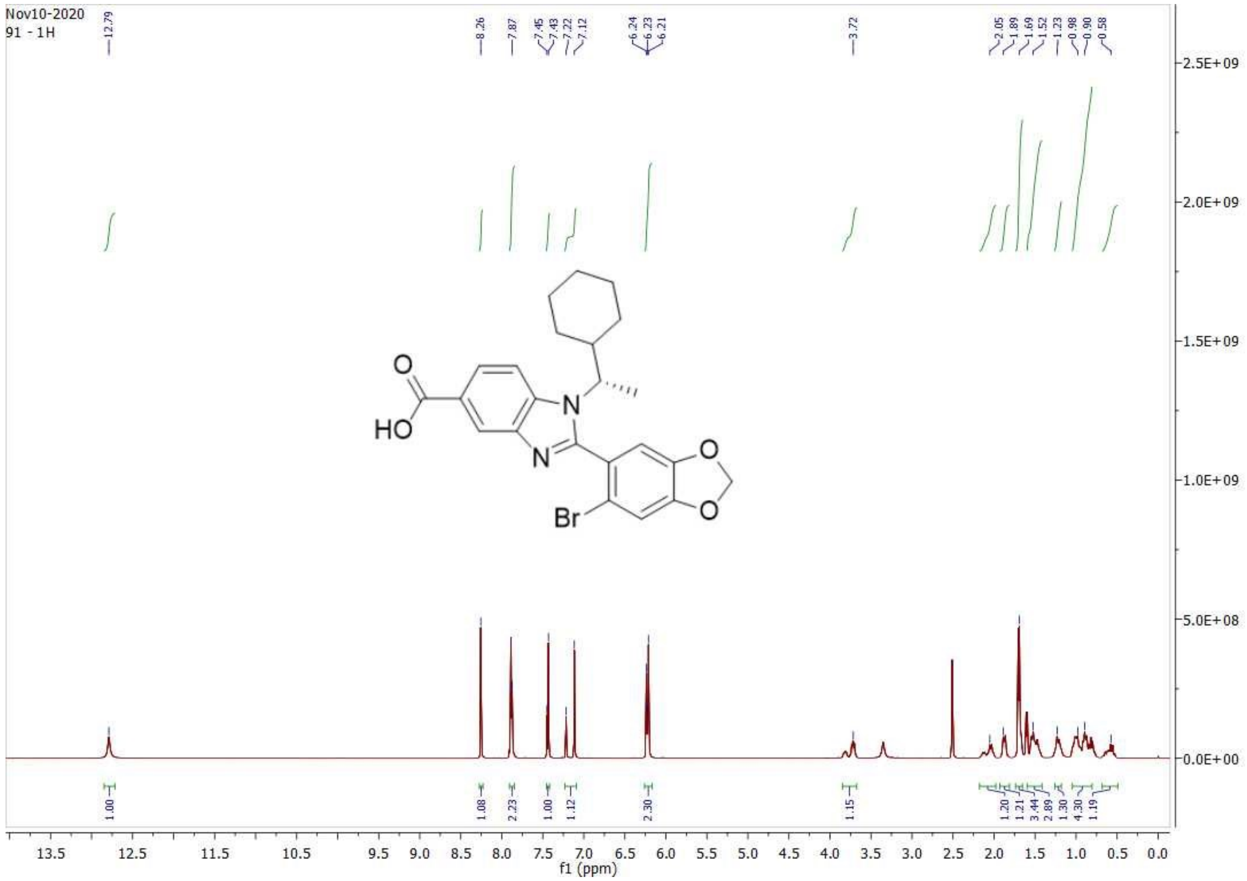
Nov10-2020
91 - 1H
12.79
8.26
7.87
7.45
7.43
7.22
7.12
6.24
6.23
6.21
3.72
2.05
1.89
1.69
1.52
1.23
0.98
0.90
0.58
2.5E+09
2.0E+09
1.5E+09
1.0E+09
5.0E+08
0.0E+00
1.00
1.08
2.23
1.00
1.12
2.30
1.15
1.20
1.21
3.44
2.89
1.30
4.30
1.19
13.5
12.5
11.5
10.5
9.5
9.0
8.5
8.0
7.5
7.0
6.5
6.0
5.5
5.0
4.5
4.0
3.5
3.0
2.5
2.0
1.5
1.0
0.5
0.0
f1 (ppm)
O
HO
N
N
O
O
Br

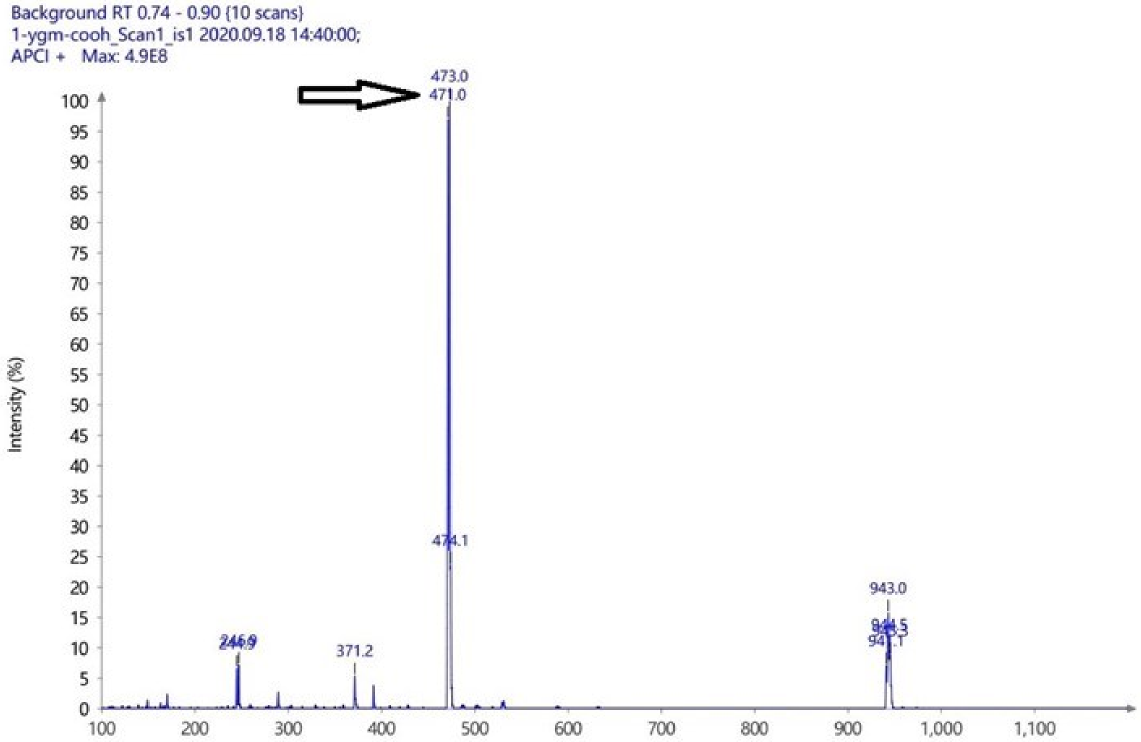

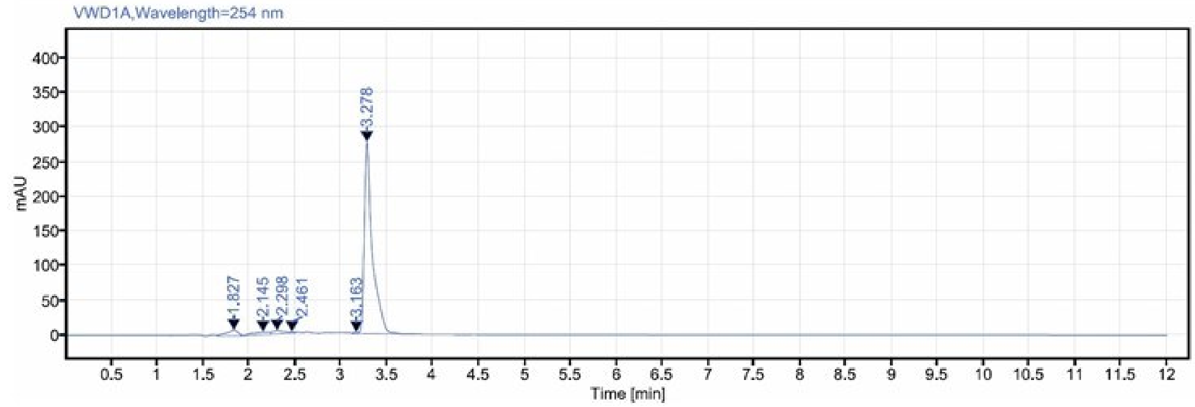

Signal: VWD1A,Wavelength=254 nm

RT [min]	Type	Width [min]	Area	Height	Area%	Name
1.827	VB	0.28	71.98	7.97	3.83	
2.145	BV	0.30	52.82	3.86	2.81	
2.298	VV	0.21	42.96	4.56	2.29	
2.461	VV	0.07	6.90	1.84	0.37	
3.163	VV	0.07	6.44	1.80	0.34	
3.278	VB	0.62	1696.27	276.07	90.35	
		Sum	1877.36			

AZ3451. 2-(6-Bromo-1,3-benzodioxol-5-yl)-N-(4-cyanophenyl)-1-[(1S)-1-cyclohexylethyl]-1H-benzimidazole-5-carboxamide.

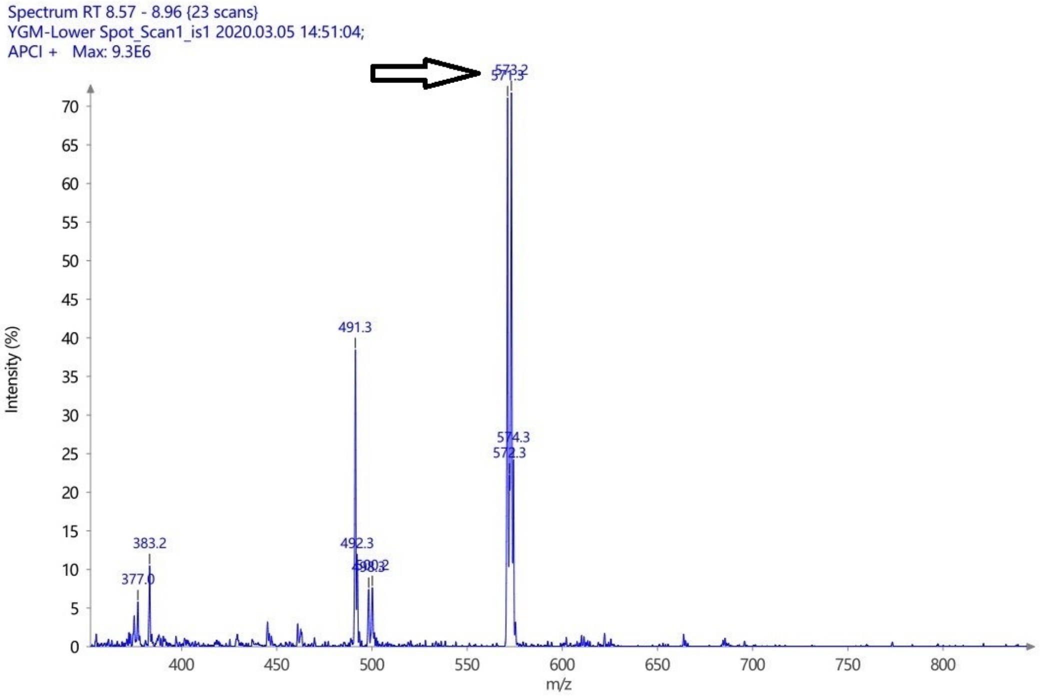

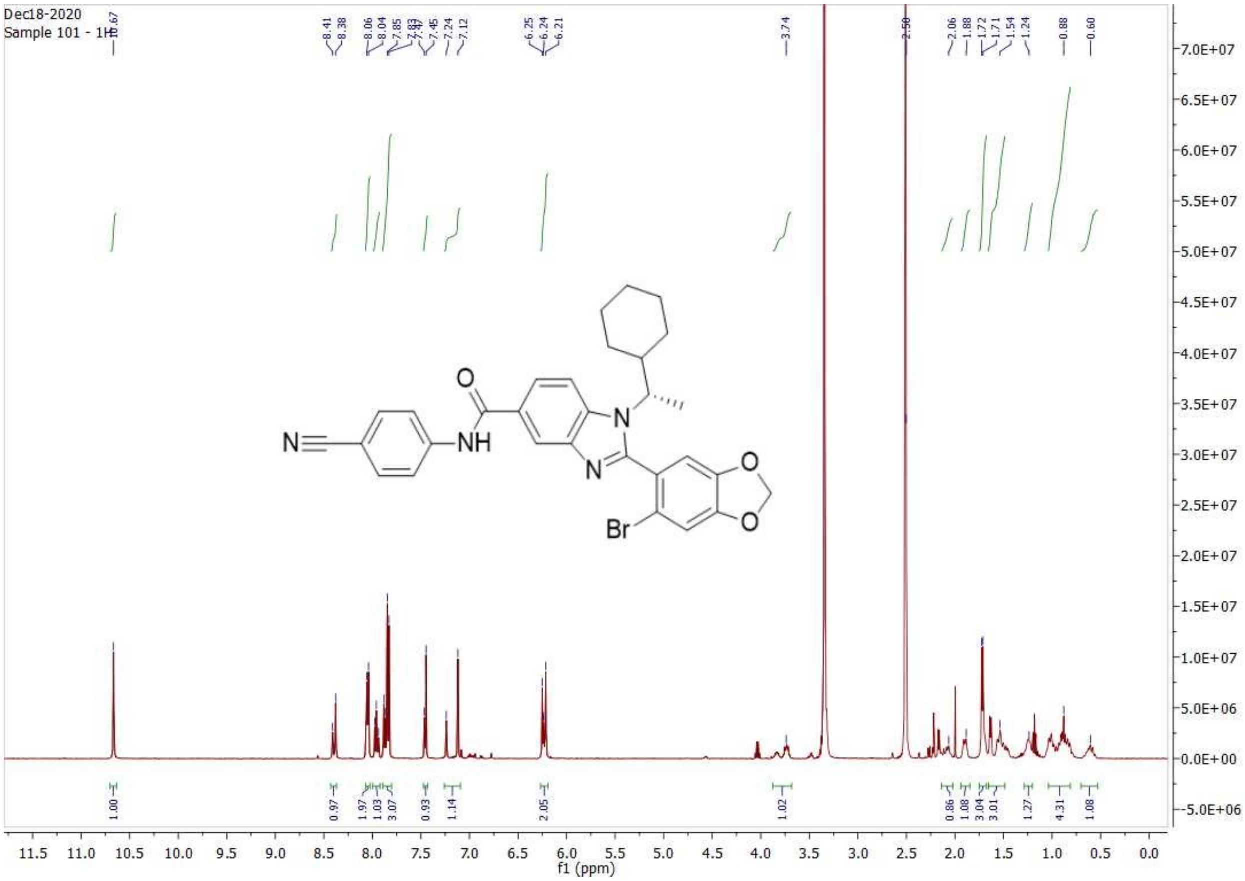
Dec18-2020
Sample 101 - 1H
10.67
8.41
8.38
8.06
8.04
7.85
7.83
7.47
7.45
7.24
7.12
6.25
6.24
6.21
3.74
2.50
2.06
1.88
1.72
1.71
1.54
1.24
0.88
0.60
1.00
0.97
1.97
1.03
3.07
0.93
1.14
2.05
1.02
0.86
1.08
3.04
3.01
1.27
4.31
1.08
7.0E+07
6.5E+07
6.0E+07
5.5E+07
5.0E+07
4.5E+07
4.0E+07
3.5E+07
3.0E+07
2.5E+07
2.0E+07
1.5E+07
1.0E+07
5.0E+06
0.0E+00
-5.0E+06
11.5
11.0
10.5
10.0
9.5
9.0
8.5
8.0
7.5
7.0
6.5
6.0
5.5
5.0
4.5
4.0
3.5
3.0
2.5
2.0
1.5
1.0
0.5
0.0
f1 (ppm)
O
N
NH
N
N
O
O
Br

Appendix 3: Characterization Data (Mass Spectroscopy, HPLC and ^{1}H-NMR) for AZ3451 analogues.

Compound 6a. (S)-2-(6-bromobenzo-1,3-dioxol-5-yl)-1-(1-cyclohexylethyl)-N-(2-fluorophenyl)-1H-benzo[d]imidazole-5-carboxamide.

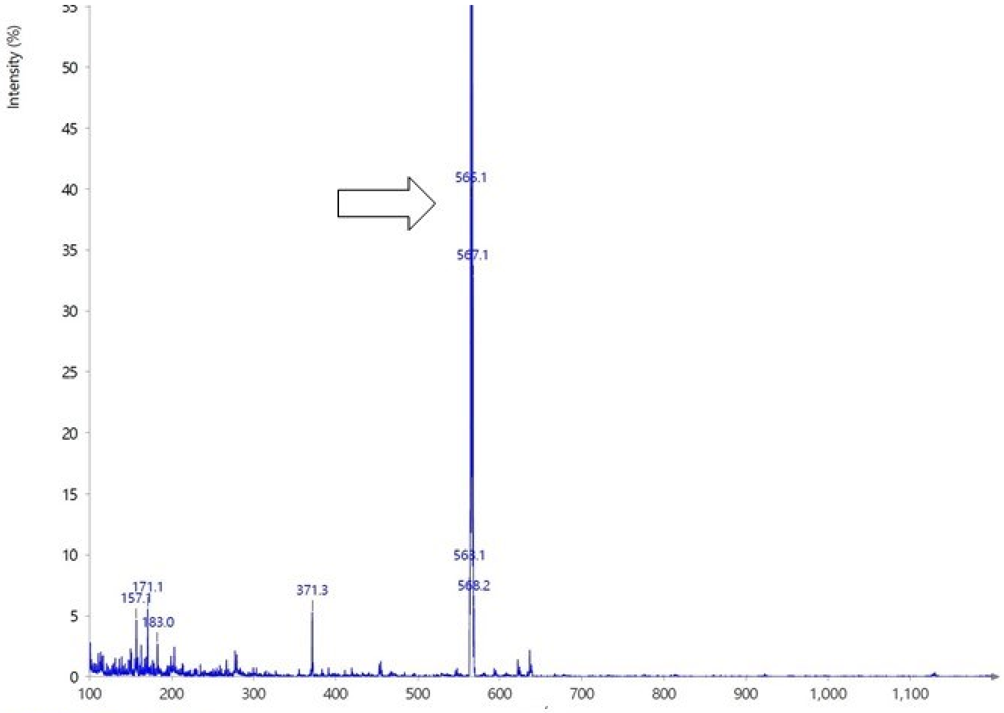

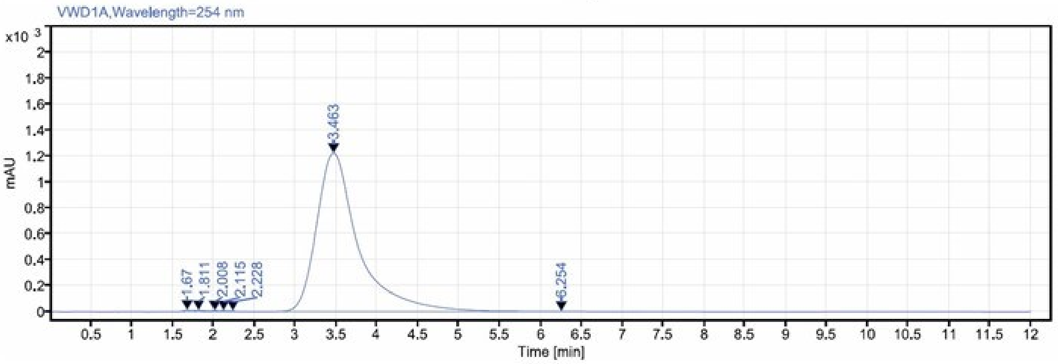

Signal: VWD1A,Wavelength=254 nm

RT [min]	Type	Width [min]	Area	Height	Area%	Name
1.670	BV	0.24	103.27	12.45	0.24	
1.811	VV	0.19	92.56	10.08	0.21	
2.008	VV	0.10	46.19	8.80	0.11	
2.115	VV	0.14	55.70	8.40	0.13	
2.228	VB	0.34	24.58	6.40	0.06	
3.463	BV	3.43	43498.47	1220.43	99.00	
6.254	VB	1.26	118.50	3.57	0.27	
		Sum	43939.29			

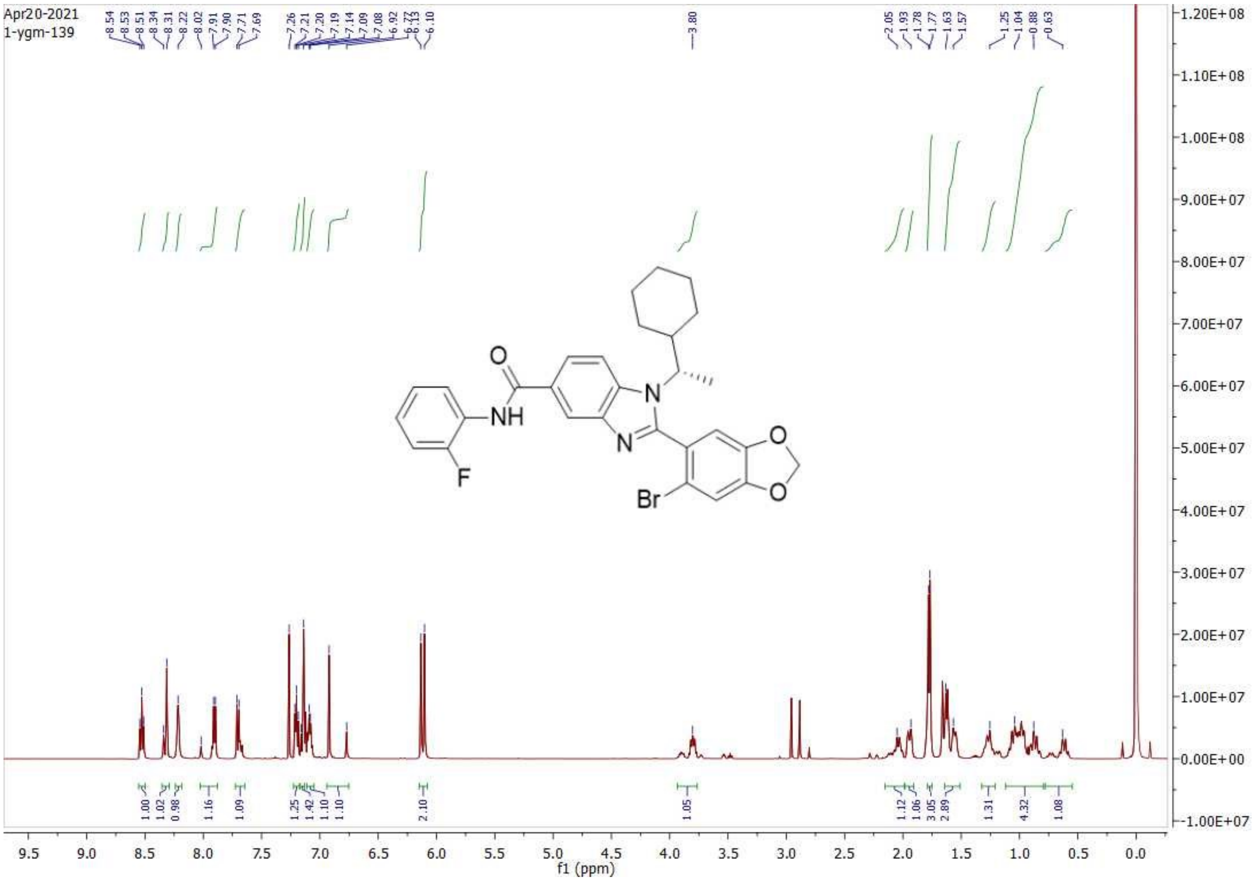
Apr20-2021
1-ygm-139
8.54
8.53
8.51
8.34
8.31
8.22
8.02
7.91
7.90
7.71
7.69
7.26
7.21
7.20
7.19
7.14
7.09
7.08
6.92
6.77
6.13
6.10
3.80
2.05
1.93
1.78
1.77
1.63
1.57
1.25
1.04
0.88
0.63
O
NH
N
N
F
O
O
Br
1.00
1.02
0.98
1.16
1.09
1.25
1.42
1.10
1.10
2.10
1.05
1.12
1.06
3.05
2.89
1.31
4.32
1.08
1.20E+08
1.10E+08
1.00E+08
9.00E+07
8.00E+07
7.00E+07
6.00E+07
5.00E+07
4.00E+07
3.00E+07
2.00E+07
1.00E+07
0.00E+00
-1.00E+07
9.5
9.0
8.5
8.0
7.5
7.0
6.5
6.0
5.5
5.0
4.5
4.0
3.5
3.0
2.5
2.0
1.5
1.0
0.5
0.0
f1 (ppm)

Compound 6b.(S)-2-(6-bromobenzo-1,3-dioxol-5-yl)-1-(1-cyclohexylethyl)-N-(3-fluorophenyl)-1H-benzo[d]imidazole-5-carboxamide.

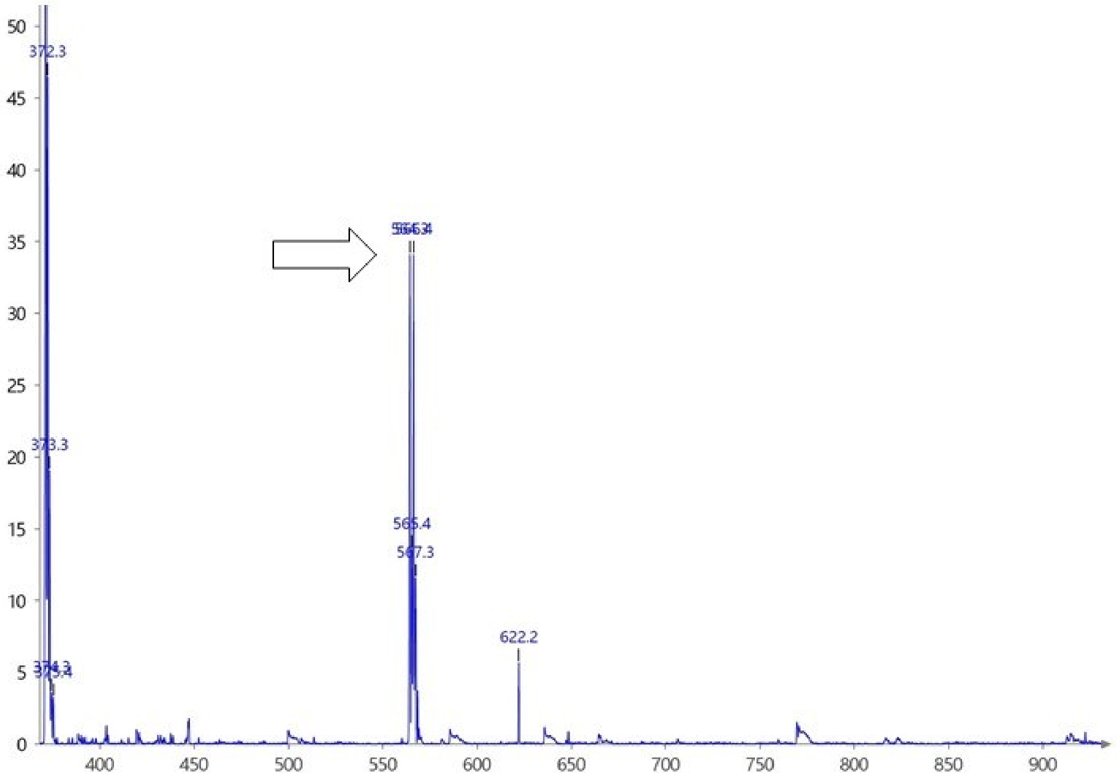

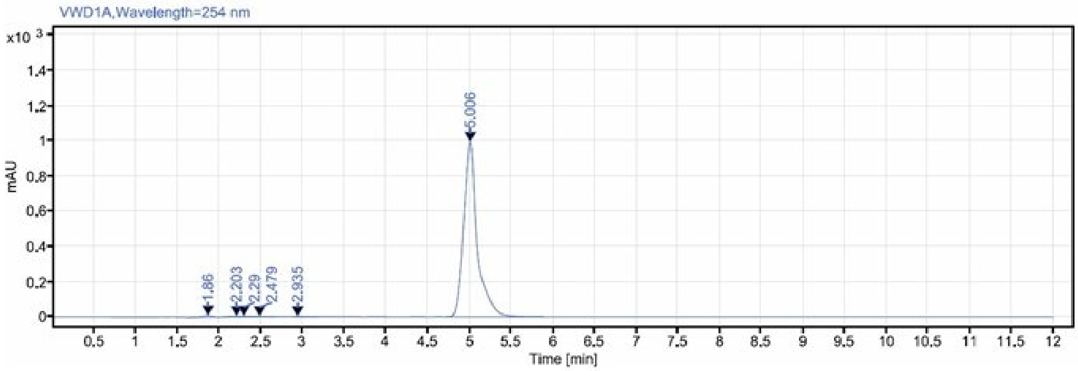

Signal: VWD1A,Wavelength=254 nm

RT [min]	Type	Width [min]	Area	Height	Area%	Name
1.860	BB	0.37	69.86	8.01	0.61	
2.203	BV	0.26	39.65	3.62	0.35	
2.290	VV	0.19	32.10	3.67	0.28	
2.479	VB	0.24	13.60	2.13	0.12	
2.935	VB	0.31	11.31	1.94	0.10	
5.006	VB	1.54	11249.73	993.99	98.54	
		Sum	11416.24			

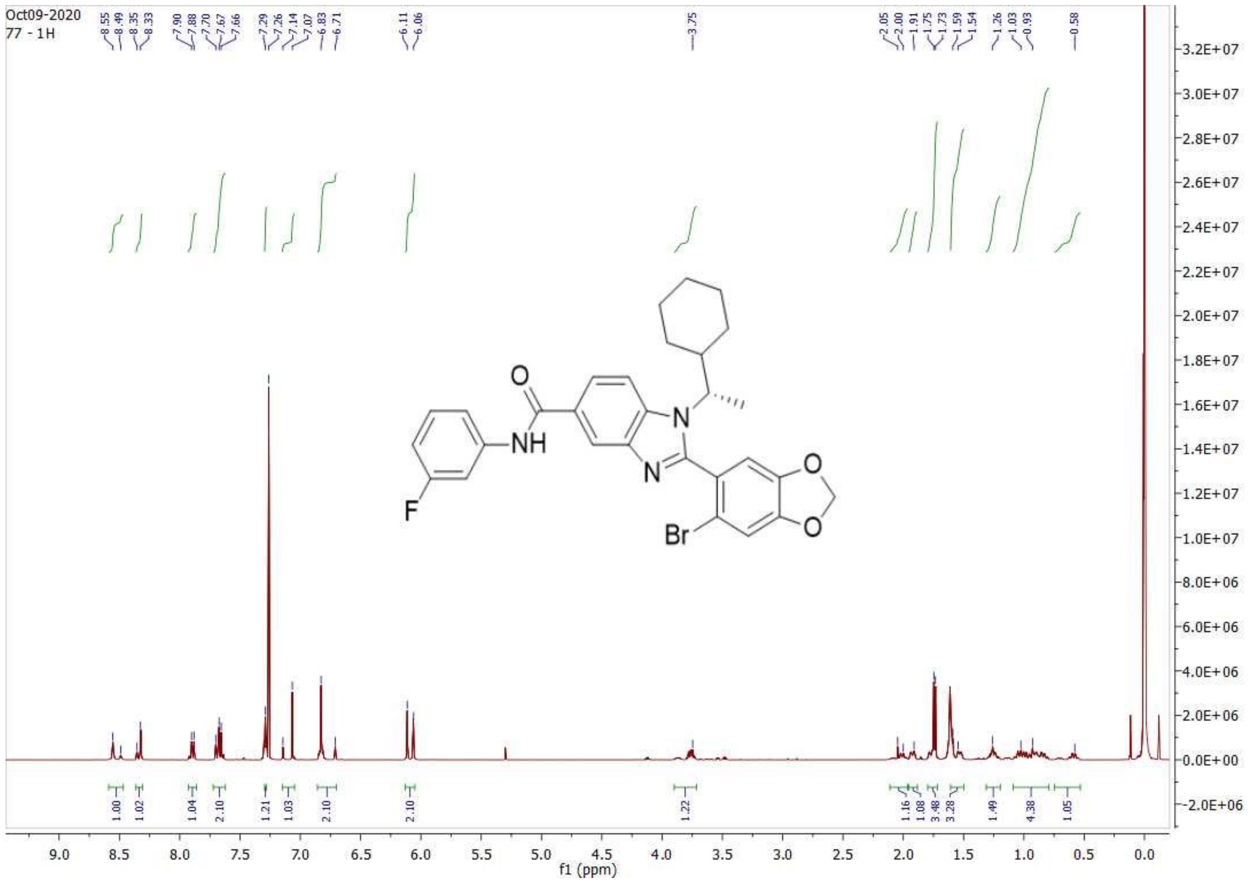
Oct09-2020
77 - 1H
8.55
8.49
8.35
8.33
7.90
7.88
7.70
7.67
7.66
7.29
7.26
7.14
7.07
6.83
6.71
6.11
6.06
3.75
2.05
2.00
1.91
1.75
1.73
1.59
1.54
1.26
1.03
0.93
0.58
1.00
1.02
1.04
2.10
1.21
1.03
2.10
2.10
1.22
1.16
1.08
3.48
3.28
1.49
4.38
1.05
3.2E+07
3.0E+07
2.8E+07
2.6E+07
2.4E+07
2.2E+07
2.0E+07
1.8E+07
1.6E+07
1.4E+07
1.2E+07
1.0E+07
8.0E+06
6.0E+06
4.0E+06
2.0E+06
0.0E+00
-2.0E+06
9.0
8.5
8.0
7.5
7.0
6.5
6.0
5.5
5.0
4.5
4.0
3.5
3.0
2.5
2.0
1.5
1.0
0.5
0.0
f1 (ppm)
O
NH
F
N
N
O
O
Br

Compound 6c. (S)-2-(6-bromobenzo-1,3-dioxol-5-yl)-1-(1-cyclohexylethyl)-N-(4-fluorophenyl)-1H-benzo[d]imidazole-5-carboxamide.

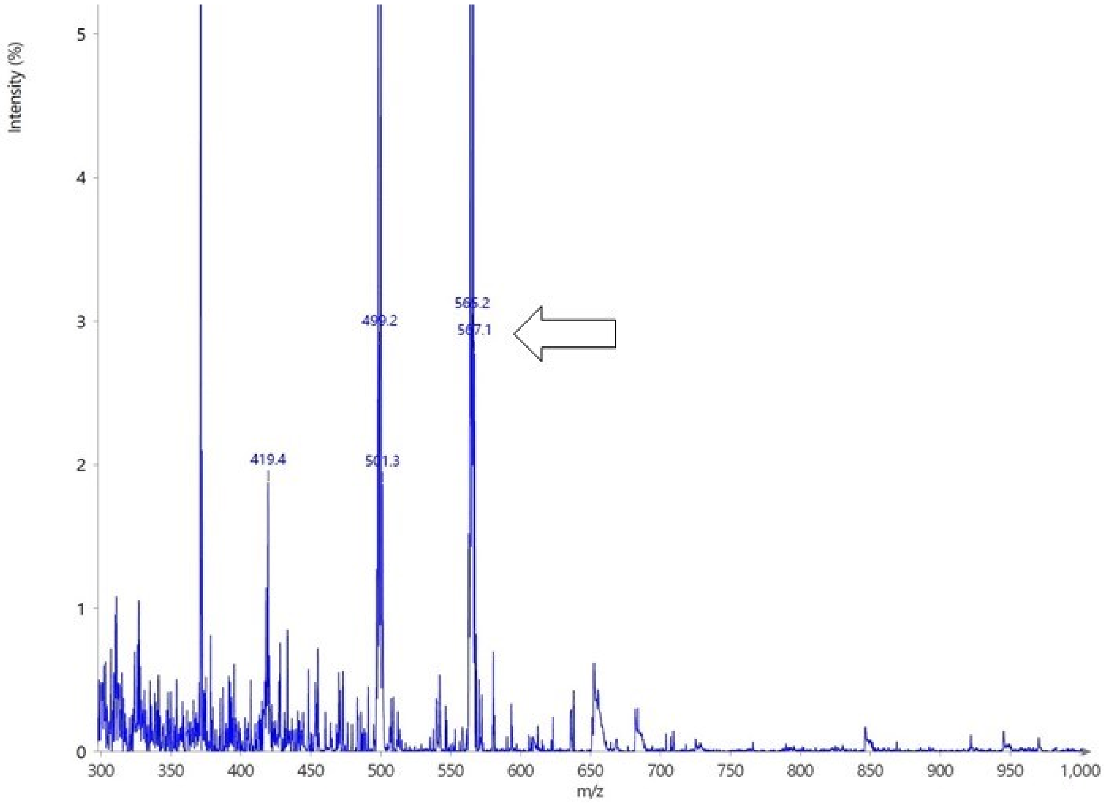

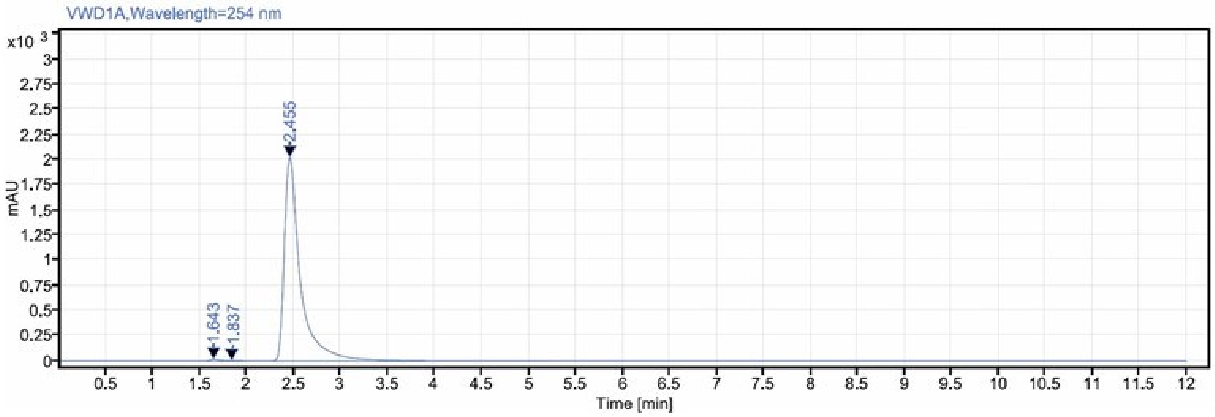

Signal: VWD1A,Wavelength=254 nm

RT [min]	Type	Width [min]	Area	Height	Area%	Name
1.643	BV	0.27	119.99	17.66	0.49	
1.837	VV	0.27	37.93	3.97	0.15	
2.455	VB	3.02	24333.63	2024.68	99.36	
		Sum	24491.56			

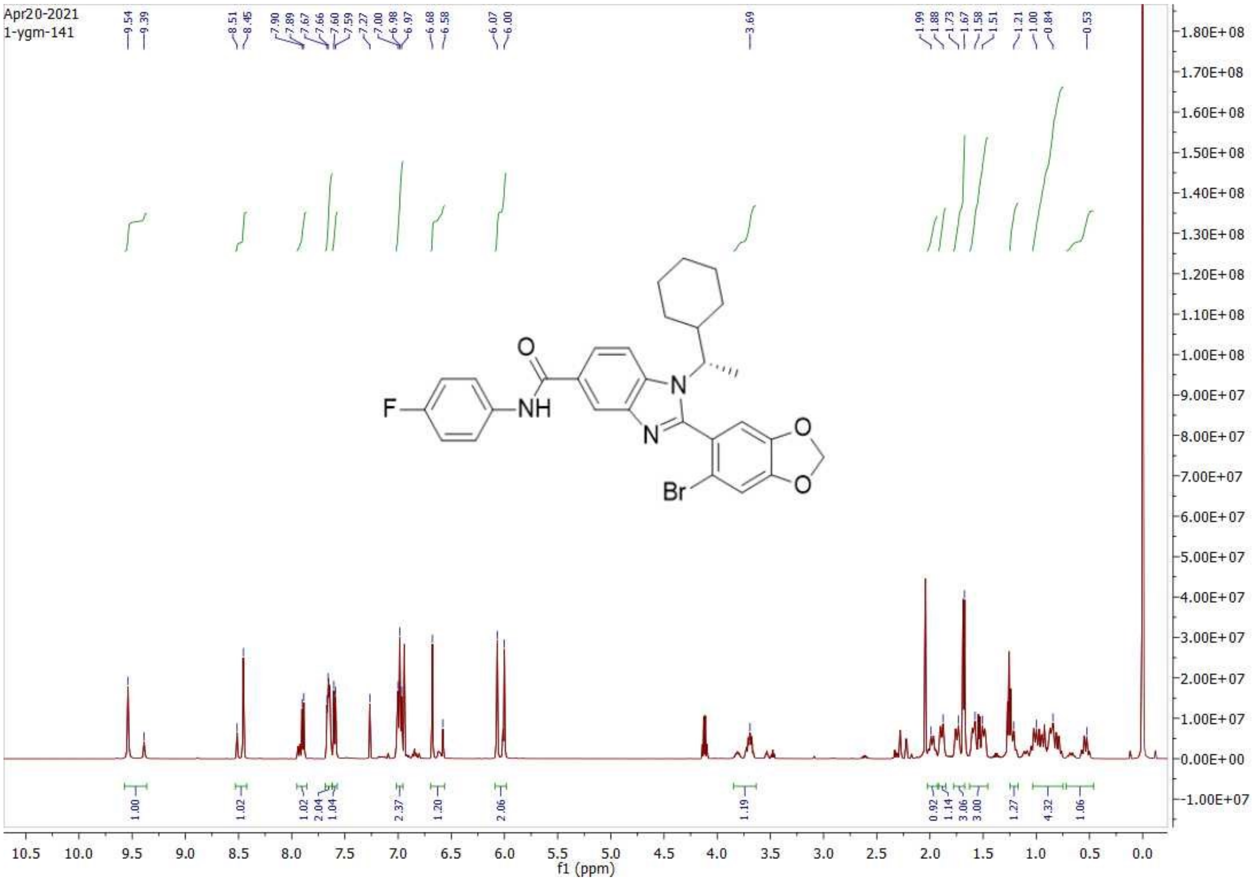
Apr20-2021
1-ygm-141
9.54
9.39
8.51
8.45
7.90
7.89
7.67
7.66
7.60
7.59
7.27
7.00
6.98
6.97
6.68
6.58
6.07
6.00
3.69
1.99
1.88
1.73
1.67
1.58
1.51
1.21
1.00
0.84
0.53
1.00
1.02
1.02
2.04
1.04
2.37
1.20
2.06
1.19
0.92
1.14
3.06
3.00
1.27
4.32
1.06
O
F
NH
N
N
O
O
Br
1.80E+08
1.70E+08
1.60E+08
1.50E+08
1.40E+08
1.30E+08
1.20E+08
1.10E+08
1.00E+08
9.00E+07
8.00E+07
7.00E+07
6.00E+07
5.00E+07
4.00E+07
3.00E+07
2.00E+07
1.00E+07
0.00E+00
-1.00E+07
10.5
10.0
9.5
9.0
8.5
8.0
7.5
7.0
6.5
6.0
5.5
5.0
4.5
4.0
3.5
3.0
2.5
2.0
1.5
1.0
0.5
0.0
f1 (ppm)

Compound 7a. (S)-2-(6-bromobenzo-1,3-dioxol-5-yl)-1-(1-cyclohexylethyl)-N-(2-fluorobenzyl)-1H-benzo[d]imidazole-5-carboxamide.

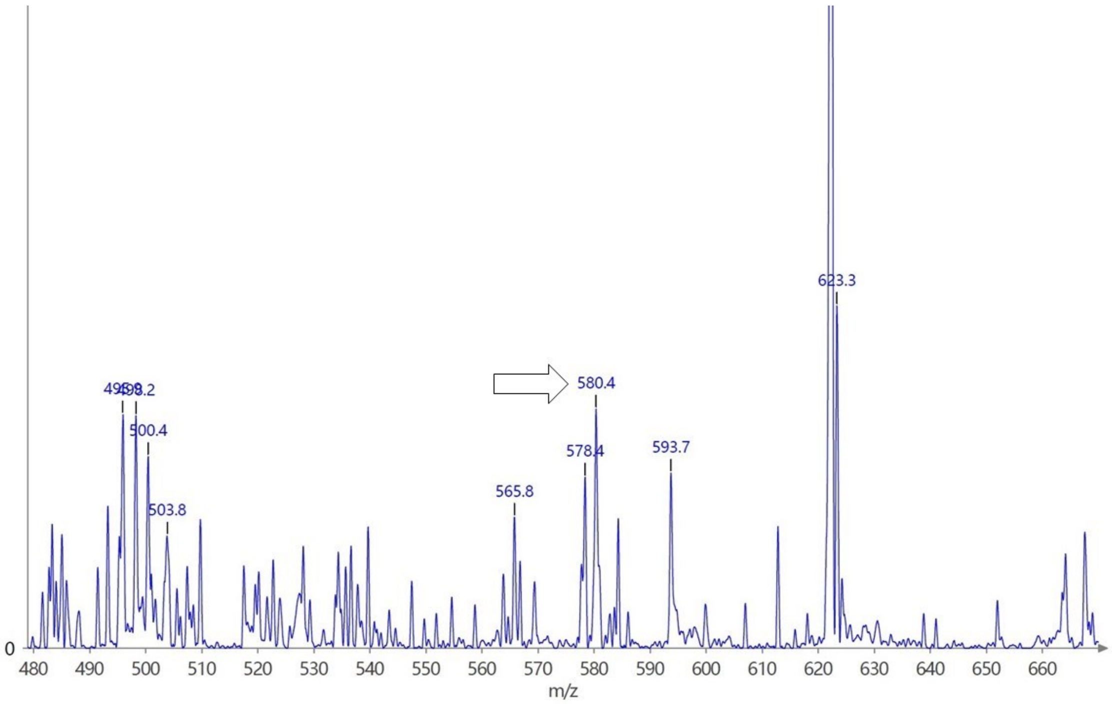

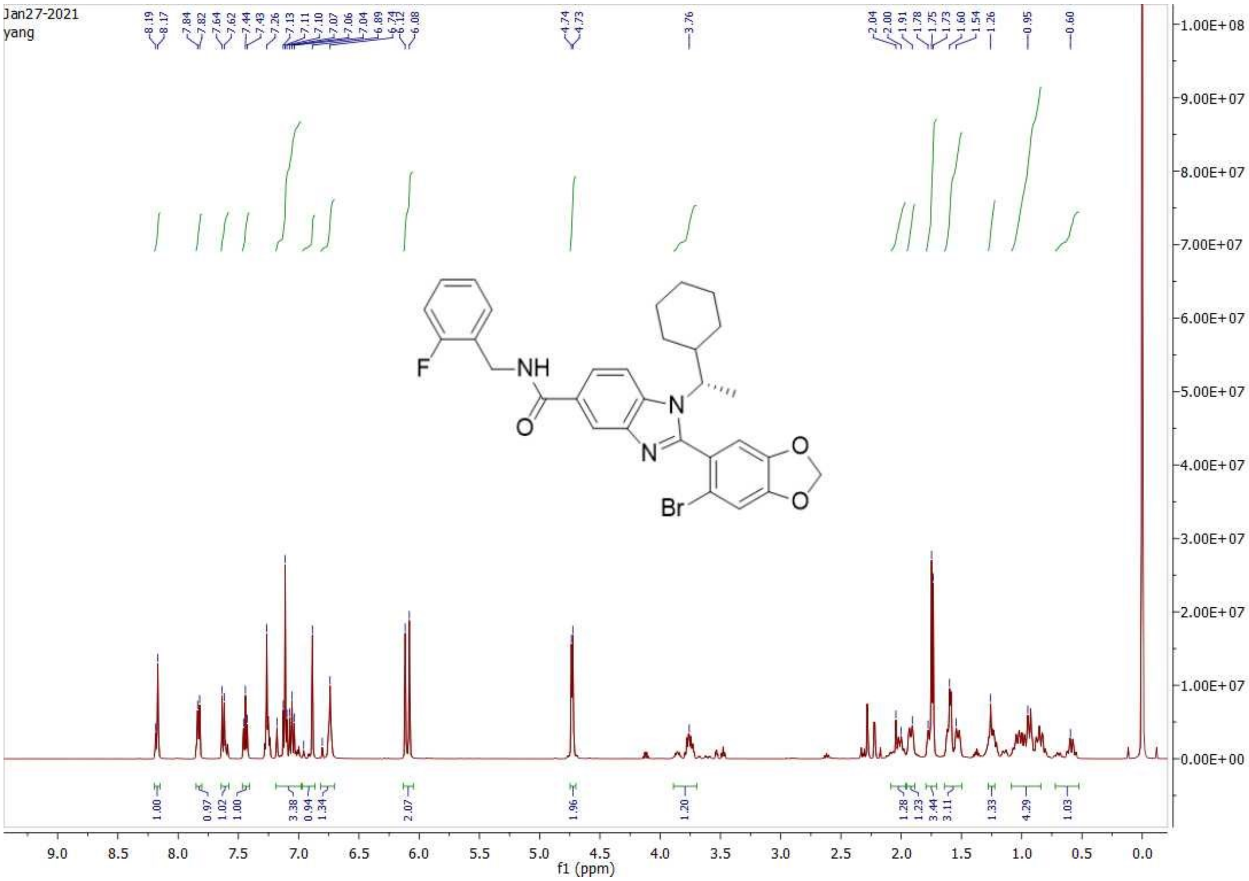
Jan27-2021
yang
8.19
8.17
7.84
7.82
7.64
7.62
7.44
7.43
7.26
7.13
7.11
7.10
7.07
7.06
7.04
6.89
6.74
6.12
6.08
4.74
4.73
3.76
2.04
2.00
1.91
1.78
1.75
1.73
1.60
1.54
1.26
0.95
0.60
F
NH
O
N
N
O
O
Br
1.00E+08
9.00E+07
8.00E+07
7.00E+07
6.00E+07
5.00E+07
4.00E+07
3.00E+07
2.00E+07
1.00E+07
0.00E+00
1.00
0.97
1.02
1.00
3.38
0.94
1.34
2.07
1.96
1.20
1.28
1.23
3.44
3.11
1.33
4.29
1.03
9.0
8.5
8.0
7.5
7.0
6.5
6.0
5.5
5.0
4.5
4.0
3.5
3.0
2.5
2.0
1.5
1.0
0.5
0.0
f1 (ppm)

Compound 7b.(S)-2-(6-bromobenzo-1,3-dioxol-5-yl)-1-(1-cyclohexylethyl)-N-(3-fluorobenzyl)-1H-benzo[d]imidazole-5-carboxamide.

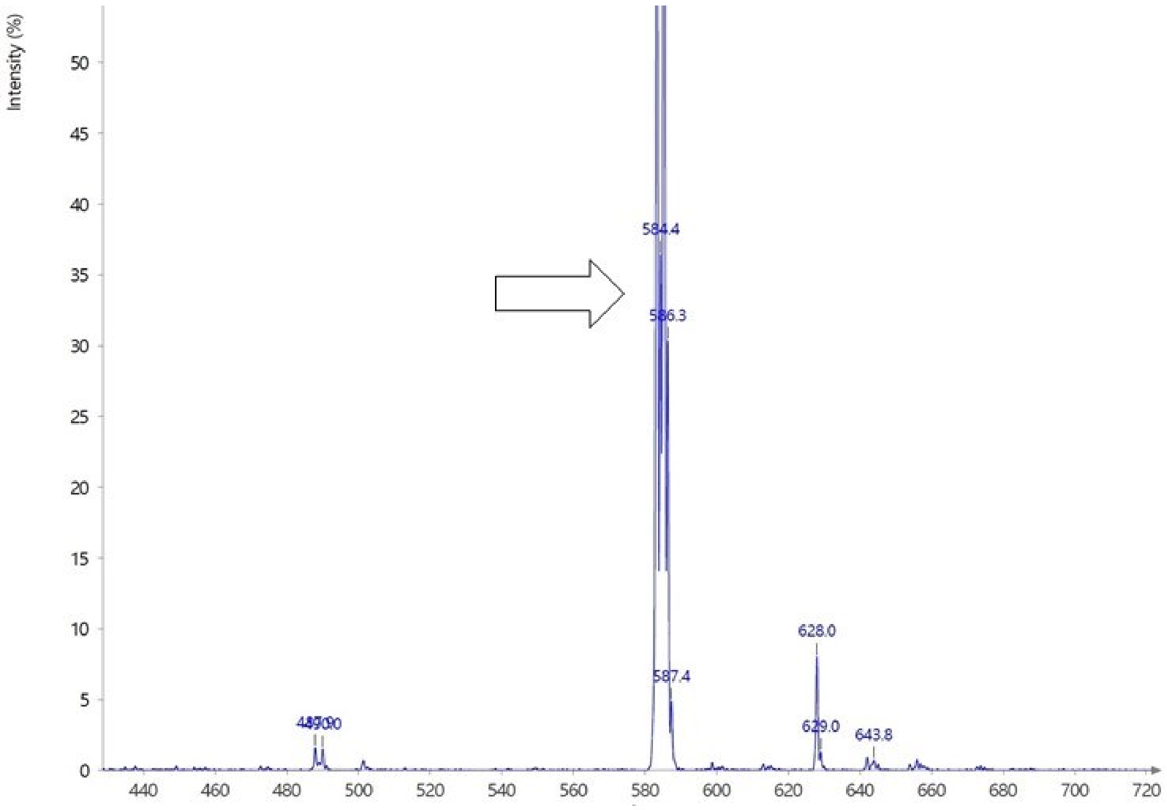

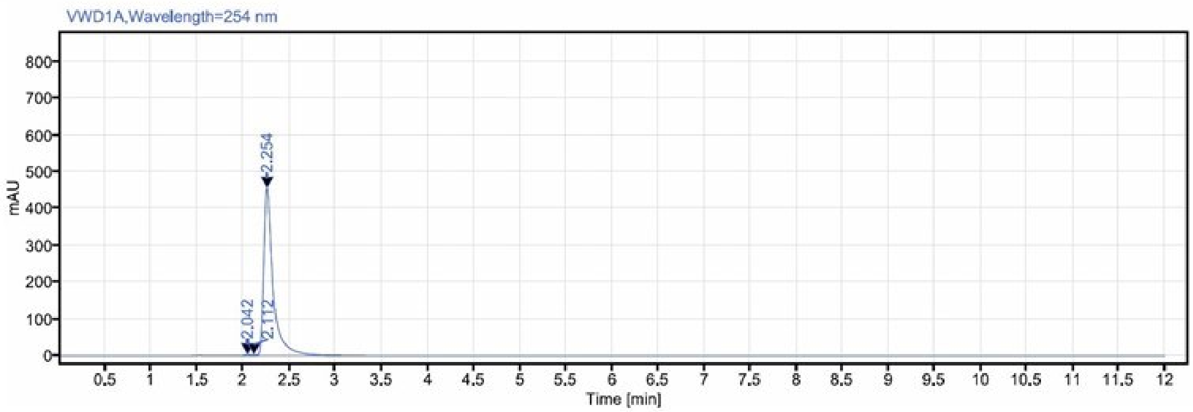

Signal: VWD1A,Wavelength=254 nm

RT [min]	Type	Width [min]	Area	Height	Area%	Name
2.042	BV	0.12	13.33	3.23	0.41	
2.112	VV	0.06	9.36	2.72	0.29	
2.254	VB	1.61	3256.51	455.61	99.31	
		Sum	3279.19			

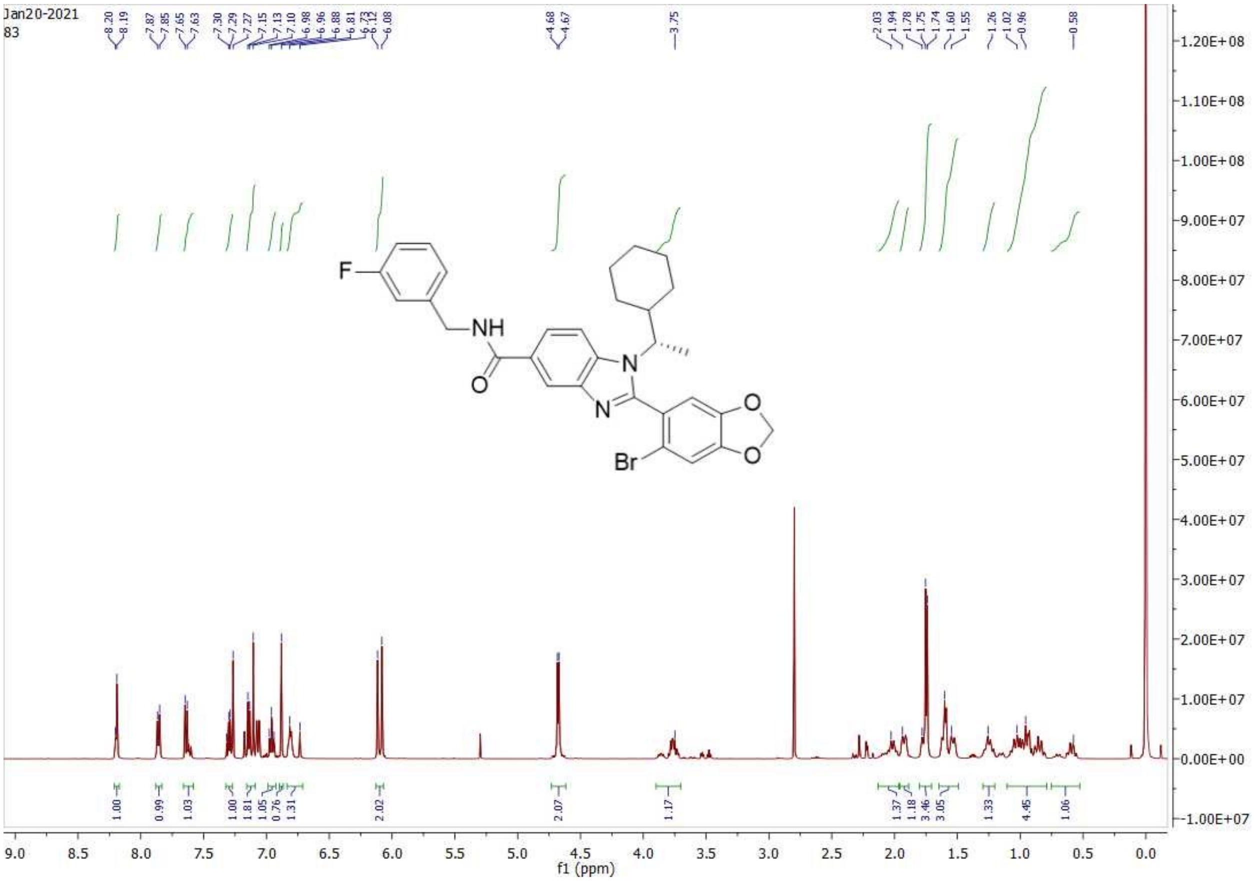
Jan20-2021
83
8.20
8.19
7.87
7.85
7.65
7.63
7.30
7.29
7.27
7.15
7.13
7.10
6.98
6.96
6.88
6.81
6.73
6.12
6.08
4.68
4.67
3.75
2.03
1.94
1.78
1.75
1.74
1.60
1.55
1.26
1.02
0.96
0.58
F
NH
O
N
N
O
O
Br
1.20E+08
1.10E+08
1.00E+08
9.00E+07
8.00E+07
7.00E+07
6.00E+07
5.00E+07
4.00E+07
3.00E+07
2.00E+07
1.00E+07
0.00E+00
-1.00E+07
1.00
0.99
1.03
1.00
1.81
1.05
0.76
1.31
2.02
2.07
1.17
1.37
1.18
3.46
3.05
1.33
4.45
1.06
9.0
8.5
8.0
7.5
7.0
6.5
6.0
5.5
5.0
4.5
4.0
3.5
3.0
2.5
2.0
1.5
1.0
0.5
0.0
f1 (ppm)

Compound 7c. (S)-2-(6-bromobenzo-1,3-dioxol-5-yl)-1-(1-cyclohexylethyl)-N-(4-fluorobenzyl)-1H-benzo[d]imidazole-5-carboxamide.

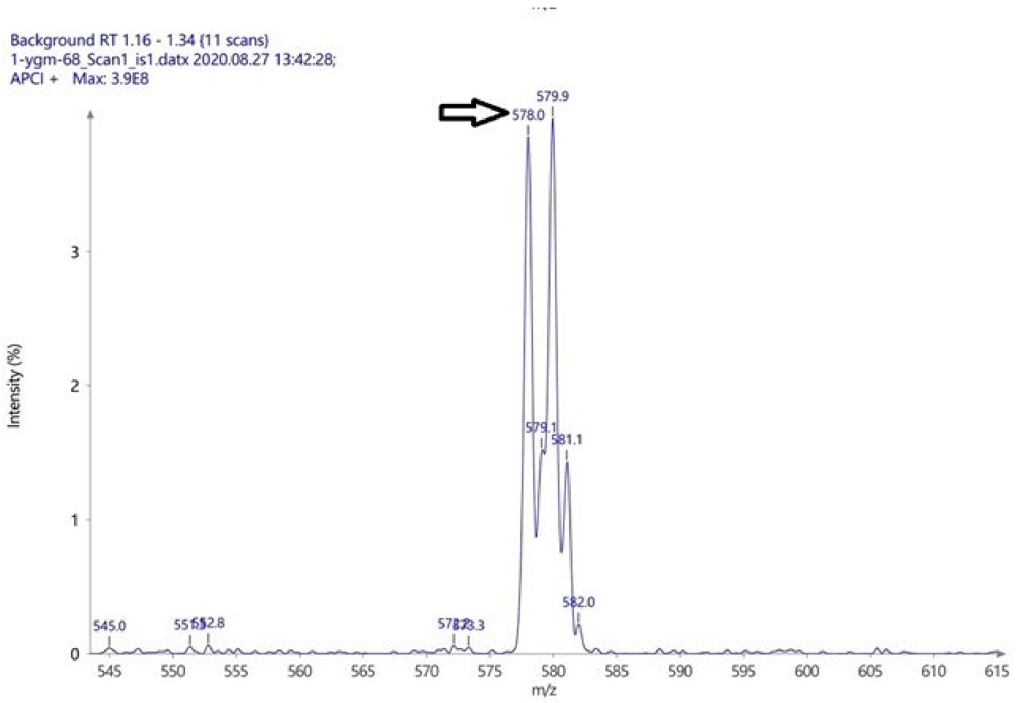

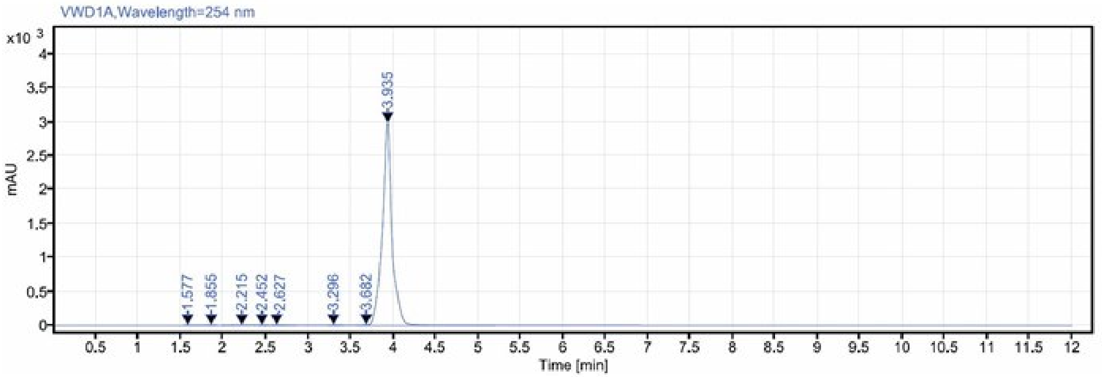

Signal: VWD1A,Wavelength=254 nm

RT [min]	Type	Width [min]	Area	Height	Area%	Name
1.577	VV	0.21	31.15	5.31	0.13	
1.855	VB	0.25	60.65	8.06	0.25	
2.215	BV	0.47	137.30	7.52	0.57	
2.452	VV	0.11	25.18	4.31	0.11	
2.627	VV	0.32	50.88	3.94	0.21	
3.296	VV	0.20	25.41	4.29	0.11	
3.682	BV	0.13	25.22	8.00	0.11	
3.935	VB	1.49	23540.83	2983.21	98.51	
		Sum	23896.61			

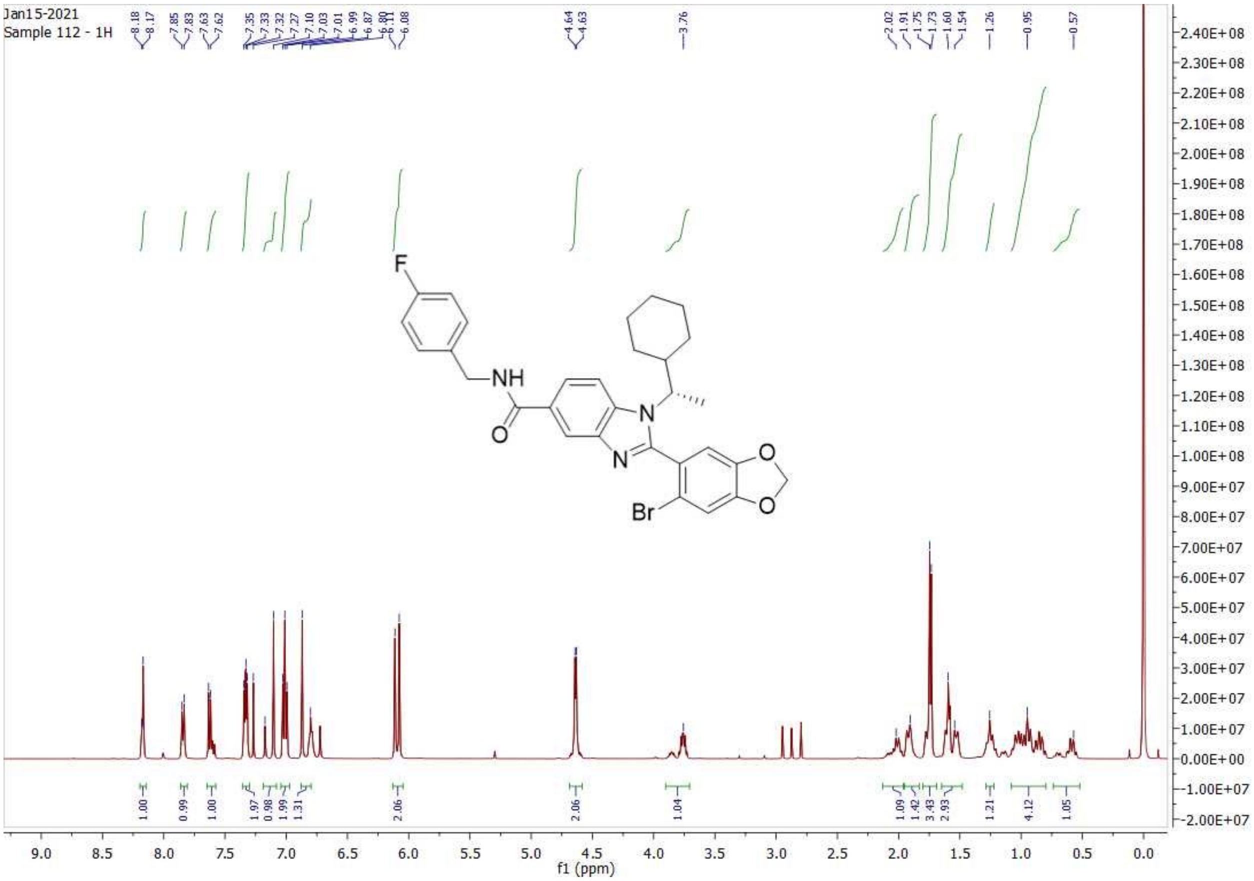
Jan15-2021
Sample 112 - 1H
8.18
8.17
7.85
7.83
7.63
7.62
7.35
7.33
7.32
7.27
7.10
7.03
7.01
6.99
6.87
6.80
6.11
6.08
4.64
4.63
3.76
2.02
1.91
1.75
1.73
1.60
1.54
1.26
0.95
0.57
F
NH
O
N
N
O
O
Br
1.00
0.99
1.00
1.97
0.98
1.99
1.31
2.06
2.06
1.04
1.09
1.42
3.43
2.93
1.21
4.12
1.05
2.40E+08
2.30E+08
2.20E+08
2.10E+08
2.00E+08
1.90E+08
1.80E+08
1.70E+08
1.60E+08
1.50E+08
1.40E+08
1.30E+08
1.20E+08
1.10E+08
1.00E+08
9.00E+07
8.00E+07
7.00E+07
6.00E+07
5.00E+07
4.00E+07
3.00E+07
2.00E+07
1.00E+07
0.00E+00
-1.00E+07
-2.00E+07
9.0
8.5
8.0
7.5
7.0
6.5
6.0
5.5
5.0
4.5
4.0
3.5
3.0
2.5
2.0
1.5
1.0
0.5
0.0
f1 (ppm)

Compound 8a. (S)-2-(6-bromobenzo-1,3-dioxol-5-yl)-1-(1-cyclohexylethyl)-N-(pyridin-2-yl)-1H-benzo[d]imidazole-5-carboxamide.

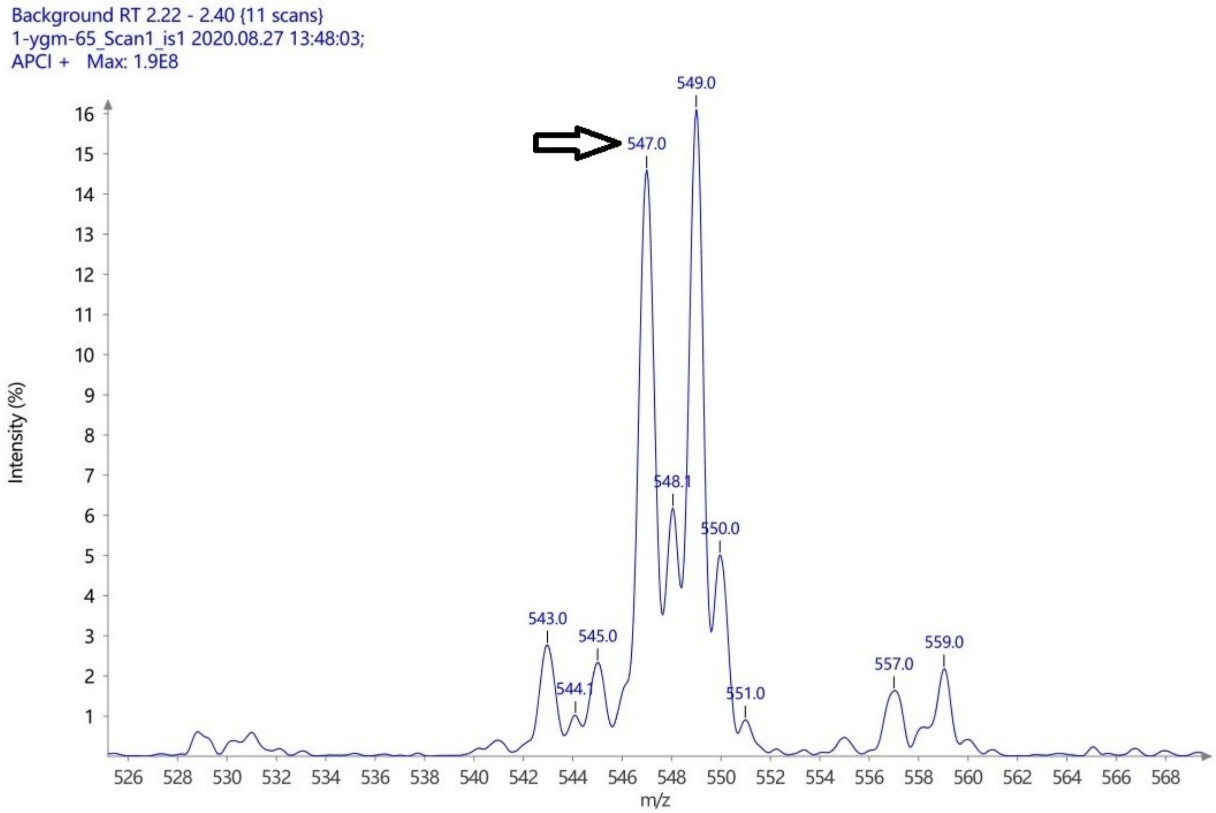

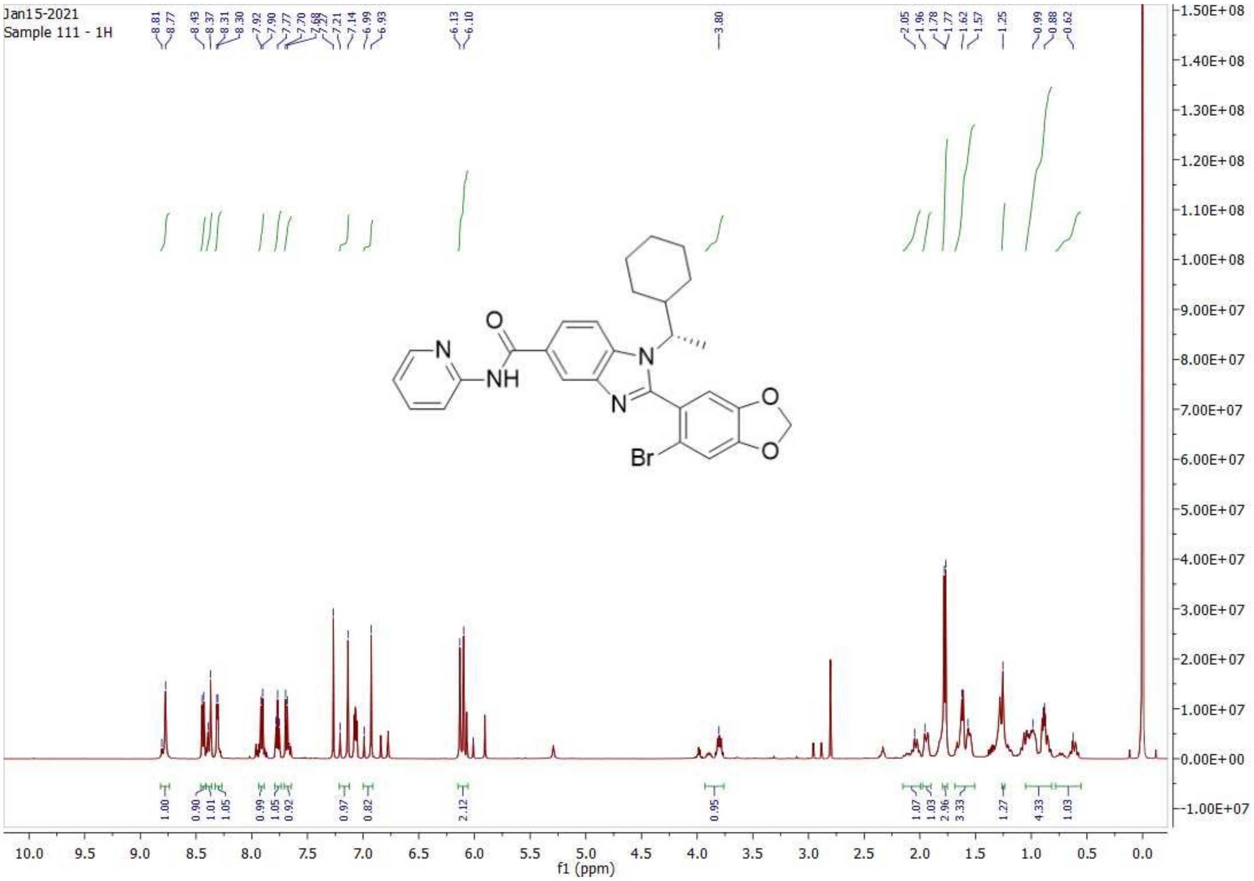
Jan15-2021
Sample 111 - 1H
8.81
8.77
8.43
8.37
8.31
8.30
7.92
7.90
7.77
7.70
7.68
7.27
7.21
7.14
6.99
6.93
6.13
6.10
3.80
2.05
1.96
1.78
1.77
1.62
1.57
1.25
0.99
0.88
0.62
O
N
NH
N
N
O
O
Br
1.00
0.90
1.01
1.05
0.99
1.05
0.92
0.97
0.82
2.12
0.95
1.07
1.03
2.96
3.33
1.27
4.33
1.03
1.50E+08
1.40E+08
1.30E+08
1.20E+08
1.10E+08
1.00E+08
9.00E+07
8.00E+07
7.00E+07
6.00E+07
5.00E+07
4.00E+07
3.00E+07
2.00E+07
1.00E+07
0.00E+00
-1.00E+07
10.0
9.5
9.0
8.5
8.0
7.5
7.0
6.5
6.0
5.5
5.0
4.5
4.0
3.5
3.0
2.5
2.0
1.5
1.0
0.5
0.0
f1 (ppm)

Compound 8b. (S)-2-(6-bromobenzo-1,3-dioxol-5-yl)-1-(1-cyclohexylethyl)-N-(pyridin-3-yl)-1H-benzo[d]imidazole-5-carboxamide.

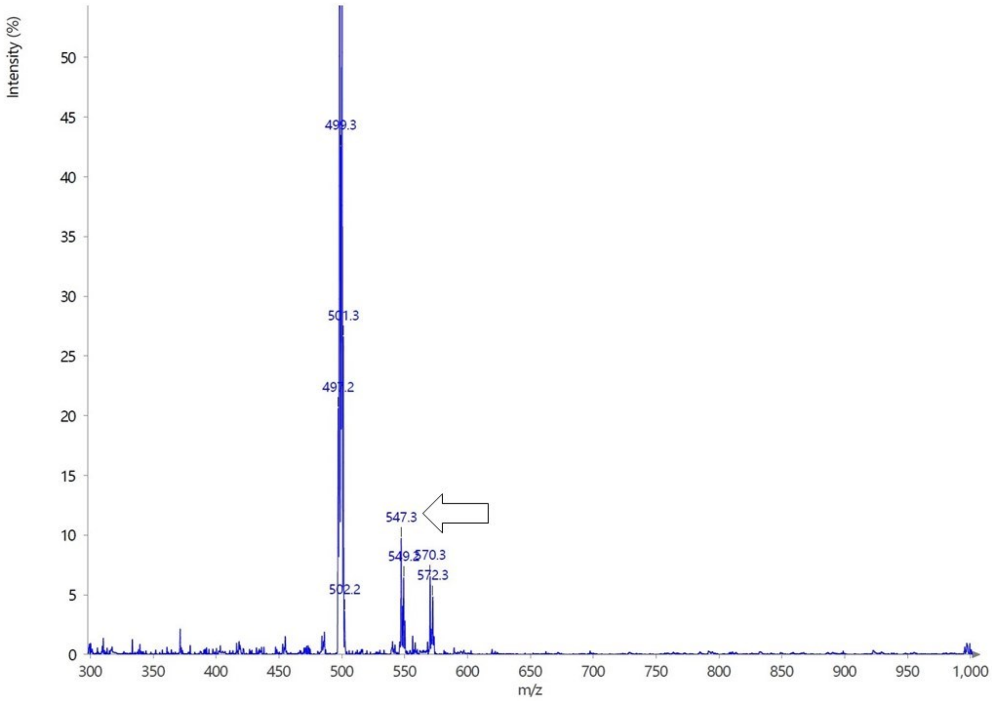

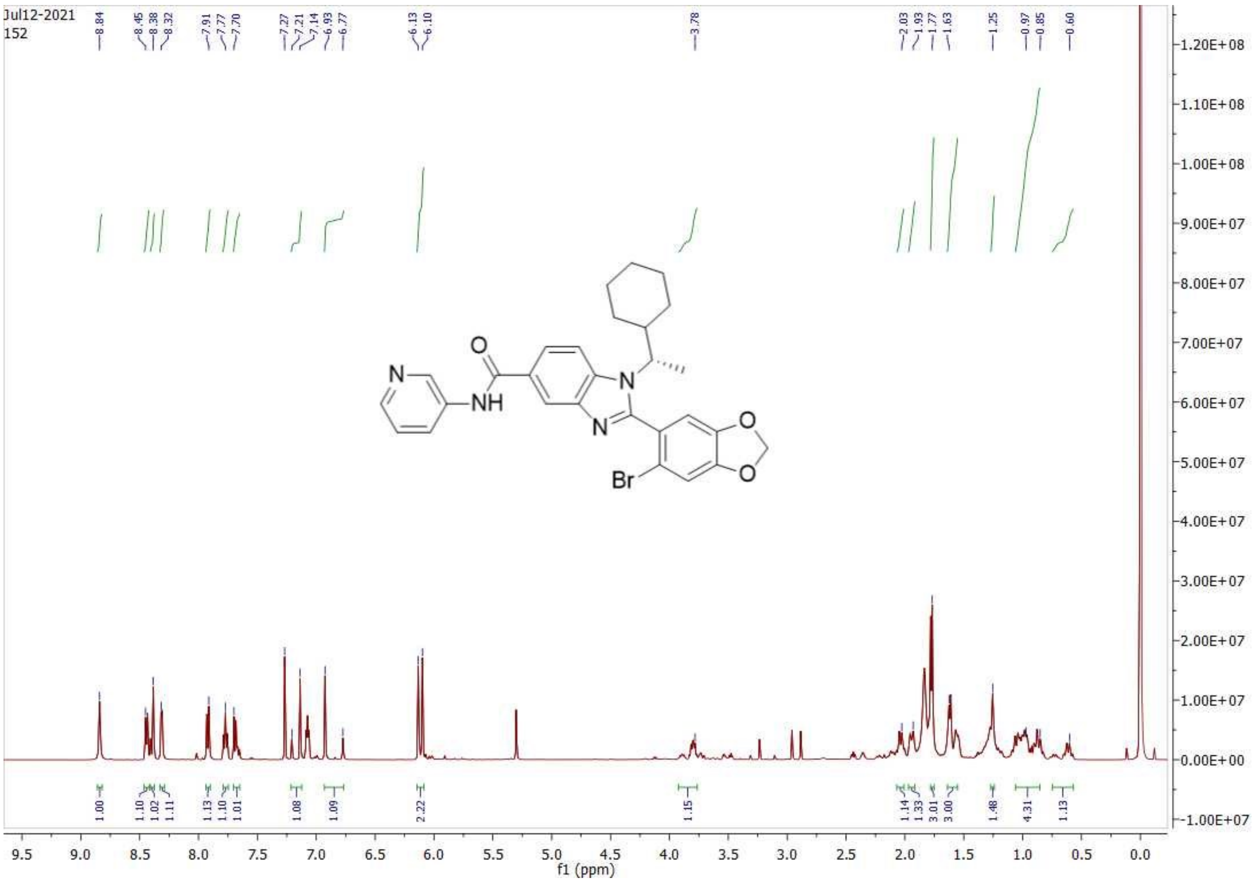

Jul12-2021
152
8.84
8.45
8.38
8.32
7.91
7.77
7.70
7.27
7.21
7.14
6.93
6.77
6.13
6.10
3.78
2.03
1.93
1.77
1.63
1.25
0.97
0.85
0.60
1.00
1.10
1.02
1.11
1.13
1.10
1.01
1.08
1.09
2.22
1.15
1.14
1.33
3.01
3.00
1.48
4.31
1.13
1.20E+08
1.10E+08
1.00E+08
9.00E+07
8.00E+07
7.00E+07
6.00E+07
5.00E+07
4.00E+07
3.00E+07
2.00E+07
1.00E+07
0.00E+00
-1.00E+07
9.5
9.0
8.5
8.0
7.5
7.0
6.5
6.0
5.5
5.0
4.5
4.0
3.5
3.0
2.5
2.0
1.5
1.0
0.5
0.0
f1 (ppm)
O
N
NH
N
N
O
O
Br

Compound 8c. (S)-2-(6-bromobenzo-1,3-dioxol-5-yl)-1-(1-cyclohexylethyl)-N-(pyridin-4-yl)-1H-benzo[d]imidazole-5-carboxamide.

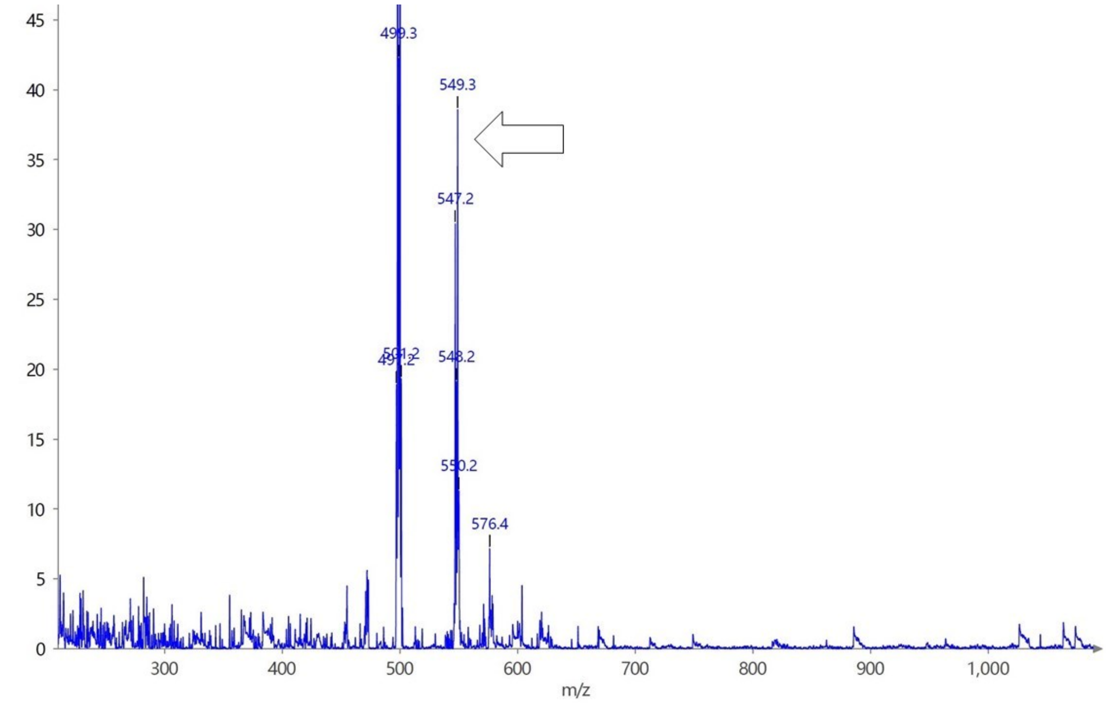

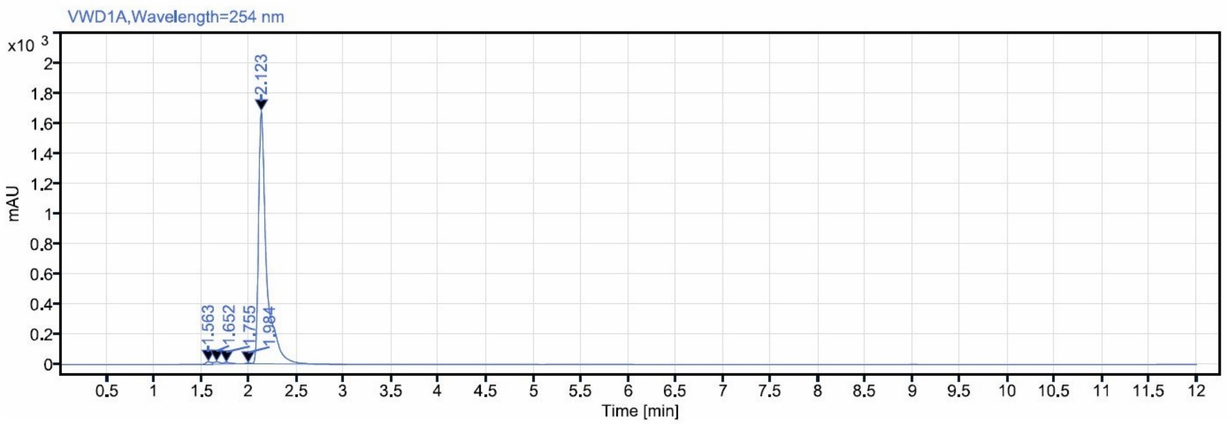

Signal: VWD1A,Wavelength=254 nm

RT [min]	Type	Width [min]	Area	Height	Area%	Name
1.563	BV	0.12	64.75	17.44	0.64	
1.652	VV	0.10	76.19	16.59	0.75	
1.755	VB	0.21	60.51	10.72	0.59	
1.984	BV	0.10	16.47	4.61	0.16	
2.123	VB	0.99	9973.47	1679.07	97.86	
		Sum	10191.40			

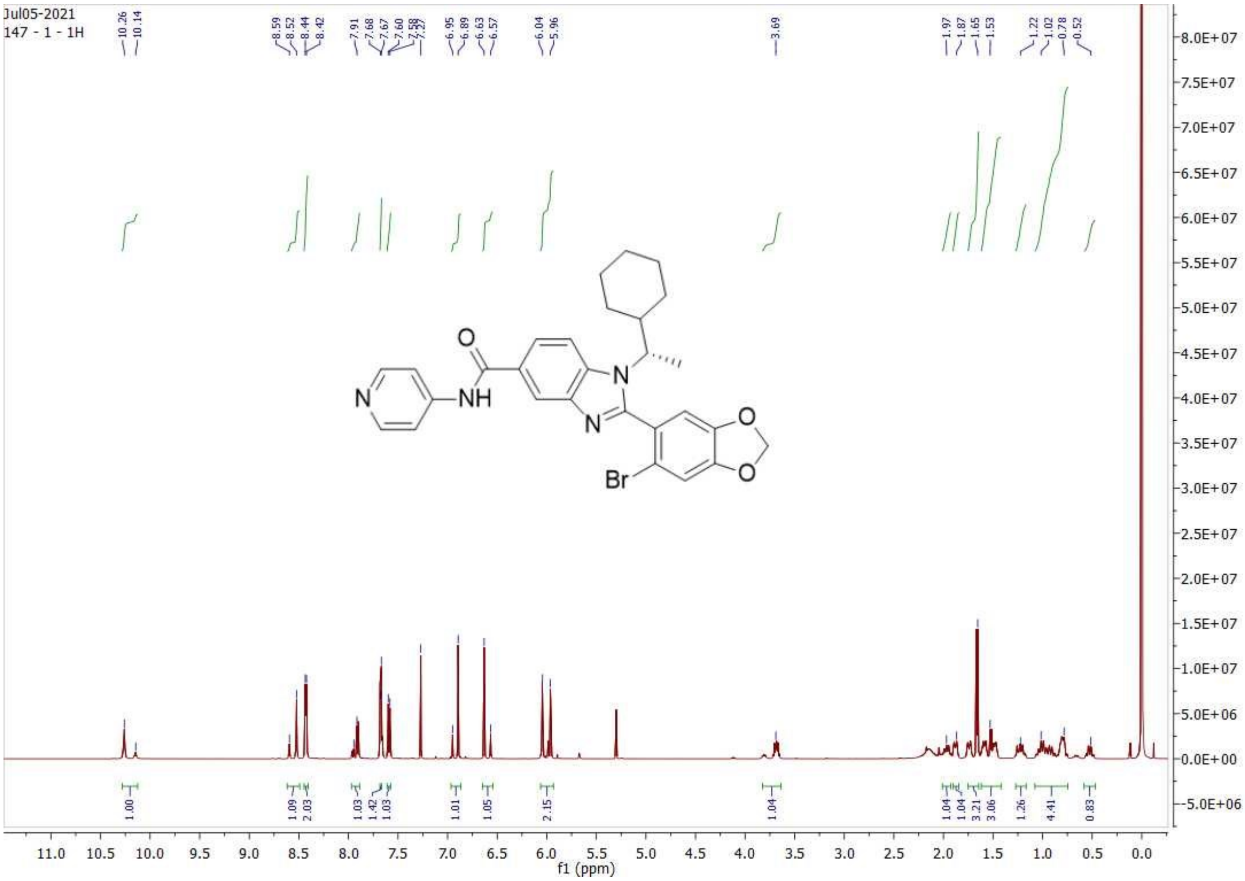
Jul05-2021
147 - 1 - 1H
10.26
10.14
8.59
8.52
8.44
8.42
7.91
7.68
7.67
7.60
7.58
7.27
6.95
6.89
6.63
6.57
6.04
5.96
3.69
1.97
1.87
1.65
1.53
1.22
1.02
0.78
0.52
1.00
1.09
2.03
1.03
1.42
1.03
1.01
1.05
2.15
1.04
1.04
1.04
3.21
3.06
1.26
4.41
0.83
f1 (ppm)
N
NH
O
N
N
O
O
Br

Compound 9a. (S)-2-(6-bromobenzo-1,3-dioxol-5-yl)-1-(1-cyclohexylethyl)-N-(quinolin-3-yl)-1H-benzo[d]imidazole-5-carboxamide.

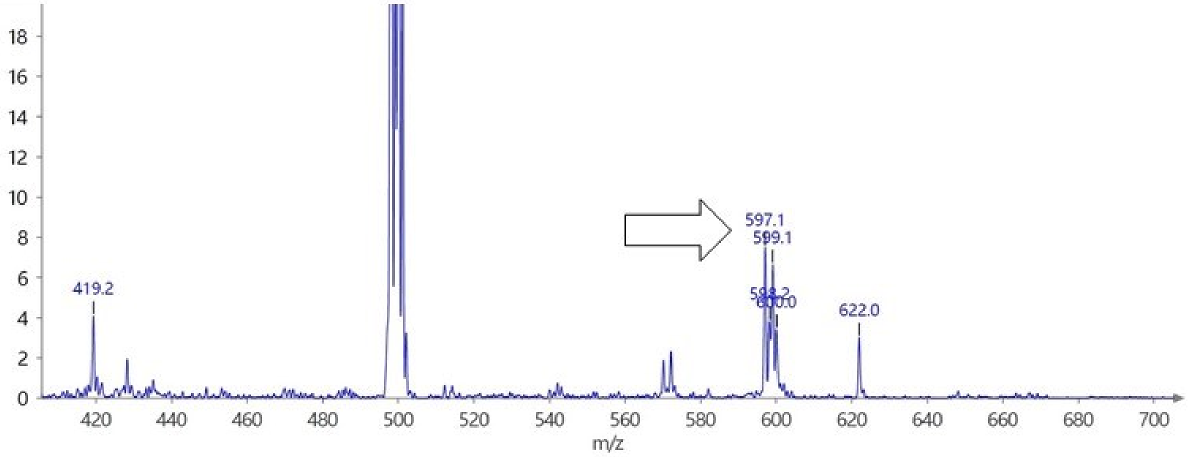

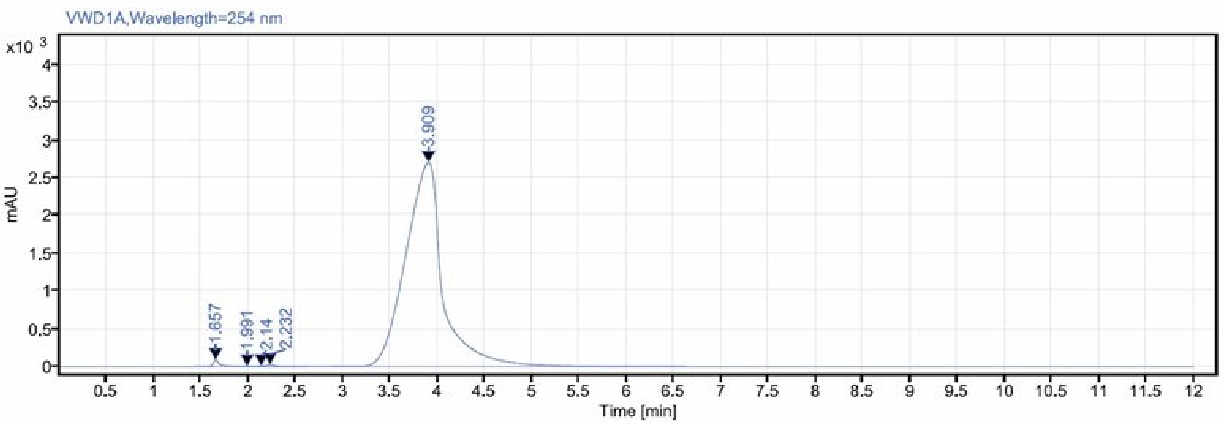

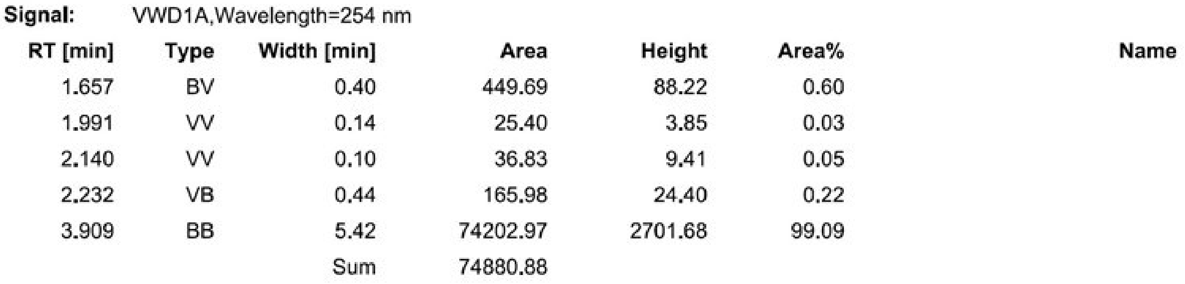
Signal: VWD1A,Wavelength=254 nm

RT [min]	Type	Width [min]	Area	Height	Area%	Name
1.657	BV	0.40	449.69	88.22	0.60	
1.991	VV	0.14	25.40	3.85	0.03	
2.140	VV	0.10	36.83	9.41	0.05	
2.232	VB	0.44	165.98	24.40	0.22	
3.909	BB	5.42	74202.97	2701.68	99.09	
		Sum	74880.88			

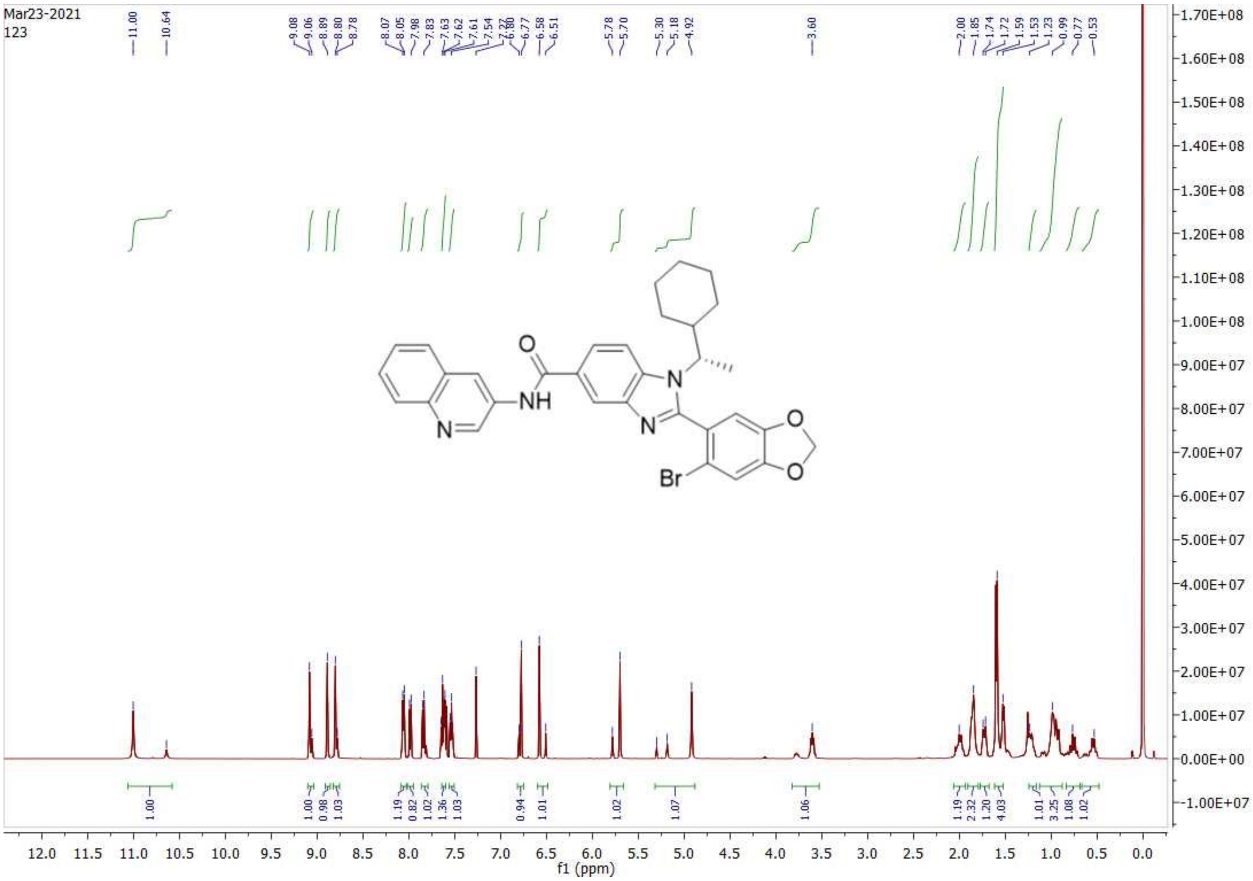
Mar23-2021
123
11.00
10.64
9.08
9.06
8.89
8.80
8.78
8.07
8.05
7.98
7.83
7.63
7.62
7.61
7.54
7.27
6.80
6.77
6.58
6.51
5.78
5.70
5.30
5.18
4.92
3.60
2.00
1.85
1.74
1.72
1.59
1.53
1.23
0.99
0.77
0.53
O
NH
N
N
N
O
O
Br
1.00
1.00
0.98
1.03
1.19
0.82
1.02
1.36
1.03
0.94
1.01
1.02
1.07
1.06
1.19
2.32
1.20
4.03
1.01
3.25
1.08
1.02
1.70E+08
1.60E+08
1.50E+08
1.40E+08
1.30E+08
1.20E+08
1.10E+08
1.00E+08
9.00E+07
8.00E+07
7.00E+07
6.00E+07
5.00E+07
4.00E+07
3.00E+07
2.00E+07
1.00E+07
0.00E+00
-1.00E+07
12.0
11.5
11.0
10.5
10.0
9.5
9.0
8.5
8.0
7.5
7.0
6.5
6.0
5.5
5.0
4.5
4.0
3.5
3.0
2.5
2.0
1.5
1.0
0.5
0.0
f1 (ppm)

Compound 9b.(S)-2-(6-bromobenzo-1,3-dioxol-5-yl)-1-(1-cyclohexylethyl)-N-(quinolin-6-yl)-1H-benzo[d]imidazole-5-carboxamide.

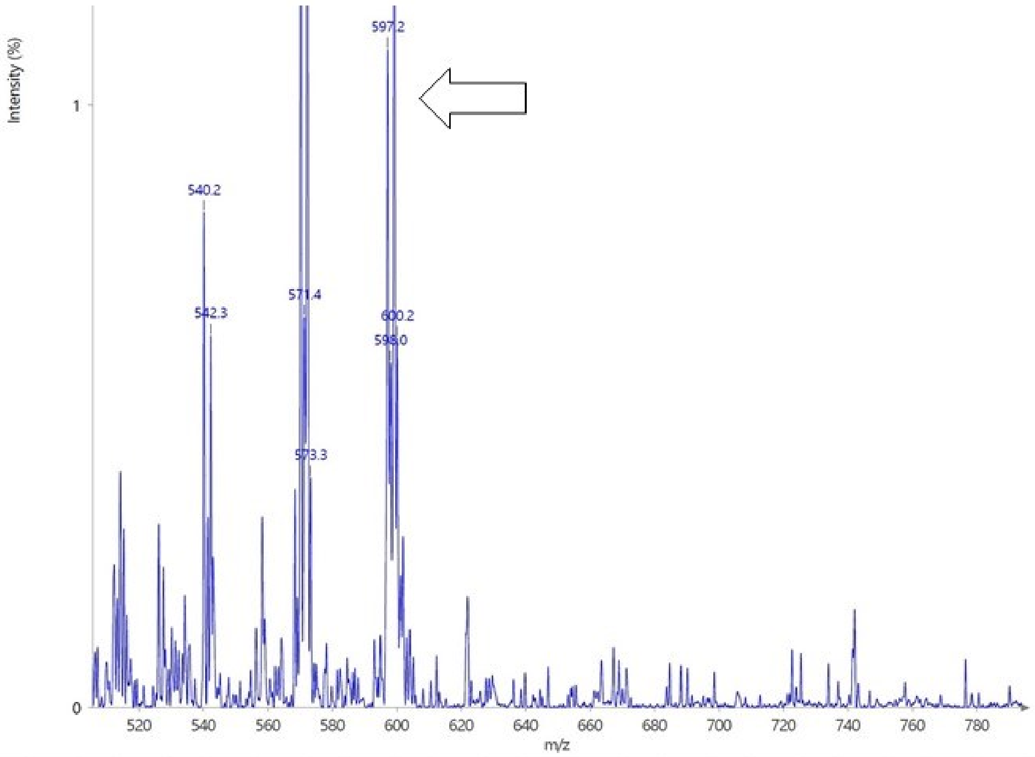

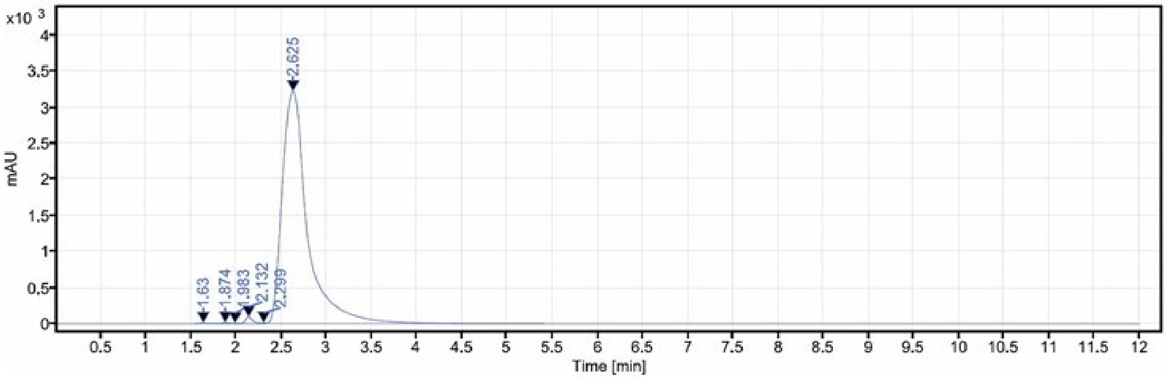

Signal: VWD1A,Wavelength=254 nm

RT [min]	Type	Width [min]	Area	Height	Area%	Name
1.630	BB	0.24	49.35	10.84	0.08	
1.874	BV	0.18	60.72	11.38	0.10	
1.983	VB	0.07	6.78	2.40	0.01	
2.132	BV	0.24	505.09	90.01	0.79	
2.299	VV	0.05	24.56	8.54	0.04	
2.625	VB	3.25	62916.63	3217.42	98.98	
		Sum	63563.12			

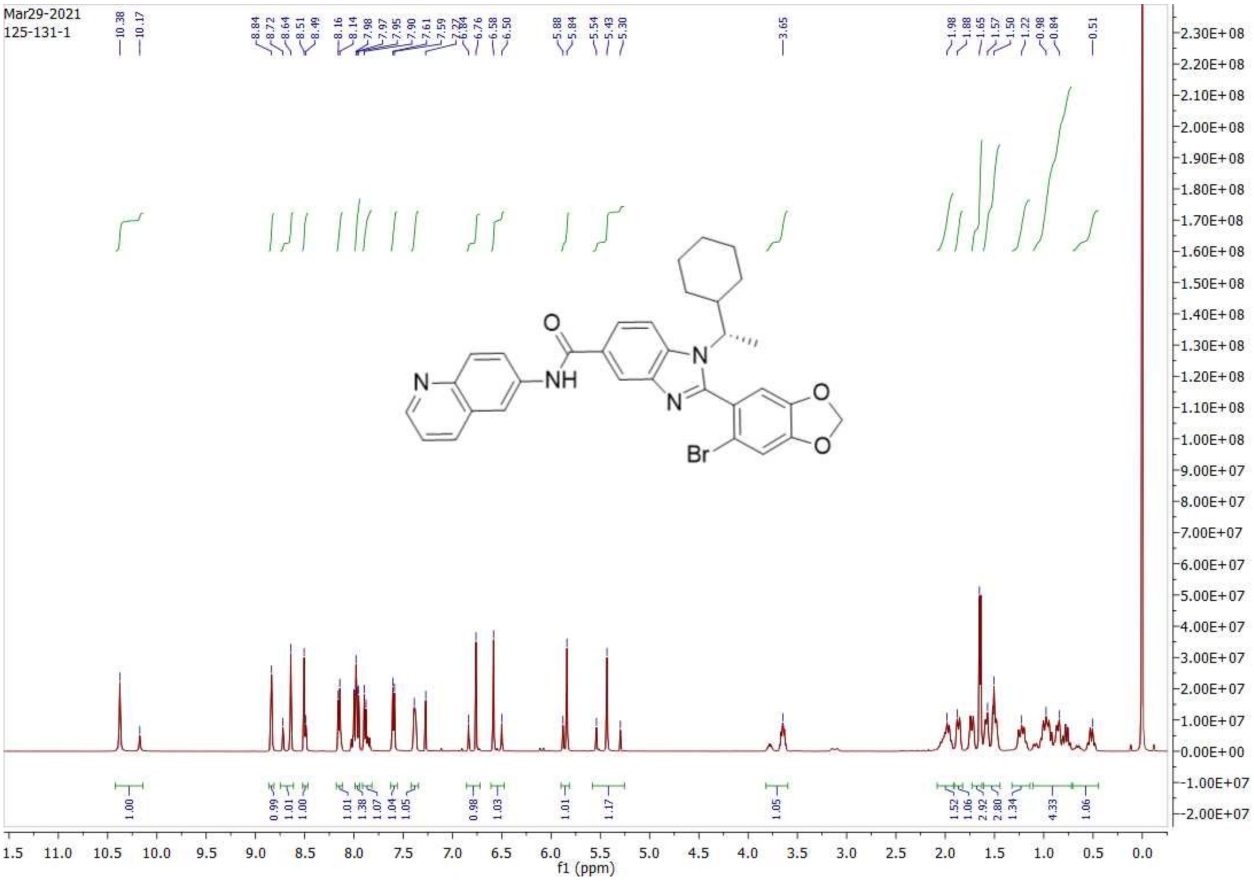
Mar29-2021
125-131-1
10.38
10.17
8.84
8.72
8.64
8.51
8.49
8.16
8.14
7.98
7.97
7.95
7.90
7.61
7.59
7.27
6.84
6.76
6.58
6.50
5.88
5.84
5.54
5.43
5.30
3.65
1.98
1.88
1.65
1.57
1.50
1.22
0.98
0.84
0.51
O
NH
N
N
N
O
O
Br
1.00
0.99
1.01
1.00
1.01
1.38
1.07
1.04
1.05
0.98
1.03
1.01
1.17
1.05
1.52
1.06
2.92
2.80
1.34
4.33
1.06
f1 (ppm)

Compound 9c. (S)-2-(6-bromobenzo-1,3-dioxol-5-yl)-1-(1-cyclohexylethyl)-N-(quinolin-8-yl)-1H-benzo[d]imidazole-5-carboxamide.

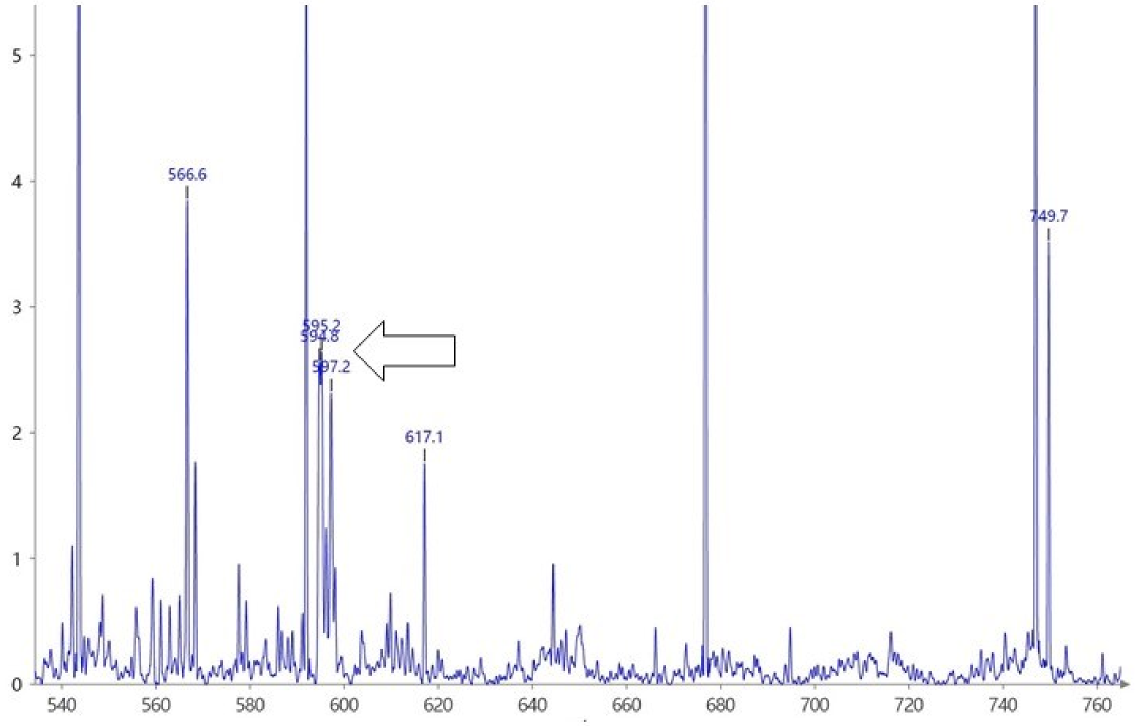

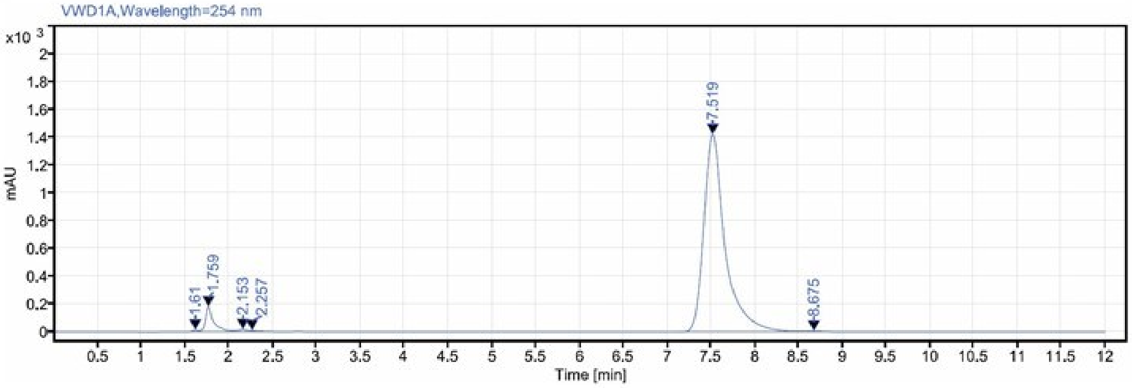

Signal: VWD1A,Wavelength=254 nm

RT [min]	Type	Width [min]	Area	Height	Area%	Name
1.610	BV	0.14	51.68	11.84	0.20	
1.759	VV	0.38	1193.38	179.06	4.68	
2.153	VV	0.20	134.00	15.66	0.53	
2.257	VB	0.40	68.81	9.06	0.27	
7.519	VV	1.44	23981.03	1419.52	93.98	
8.675	VB	0.83	87.30	4.87	0.34	
		Sum	25516.20			

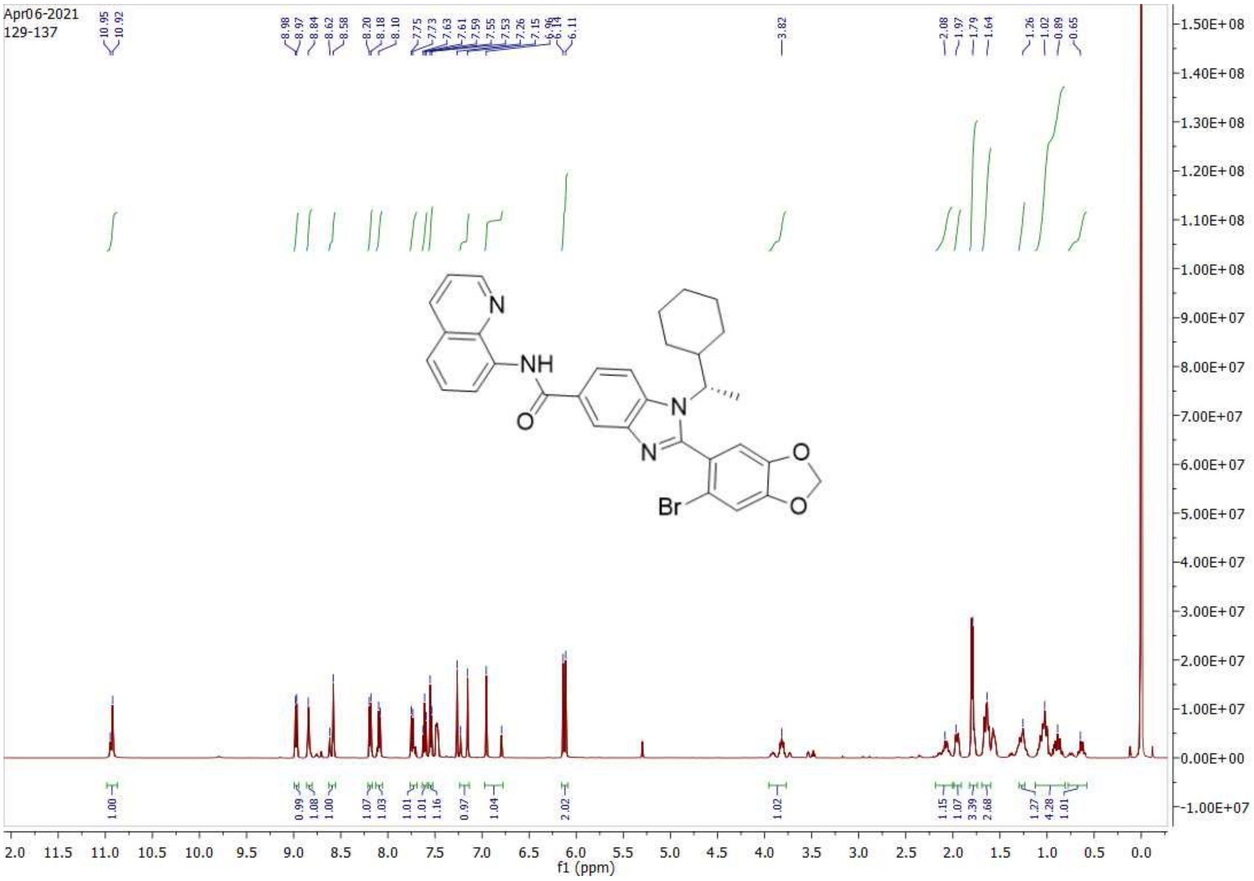
Apr06-2021
129-137
10.95
10.92
8.98
8.97
8.84
8.62
8.58
8.20
8.18
8.10
7.75
7.73
7.63
7.61
7.59
7.55
7.53
7.26
7.15
6.96
6.14
6.11
3.82
2.08
1.97
1.79
1.64
1.26
1.02
0.89
0.65
N
NH
O
N
N
O
O
Br
1.00
0.99
1.08
1.00
1.07
1.03
1.01
1.01
1.16
0.97
1.04
2.02
1.02
1.15
1.07
3.39
2.68
1.27
4.28
1.01
2.0
11.5
11.0
10.5
10.0
9.5
9.0
8.5
8.0
7.5
7.0
6.5
6.0
5.5
5.0
4.5
4.0
3.5
3.0
2.5
2.0
1.5
1.0
0.5
0.0
f1 (ppm)
1.50E+08
1.40E+08
1.30E+08
1.20E+08
1.10E+08
1.00E+08
9.00E+07
8.00E+07
7.00E+07
6.00E+07
5.00E+07
4.00E+07
3.00E+07
2.00E+07
1.00E+07
0.00E+00
-1.00E+07

Compound 10a. (S)-2-(6-bromobenzo-1,3-dioxol-5-yl)-1-(1-cyclohexylethyl)-N-(3-ethynylphenyl)-1H-benzo[d]imidazole-5-carboxamide.

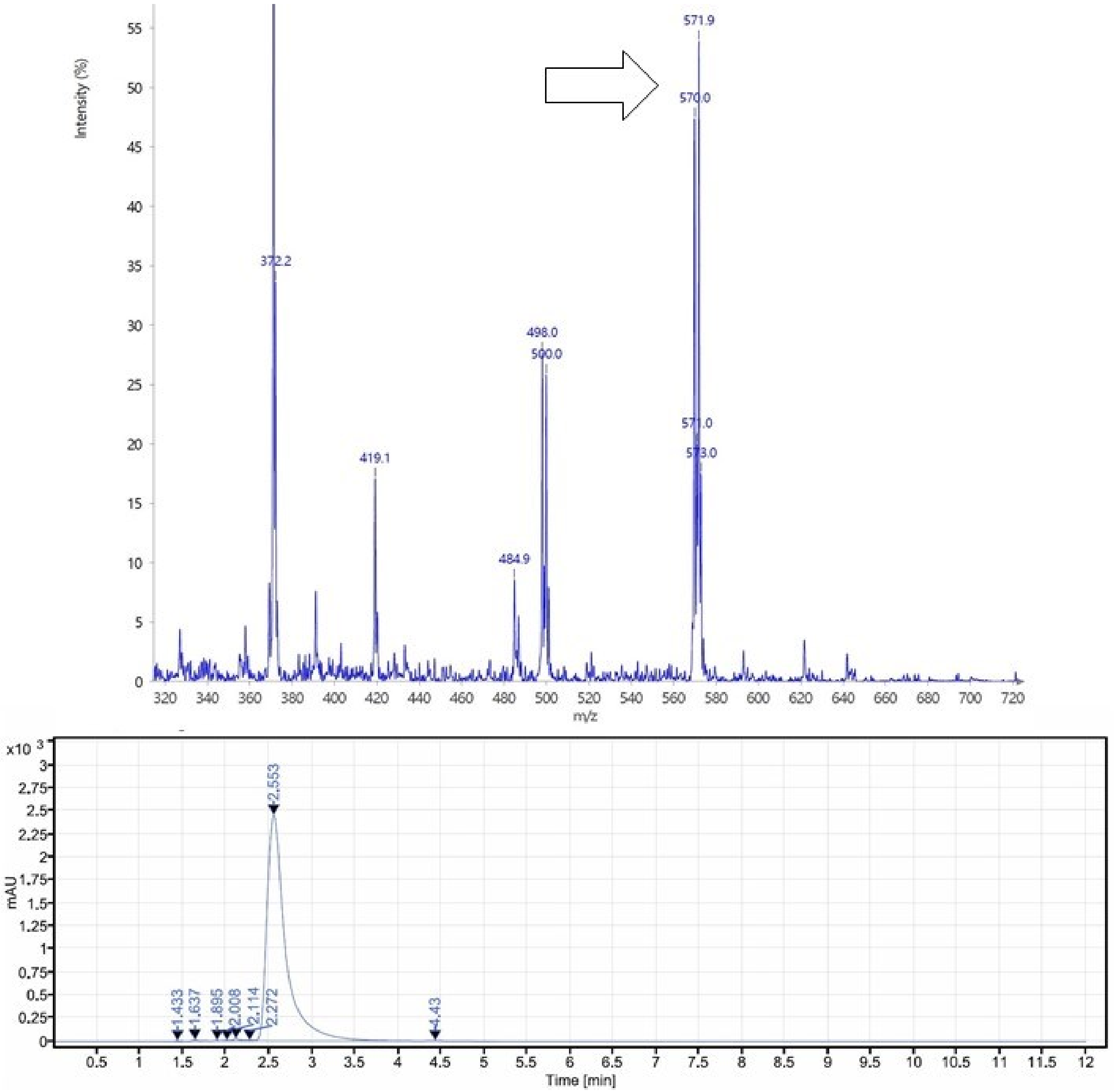

Signal: VWD1A,Wavelength=254 nm

RT [min]	Type	Width [min]	Area	Height	Area%	Name
1.433	BB	0.29	24.89	4.81	0.07	
1.637	BB	0.29	67.03	12.53	0.18	
1.895	BB	0.11	8.38	2.56	0.02	
2.008	BV	0.10	12.95	3.36	0.03	
2.114	VV	0.18	120.40	22.40	0.32	
2.272	VV	0.10	36.80	7.19	0.10	
2.553	VV	1.92	37089.86	2451.61	99.05	
4.430	VB	0.91	83.50	3.83	0.22	
		Sum	37443.81			

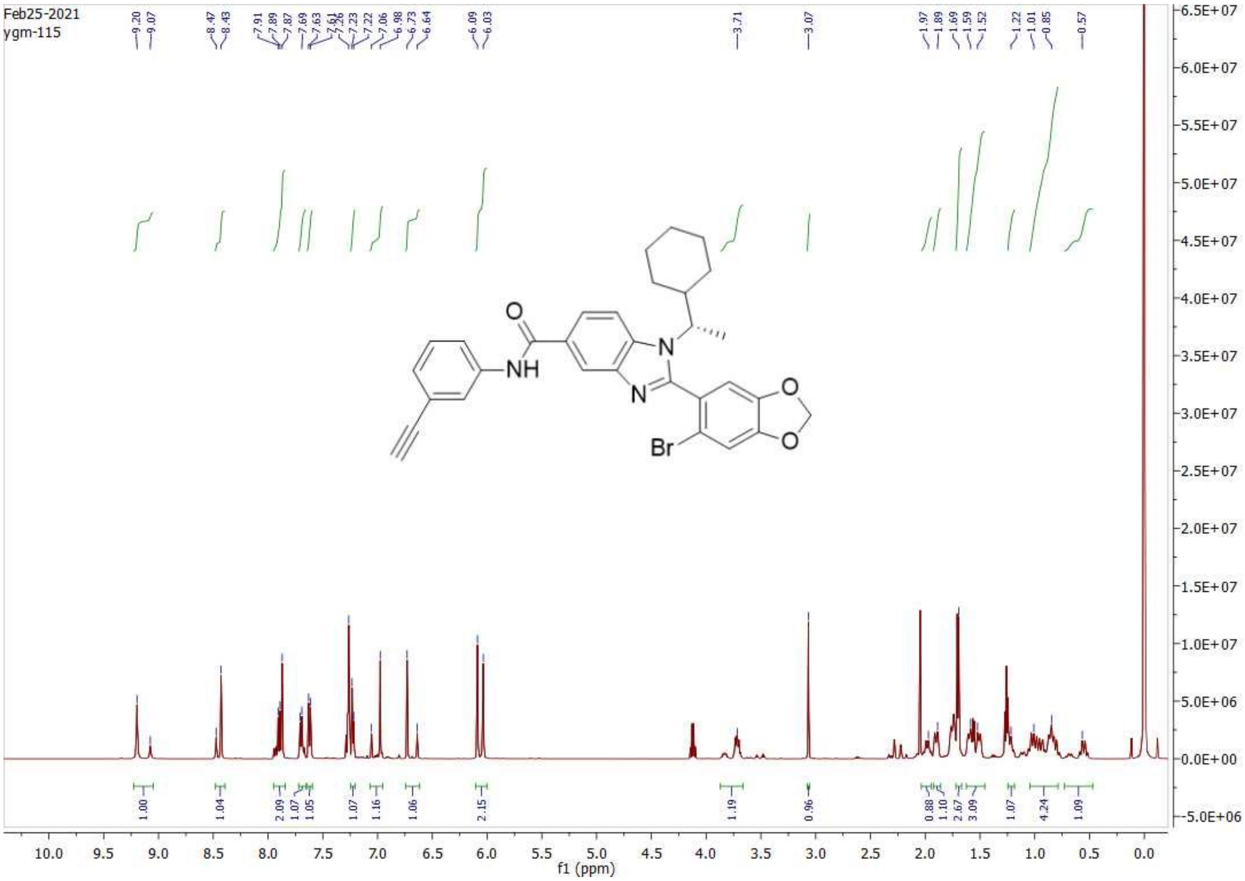
Feb25-2021
ygm-115
9.20
9.07
8.47
8.43
7.91
7.89
7.87
7.69
7.63
7.61
7.26
7.23
7.22
7.06
6.98
6.73
6.64
6.09
6.03
3.71
3.07
1.97
1.89
1.69
1.59
1.52
1.22
1.01
0.85
0.57
O
NH
N
N
O
O
Br
1.00
1.04
2.09
1.07
1.05
1.07
1.16
1.06
2.15
1.19
0.96
0.88
1.10
2.67
3.09
1.07
4.24
1.09
6.5E+07
6.0E+07
5.5E+07
5.0E+07
4.5E+07
4.0E+07
3.5E+07
3.0E+07
2.5E+07
2.0E+07
1.5E+07
1.0E+07
5.0E+06
0.0E+00
-5.0E+06
10.0
9.5
9.0
8.5
8.0
7.5
7.0
6.5
6.0
5.5
5.0
4.5
4.0
3.5
3.0
2.5
2.0
1.5
1.0
0.5
0.0
f1 (ppm)

Compound 10b. (S)-2-(6-bromobenzo-1,3-dioxol-5-yl)-1-(1-cyclohexylethyl)-N-(4-ethynylphenyl)-1H-benzo[d]imidazole-5-carboxamide.

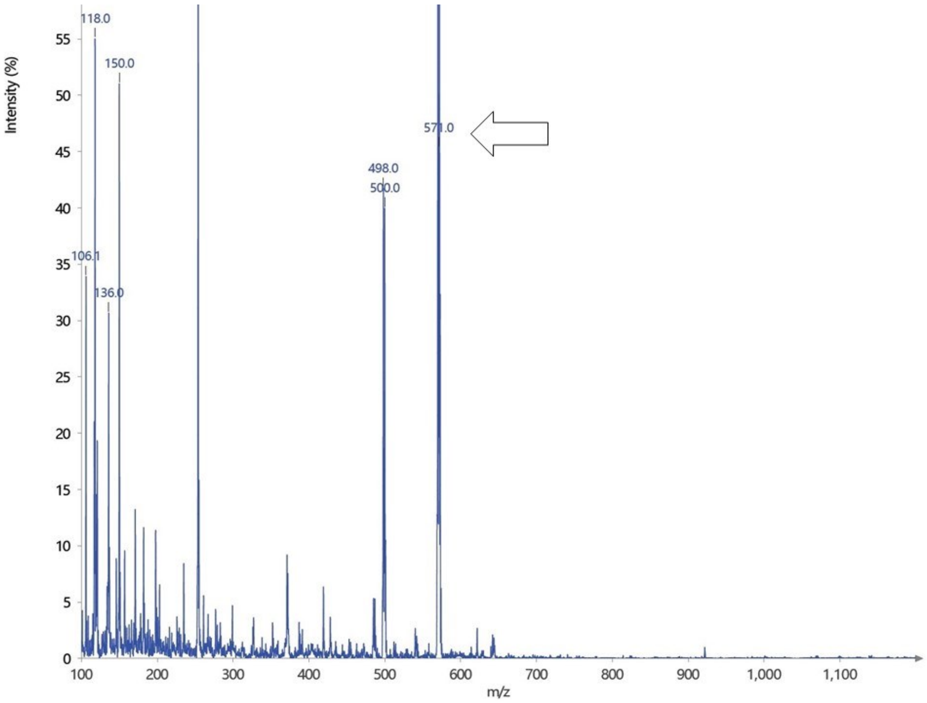

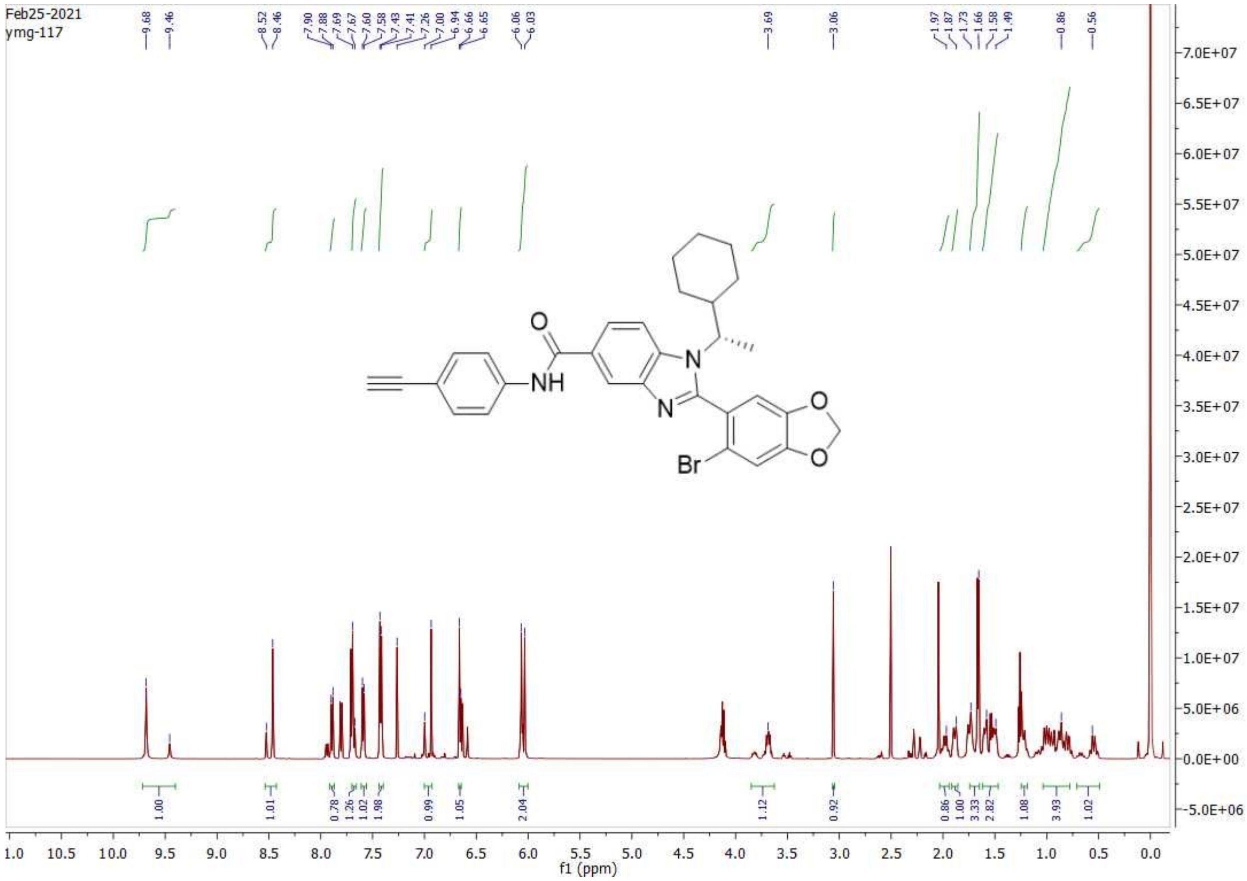
Feb25-2021
ymg-117
9.68
9.46
8.52
8.46
7.90
7.88
7.69
7.67
7.60
7.58
7.43
7.41
7.26
7.00
6.94
6.66
6.65
6.06
6.03
3.69
3.06
1.97
1.87
1.73
1.66
1.58
1.49
0.86
0.56
O
NH
N
N
O
O
Br
1.00
1.01
0.78
1.26
1.02
1.98
0.99
1.05
2.04
1.12
0.92
0.86
1.00
3.33
2.82
1.08
3.93
1.02
7.0E+07
6.5E+07
6.0E+07
5.5E+07
5.0E+07
4.5E+07
4.0E+07
3.5E+07
3.0E+07
2.5E+07
2.0E+07
1.5E+07
1.0E+07
5.0E+06
0.0E+00
-5.0E+06
1.0
10.5
10.0
9.5
9.0
8.5
8.0
7.5
7.0
6.5
6.0
5.5
5.0
4.5
4.0
3.5
3.0
2.5
2.0
1.5
1.0
0.5
0.0
f1 (ppm)

Compound 11a. (S)-2-(6-bromobenzo-1,3-dioxol-5-yl)-N-(4-bromophenyl)-1-(1-cyclohexylethyl)-1H-benzo[d]imidazole-5-carboxamide.

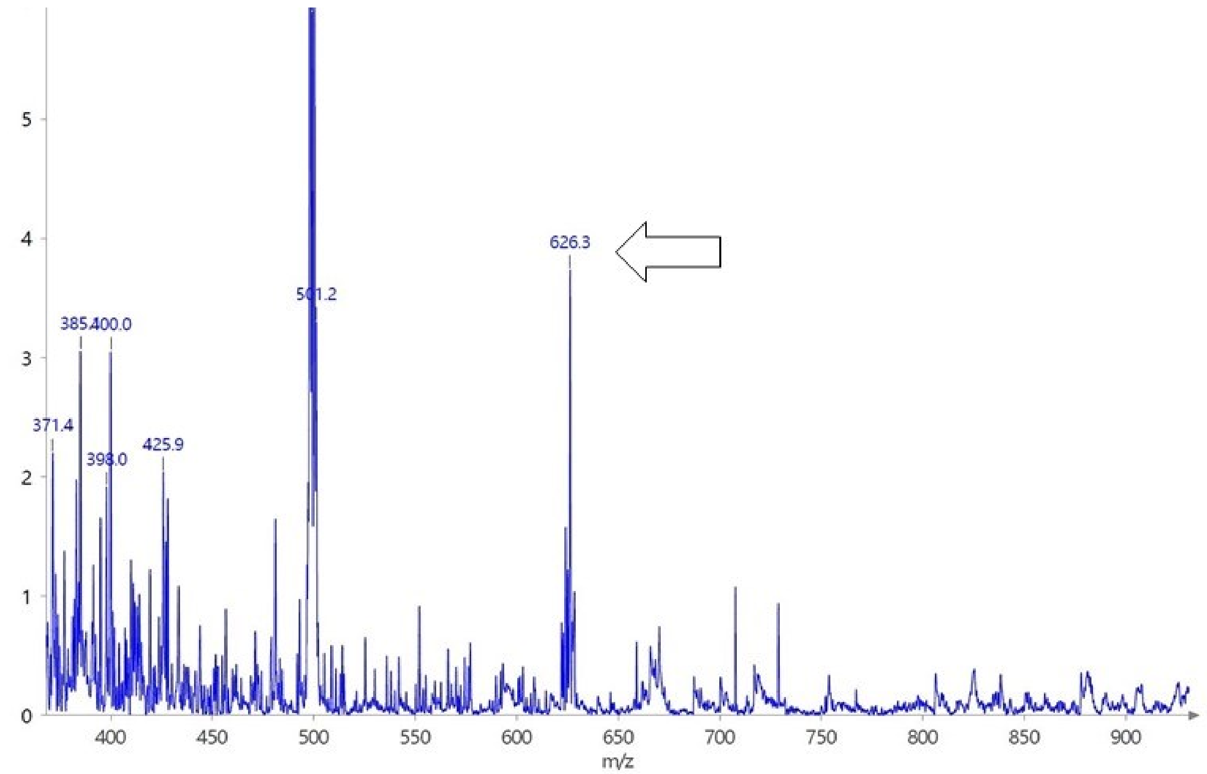

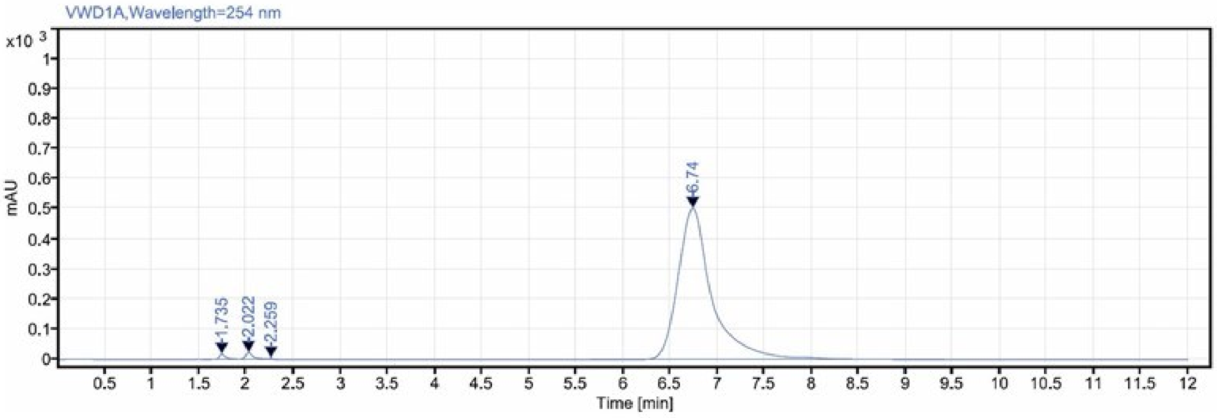

Signal: VWD1A,Wavelength=254 nm

RT [min]	Type	Width [min]	Area	Height	Area%	Name
1.735	BV	0.38	105.28	18.08	0.81	
2.022	VV	0.30	147.23	22.82	1.13	
2.259	VB	0.11	13.65	5.10	0.11	
6.740	BB	3.74	12716.83	502.44	97.95	
		Sum	12982.99			

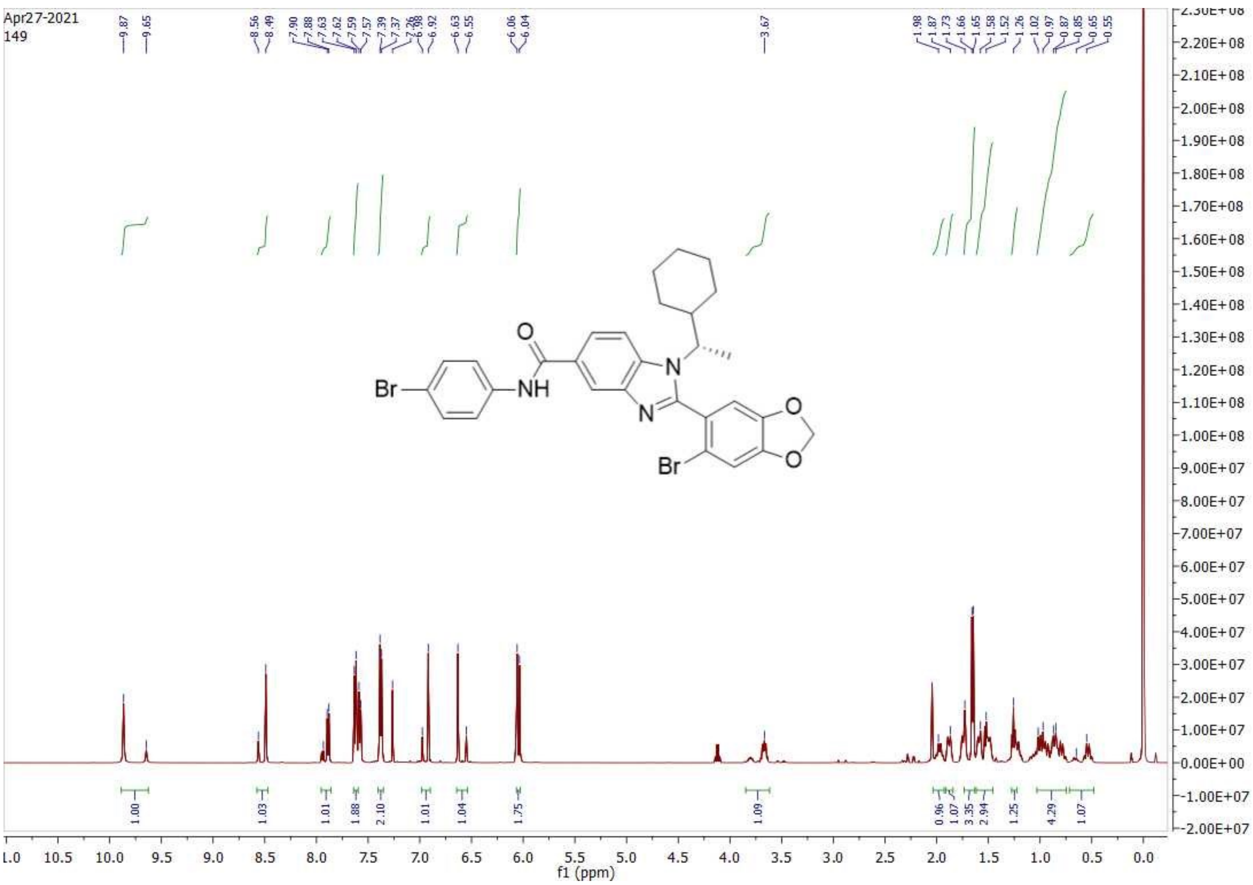

Apr27-2021
149
9.87
9.65
8.56
8.49
7.90
7.88
7.63
7.62
7.59
7.57
7.39
7.37
7.26
6.98
6.92
6.63
6.55
6.06
6.04
3.67
1.98
1.87
1.73
1.66
1.65
1.58
1.52
1.26
1.02
0.97
0.87
0.85
0.65
0.55
O
Br
NH
N
N
O
O
Br
1.00
1.03
1.01
1.88
2.10
1.01
1.04
1.75
1.09
0.96
1.07
3.35
2.94
1.25
4.29
1.07
2.30E+08
2.20E+08
2.10E+08
2.00E+08
1.90E+08
1.80E+08
1.70E+08
1.60E+08
1.50E+08
1.40E+08
1.30E+08
1.20E+08
1.10E+08
1.00E+08
9.00E+07
8.00E+07
7.00E+07
6.00E+07
5.00E+07
4.00E+07
3.00E+07
2.00E+07
1.00E+07
0.00E+00
-1.00E+07
-2.00E+07
1.0
10.5
10.0
9.5
9.0
8.5
8.0
7.5
7.0
6.5
6.0
5.5
5.0
4.5
4.0
3.5
3.0
2.5
2.0
1.5
1.0
0.5
0.0
f1 (ppm)

Compound 12a. (S)-2-(6-bromobenzo-1,3-dioxol-5-yl)-1-(1-cyclohexylethyl)-N-(pyridin-2-ylmethyl)-1H-benzo[d]imidazole-5-carboxamide.

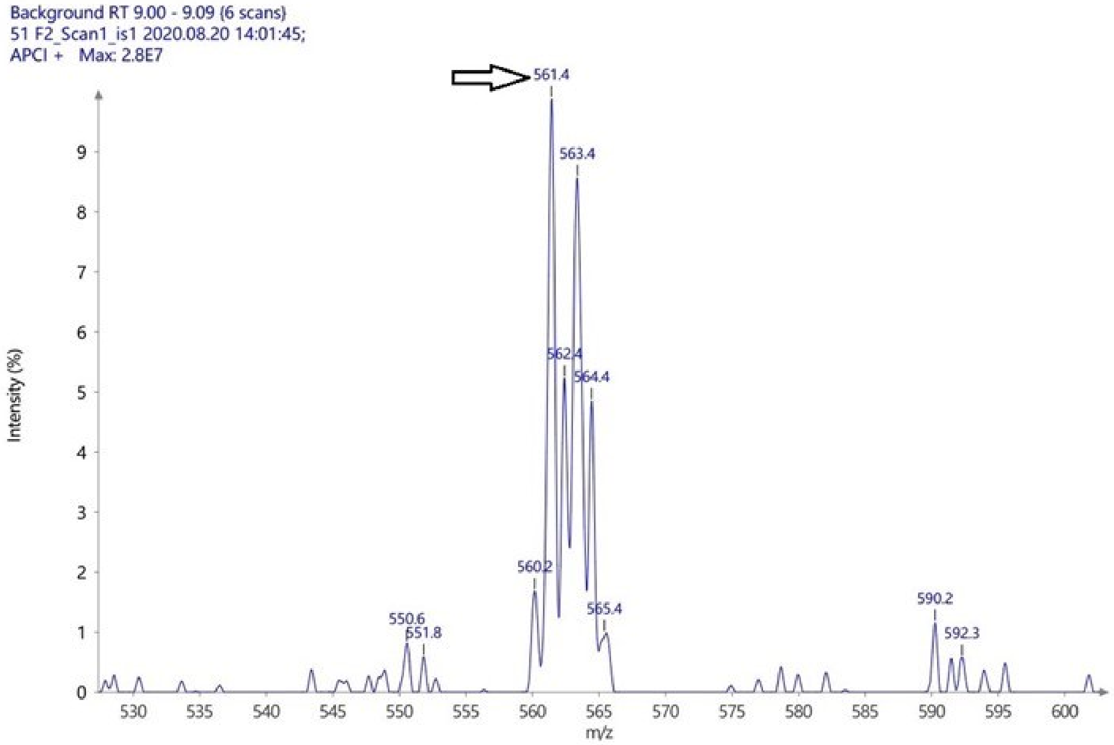

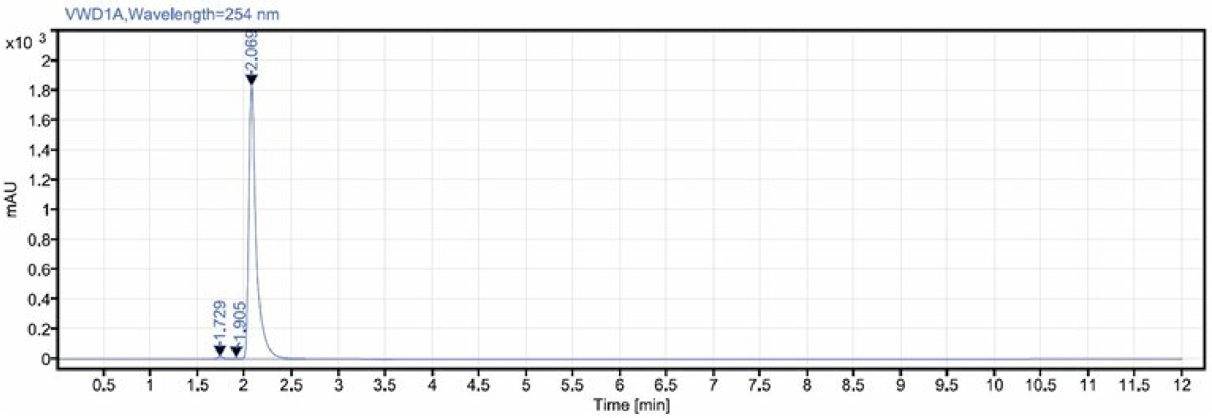

Signal: VWD1A,Wavelength=254 nm

RT [min]	Type	Width [min]	Area	Height	Area%	Name
1.729	BV	0.31	77.63	13.44	0.76	
1.905	VV	0.12	30.30	5.68	0.30	
2.069	VB	1.63	10087.35	1827.19	98.94	
		Sum	10195.29			

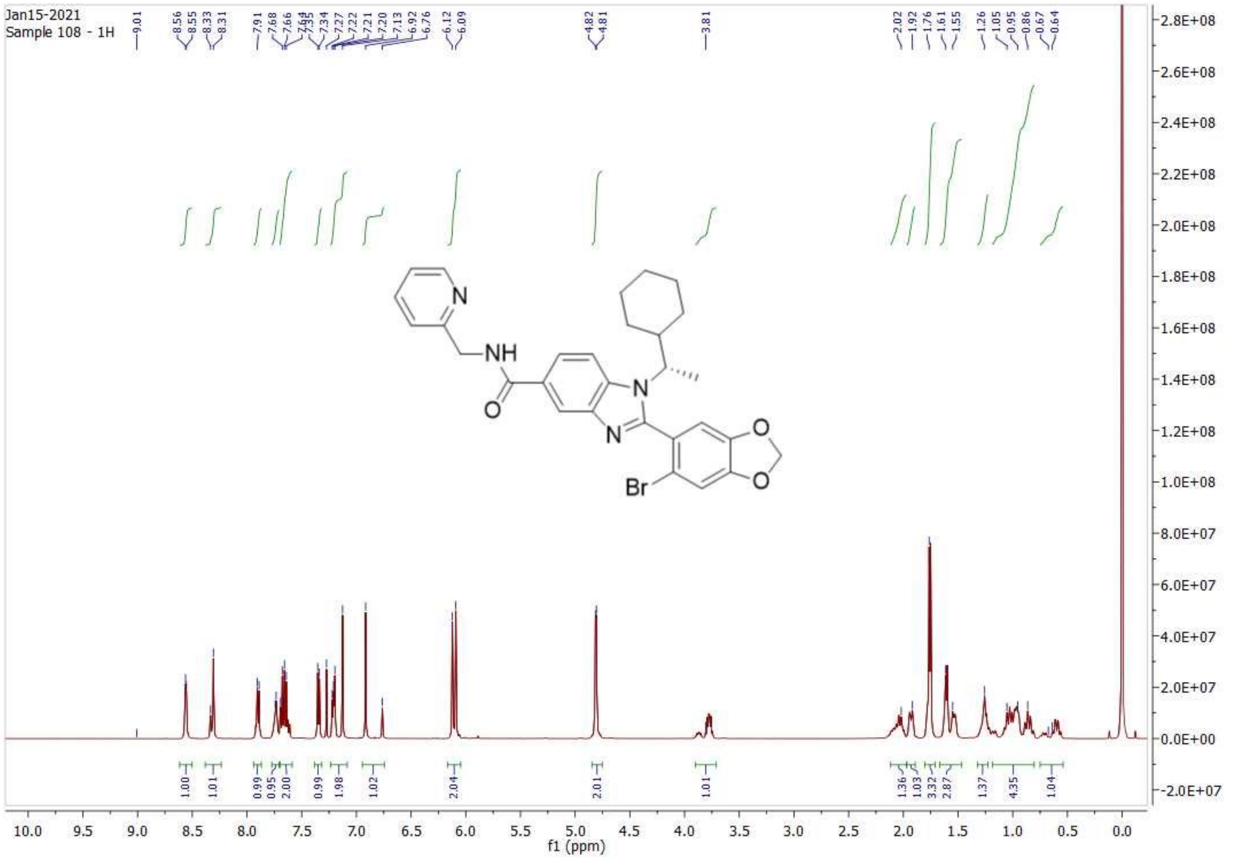
Jan15-2021
Sample 108 - 1H
9.01
8.56
8.55
8.33
8.31
7.91
7.68
7.66
7.64
7.35
7.34
7.27
7.22
7.21
7.20
7.13
6.92
6.76
6.12
6.09
4.82
4.81
3.81
2.02
1.92
1.76
1.61
1.55
1.26
1.05
0.95
0.86
0.67
0.64
N
NH
O
N
N
O
O
Br
1.00
1.01
0.99
0.95
2.00
0.99
1.98
1.02
2.04
2.01
1.01
1.36
1.03
3.32
2.87
1.37
4.35
1.04
2.8E+08
2.6E+08
2.4E+08
2.2E+08
2.0E+08
1.8E+08
1.6E+08
1.4E+08
1.2E+08
1.0E+08
8.0E+07
6.0E+07
4.0E+07
2.0E+07
0.0E+00
-2.0E+07
10.0
9.5
9.0
8.5
8.0
7.5
7.0
6.5
6.0
5.5
5.0
4.5
4.0
3.5
3.0
2.5
2.0
1.5
1.0
0.5
0.0
f1 (ppm)

Compound 13a. (S)-N-([1,1'-biphenyl]-2-yl)-2-(6-bromobenzo-1,3-dioxol-5-yl)-1-(1-cyclohexylethyl)-1H-benzo[d]imidazole-5-carboxamide.

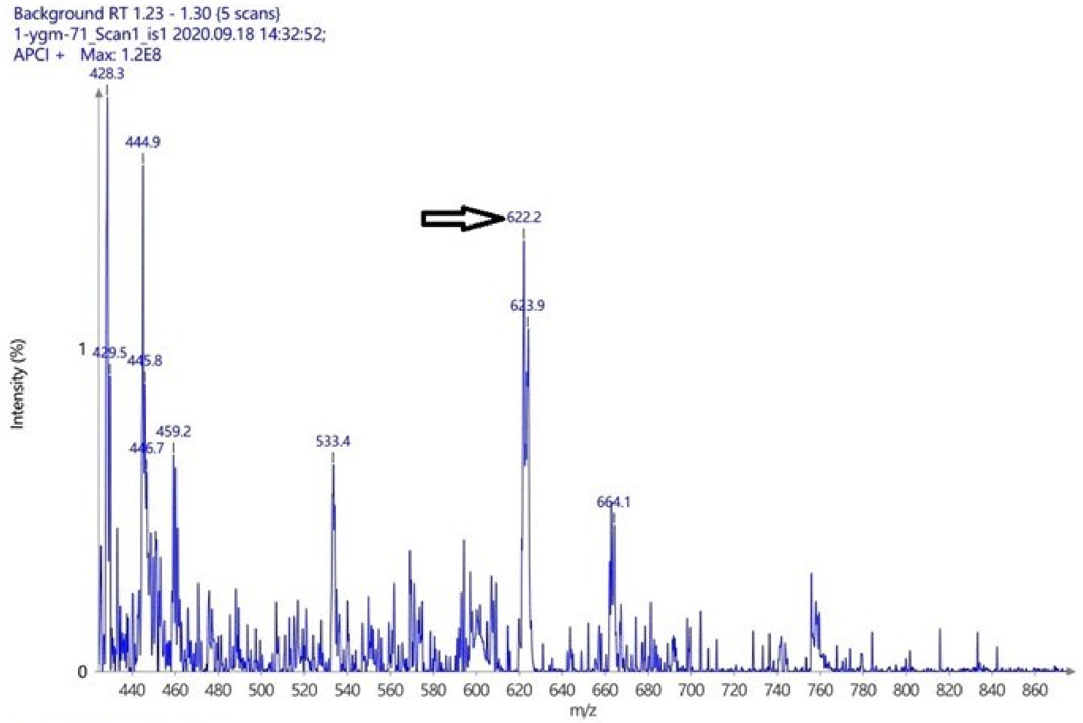

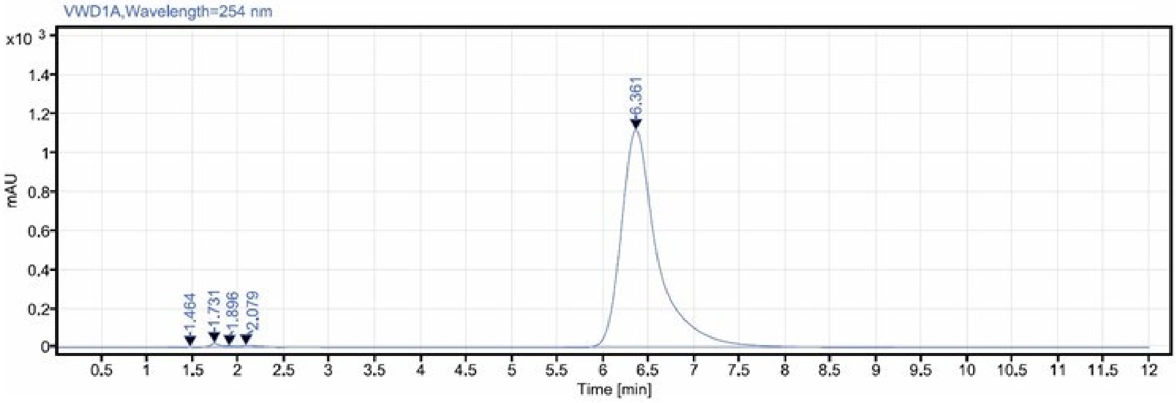

Signal: VWD1A,Wavelength=254 nm

RT [min]	Type	Width [min]	Area	Height	Area%	Name
1.464	BB	0.31	9.74	2.00	0.03	
1.731	BV	0.34	166.56	21.83	0.53	
1.896	VV	0.12	37.95	6.22	0.12	
2.079	VB	0.46	116.18	9.40	0.37	
6.361	BB	3.61	31169.00	1118.37	98.95	
		Sum	31499.43			

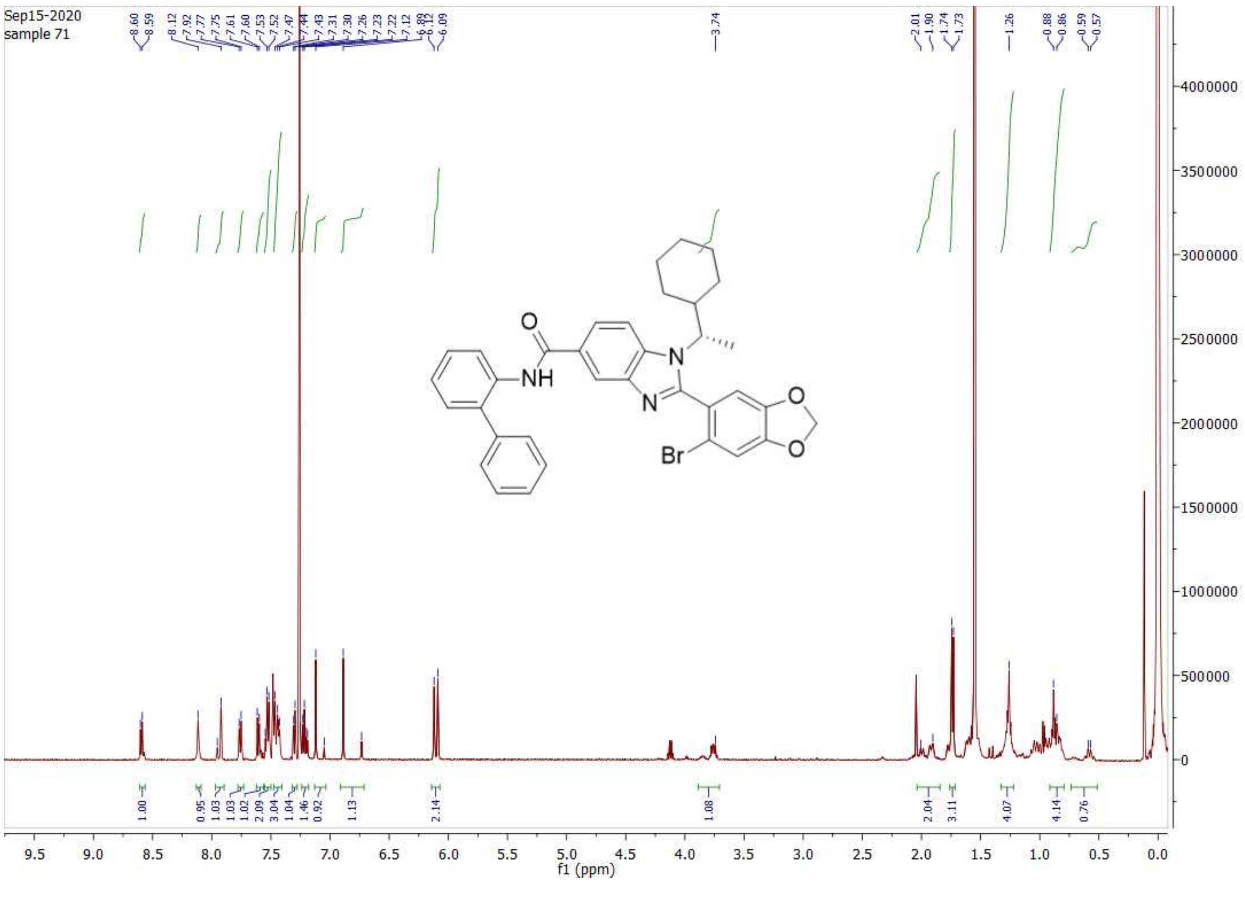
Sep15-2020
sample 71
8.60
8.59
8.12
7.92
7.77
7.75
7.61
7.60
7.53
7.52
7.47
7.44
7.43
7.31
7.30
7.26
7.23
7.22
7.12
6.89
6.12
6.09
3.74
2.01
1.90
1.74
1.73
1.26
0.88
0.86
0.59
0.57
O
NH
N
N
O
O
Br
4000000
3500000
3000000
2500000
2000000
1500000
1000000
500000
0
1.00
0.95
1.03
1.03
1.02
2.09
3.04
1.04
1.46
0.92
1.13
2.14
1.08
2.04
3.11
4.07
4.14
0.76
9.5
9.0
8.5
8.0
7.5
7.0
6.5
6.0
5.5
5.0
4.5
4.0
3.5
3.0
2.5
2.0
1.5
1.0
0.5
0.0
f1 (ppm)

Compound 14a. (S)-2-(6-bromobenzo-1,3-dioxol-5-yl)-1-(1-cyclohexylethyl)-N-(4-phenoxyphenyl)-1H-benzo[d]imidazole-5-carboxamide.

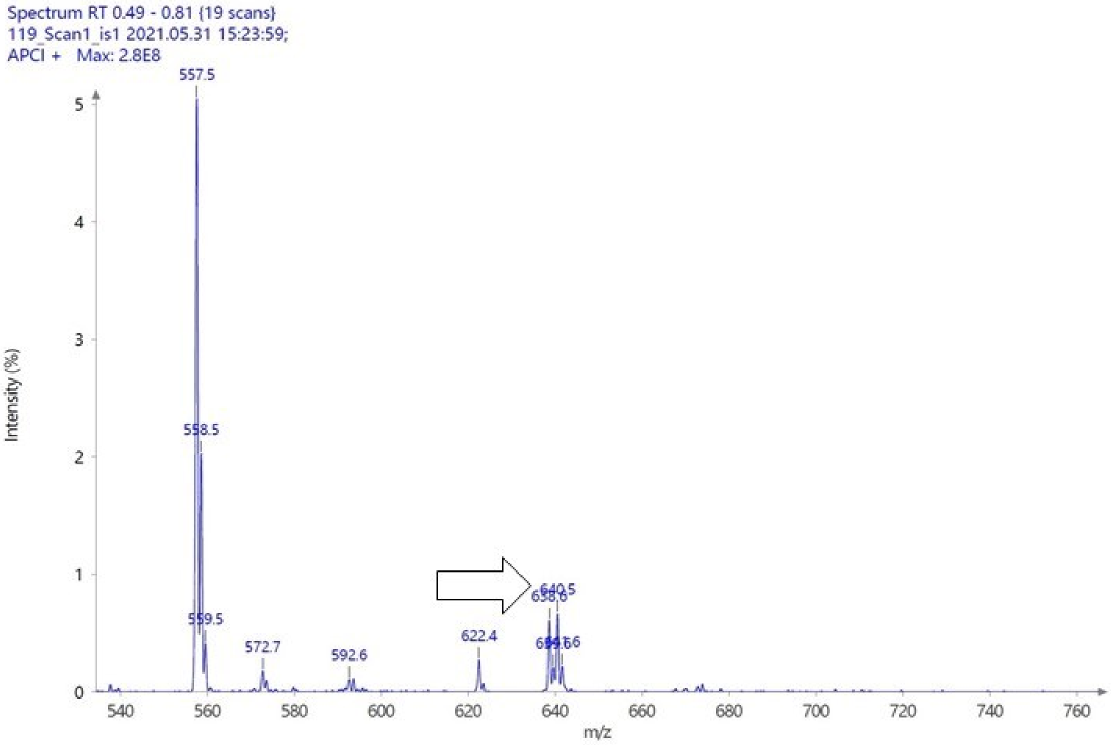

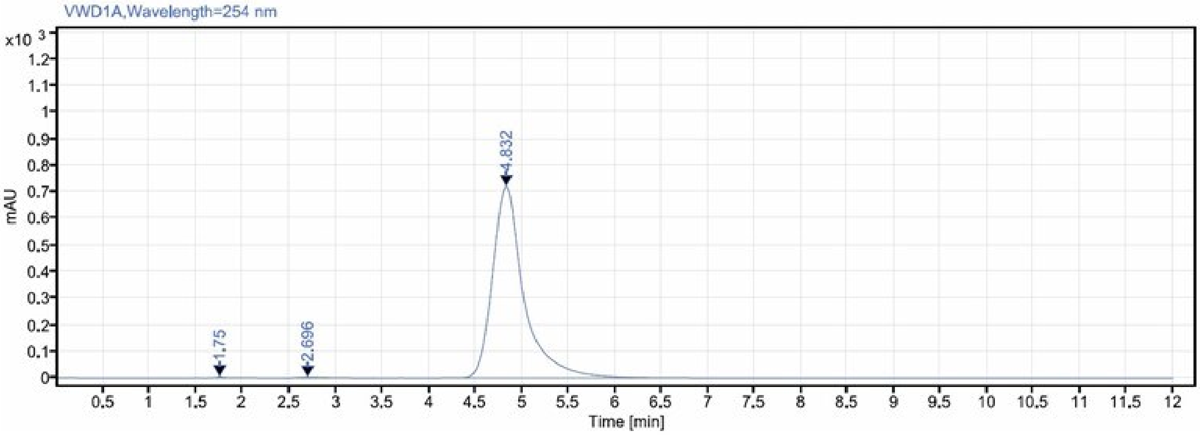

Signal: VWD1A,Wavelength=254 nm

RT [min]	Type	Width [min]	Area	Height	Area%	Name
1.750	VV	0.33	33.17	5.07	0.19	
2.696	BB	1.00	76.46	3.34	0.45	
4.832	BB	3.79	17021.17	721.65	99.36	
		Sum	17130.80			

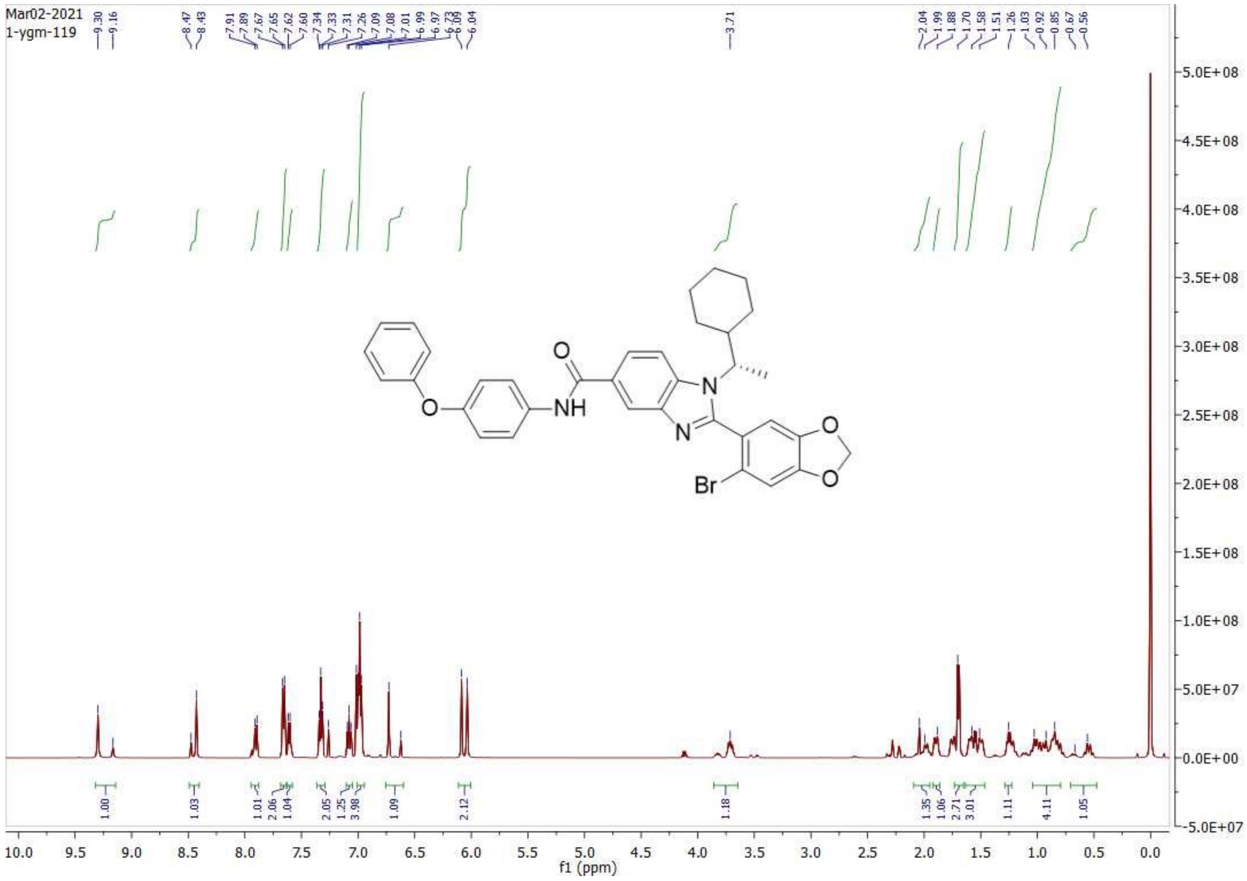
Mar02-2021
1-ygm-119
9.30
9.16
8.47
8.43
7.91
7.89
7.67
7.65
7.62
7.60
7.34
7.33
7.31
7.26
7.09
7.08
7.01
6.99
6.97
6.73
6.09
6.04
3.71
2.04
1.99
1.88
1.70
1.58
1.51
1.26
1.03
0.92
0.85
0.67
0.56
O
NH
N
N
O
O
Br
1.00
1.03
1.01
2.06
1.04
2.05
1.25
3.98
1.09
2.12
1.18
1.35
1.06
2.71
3.01
1.11
4.11
1.05
10.0
9.5
9.0
8.5
8.0
7.5
7.0
6.5
6.0
5.5
5.0
4.5
4.0
3.5
3.0
2.5
2.0
1.5
1.0
0.5
0.0
f1 (ppm)
5.0E+08
4.5E+08
4.0E+08
3.5E+08
3.0E+08
2.5E+08
2.0E+08
1.5E+08
1.0E+08
5.0E+07
0.0E+00
-5.0E+07

Appendix 4: MS and ^{1}H-NMR Spectra for Compound 15.

(S)-2-(2-bromophenyl)-1-(1-cyclohexylethyl)-1H-benzoimidazole-5-carboxylic acid.

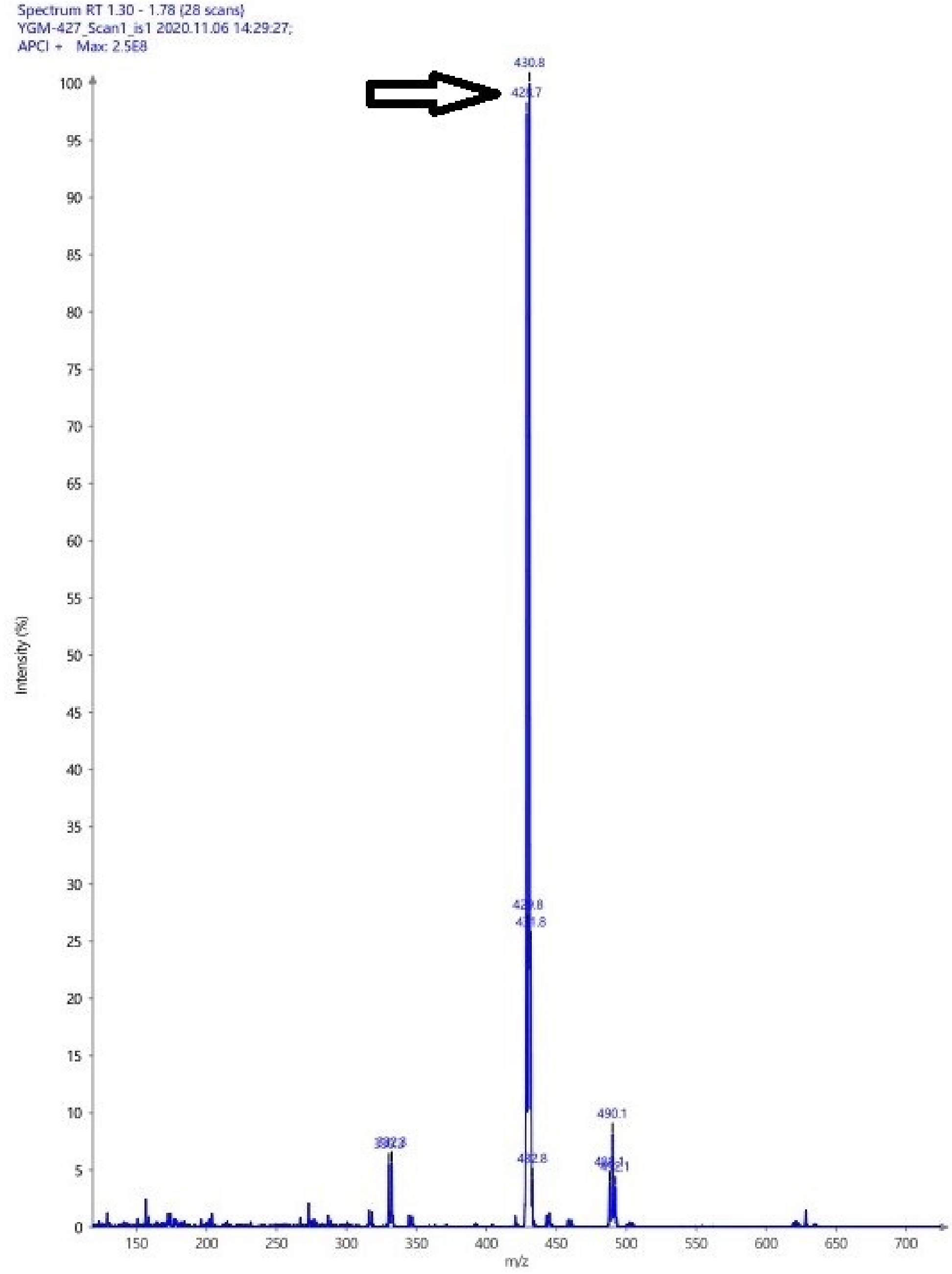

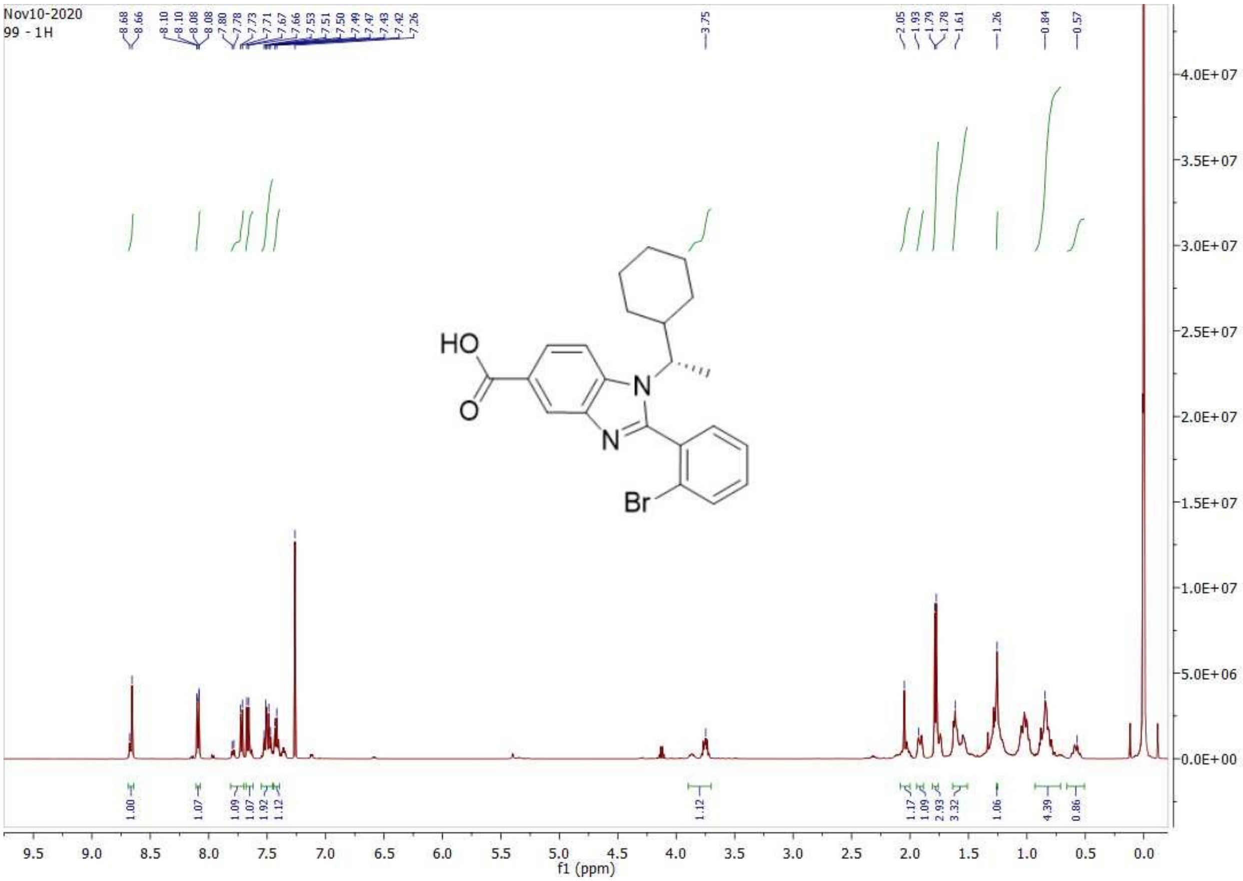
Nov10-2020
99 - 1H
8.68
8.66
8.10
8.10
8.08
8.08
7.80
7.78
7.73
7.71
7.67
7.66
7.53
7.51
7.50
7.49
7.47
7.43
7.42
7.26
3.75
2.05
1.93
1.79
1.78
1.61
1.26
0.84
0.57
HO
O
N
N
Br
1.00
1.07
1.09
1.07
1.92
1.12
1.12
1.17
1.09
2.93
3.32
1.06
4.39
0.86
-4.0E+07
-3.5E+07
-3.0E+07
-2.5E+07
-2.0E+07
-1.5E+07
-1.0E+07
-5.0E+06
-0.0E+00
9.5
9.0
8.5
8.0
7.5
7.0
6.5
6.0
5.5
5.0
4.5
4.0
3.5
3.0
2.5
2.0
1.5
1.0
0.5
0.0
f1 (ppm)